POLITECNICO DI MILANO
School of industrial and information Engineering
Master of Science degree in Energy Engineering

MODEL BASED CONTROL OF A HYBRID HEAT PUMP SYSTEM FOR BUILDING HEATING

Relatore: Prof. Aprile Marcello
Co-relatore: Prof. Kum Dongsuk

Tesi di laurea di:
Ettore Zanetti Matr. 836610

Anno accademico 2016/2017

Acknowledgements

Ringrazio il Professor Marcello Aprile e il Professor Dongsuk Kum per il loro supporto nello sviluppo di questo lavoro di tesi. Una speciale menzione anche all'ingegnere Rossano Scoccia, Erica Zavaglio, e i miei compagni del VDClab in Corea.
Ringrazio anche la mia famiglia e la mia ragazza Thao che mi hanno supportante durante lo sviluppo del lavoro.

Sintesi

L'attenzione verso l'efficienza energetica e la riduzione dei consumi nel settore dell'edilizia sta acquisendo sempre più importanza [1]. Utilizzare sistemi di generazione dell'energia alimentati da fonti rinnovabili unitamente ad un sistema di controllo supervisivo, ottimizzato per minimizzare i consumi dell'edificio garantendo allo stesso tempo la domanda elettrica e termica, va in questa direzione.
L'obiettivo generale del lavoro è dimostrare che, attraverso il controllo supervisivo, è possibile massimizzare l'efficienza di un sistema edificio-impianto complesso, costituito da edificio capacitivo dotato di impianto fotovoltaico, sistema di generazione a pompa di calore areotermica e sistema di accumulo dell'energia termica, ottenendo il minimo costo operativo e di investimento.
Questo può essere effettuato mediante l'utilizzo di un algoritmo di controllo che minimizzi il consumo energetico dell'edificio garantendo il comfort termico. A questo scopo la toolbox TOMLAB [2] per MATLAB è stata utilizzata e comparata con un controllore a regola di riferimento.

Parole chiave: Sistema riscaldamento ibrido, Accumulo termico, Modello a resistenze termiche per edificio, Ottimizzazione Controllo, Riscaldamento a pavimento, Energia rinnovabile.

Abstract

There has been increasing effort to develop energy efficient and low consumption buildings [1]. Combining renewable energies and optimal control theories is a promising approach towards achieving this goal.

The main objective of this work is to demonstrate that, by implementing supervisory control, it is possible to maximize the efficiency of a complex building system consisting of a photovoltaic power plant, an hybrid heating system and a thermal storage. The control system proposed was designed to minimize the operating costs by employing a control algorithm that would minimize the energy consumption of the building while also achieving thermal comfort. For this objective, TOMLAB [2], a MATLAB software, was used and compared to a simple reference rule-based controller.

Keywords: hybrid heating system, Thermal storage, Building model with thermal resistances, Optimal control, Floor heating, Renewable energy.

Contents

LIST OF FIGURES

LIST OF TABLES

1 INTRODUCTION

1.1 General background

There has been increasing effort to develop energy efficient and low consumption buildings [1], because buildings account for 20-40% of the total energy consumptions [3].
There are two main ways to decrease building energy consumption, retrofitting and modernization of physical properties and the application of advanced control techniques in the building automation systems.
However despite the research efforts in designing advanced control strategies, a detailed review article on this topic is [4], the most widely used approach is to use a climatic curve, based on the climatic zone, the external temperature and few building parameters. Sometimes the HVAC "heating ventilation and air conditioning system" is manually controlled by the user or by a simple "RBC" rule based controller, which uses some simple rules and "if-else" strategies to maintain the thermal comfort in each room.
However with this approach some major problems arises, first there is a lack of optimized strategy for the whole building control. Secondly during Autumn and Spring, the traditional controller may underestimate the gain contribution from the sun as shown in chapter 4, overheating the building in the morning and leading to a higher room temperature than required. Lastly, in cases such as the considered problem, when a thermal storage is present, a traditional controller would not be able to efficiently exploit the decoupling between the building energy demand and the production from the heating system.
Meanwhile an optimized controller can overcome this problems. In this work an MPC "model predictive control" strategy was applied, a review on this topic is offered in [5].
MPC controllers are linked to the physics of the building, so it is possible to create scalable models like in chapter 2 for the optimization problem.

1.2 Case study

The building taken into consideration in this work is the same as in [6]. It is a primary school located in Lombardy (North Italy), and it consists of four classroom and a cafeteria with a big hall in the middle.

There is a floor heating system which in this simulation scenario, is supported by an air source heat pump, since in mild climates the air source heat pump has a similar performance with respect to a ground source heat pump [7], a boiler in order to have a reference and a thermal storage. A photovoltaic system is also included in the analysis, since the optimal controller can exploit the decoupling between heat pump and thermal storage, allowing the heat pump to work when energy from the PV plant is available.

In Figure 1.2.1 two views of the considered building are reported, and in Figure 1.2.2 a simple infographic on the whole system is reported.

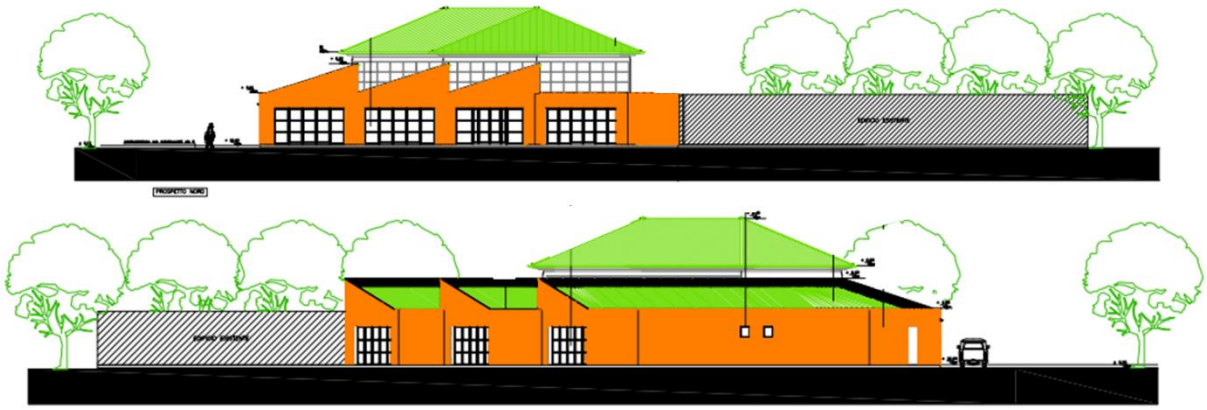

Figure 1.2.1 Building prospects

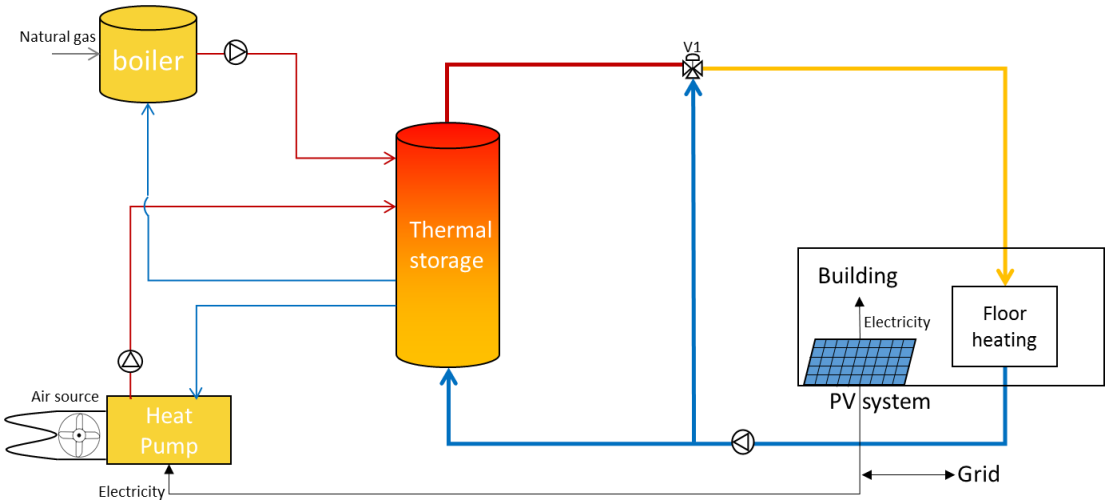

Figure 1.2.2 Schematic system scheme

1.3 System modeling

The first step when dealing with optimal control problems, is to define the physical model of the system. However there are limitations on the level of accuracy the physical system should have. In fact there is a trade off between the number of dynamic states describing the behavior of the considered system and the computational time required to find the optimal solution for the problem as discussed in [8].
In this work a reasonable model for all the components of the building was considered to represent the general thermal dynamics of the building, while not increasing the number of states and controls. The system modelling is discussed in more detail in Chapter 2.

1.4 Optimal control

The second step consists on the formulation of the optimal control problem, which can be seen as the objective that the optimal controller should accomplish within certain boundaries and constraints on states and controls. First a cost function is defined, which accounts for the objective, which in this case will be the minimization of the energy consumption of the heating system while providing thermal comfort inside the building. The boundaries and constraints are related to the physical parameters, the maximum inlet water flow rate into the floor heating for example. A detailed explanation of the cost function is given in chapter 3.1.
Once the model and problem are fully defined, a numerical simulation of the system is required.
The problem considered in this thesis is rather complex, in fact it consists of six dynamic states, three control variables, three disturbances on the dynamic system and two additional disturbances on the objective function. Furthermore the time horizon, ideally should be the whole heating season from October to April, however it would not be possible to simulate such a problem in a reasonable amount of time, therefore only five days a month from Thursday to Monday were considered. The reason behind this choice is to include the weekend which is a critical point since the building tends to cool down, and it is a period long enough, that it can be ensured the fact the summation of the results for each month, will be a very good approximation of the result obtained by considering the whole heating season.
Another key parameter is the time step, in other works sometimes an hourly time step is used [9], because of computational issues, however this choice is not realistic, since the controller ideally should be able to change the controls every instant, therefore a twenty minute time step was used.

1.5 Objective of the work

The final objective of the work is to demonstrate that the optimal controller, by exploiting the additional information given by the weather data and the prices, will outperform the rule based controller from an economic and thermal comfort point of view. There are few ways to do this. First the optimal controller should be able to exploit the thermal storage charging it when the cost of energy is the lowest and depending on the considered season use the heat pump or the boiler. Secondly the rule based controller may underestimate the gain contribution from the sun as shown in 4.3.2, overheating the building in the morning and leading to a higher room temperature than required. Furthermore the rule based controller is forced to maintain a minimum temperature in the building as shown in paragraph 4.1, especially during the weekend in order to ensure thermal comfort on Monday considering that the heating system will always start heating up the building at the same hour. The optimal controller instead can use the weather data to both prevent overheating and leave the building to cool down during the weekend, because it can start the heating system at just the right moment to guarantee thermal comfort on Monday morning.

2 SYSTEM MODELING

2.1 Thermal configuration

The plant consists of three main components, a natural gas boiler and an air heat pump which are connected to the thermal storage, and a thermal storage which is directly connected to the building. A plant scheme is reported in and the nomenclature in Table 2.4.1.1.

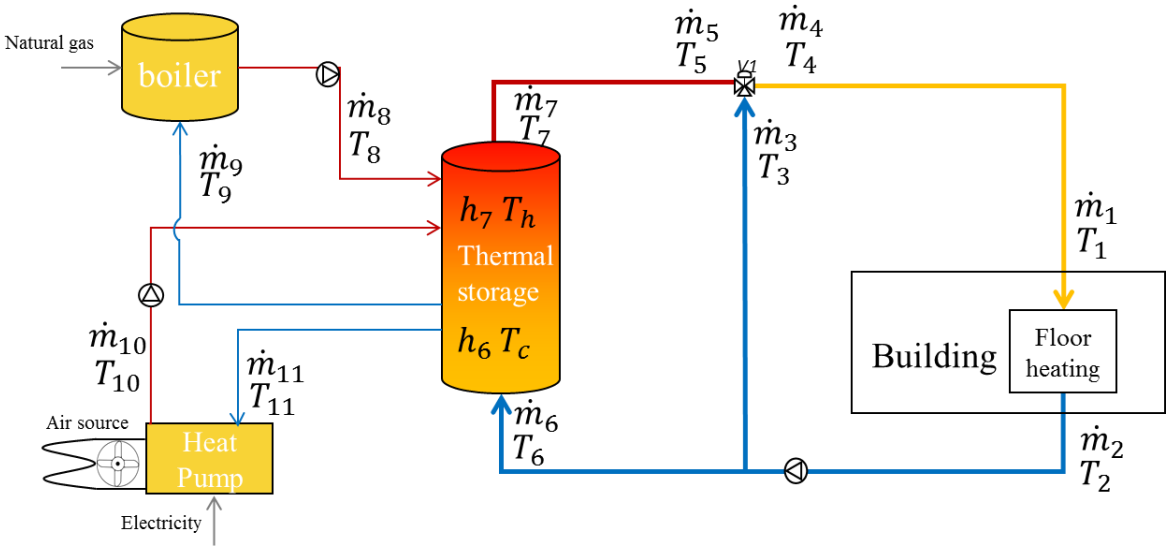

Figure 2.1.1 Plant configuration

Table 2.4.1.1 Plant configuration nomenclature

T [°C]	m [kg/s] h [m]	Description
T_1	m_1	Building Inlet
T_2	m_2	Building Outlet
$T_3 = T_2$	m_3	Recirculation Inlet from Building Outlet
T_4	m_4	Recirculation Outlet
T_5	m_5	Recirculation Inlet from Thermal storage (hot)
$T_6 = T_2$	m_6	Thermal storage Inlet (Cold)
$T_7 = T_5$	m_7	Thermal storage Outlet (hot)
T_8	m_8	Boiler outlet
T_9	m_9	Heat pump outlet
T_{10}	$m_{10} = m_8$	Boiler inlet
T_{11}	$m_{11} = m_9$	Heat pump inlet
T_h	h_7	Thermal storage (hot)
T_c	h_6	Thermal storage (cold)

The reason behind this choice is to decouple the heat pump and boiler from the heating demand of the building which is provided by the thermal storage. In this way the boiler and heat pump could work most of their operating time at maximum efficiency to charge the thermal storage.

Both heat pump and boiler can operate in modulating mode, i.e. they operate with a given set point for the supply temperature so that both heating capacity and the mass flow rate supplied to the storage vary according to the value of the return temperature, assuming equal temperature at the storage bottom.

From Figure 2.1.1 can be also noticed a recirculation of the water coming out from the building, in this way it is possible to accurately control the building inlet temperature T_1 under the assumption that the overall mass flow rate m_1 will be constant.

In summary, the independent control variables for the system are $\dot{m}_8$, $\dot{m}_{10}$ and $\dot{m}_5$, where the first one is the inlet mass flow rate from the boiler, the second one is the inlet mass flow rate from the heat pump and the third one is the outlet mass flow rate going to the mixer from the thermal storage to regulate T_1.

2.2 Building model

A realistic representation of the building dynamics is critical for the results to be meaningful. There are many different approaches with different levels of accuracy [10], mainly depending on the number of dynamic states and controls, ranging from dynamic simulations

accounting perfectly for the thermal behavior of each room in the building, such as TRSYNS, to low order models able to represent just the global behavior of the building, such as lumped RC approaches. For this application a three parameter lumped RC thermal model has been used [6] and all the parameters have been found using identification method starting from measured data, since the main goal was to understand the global thermal behavior of the building while minimizing the utilized number of dynamic states. A sketch of the building model is reported in Figure 2.2.1.

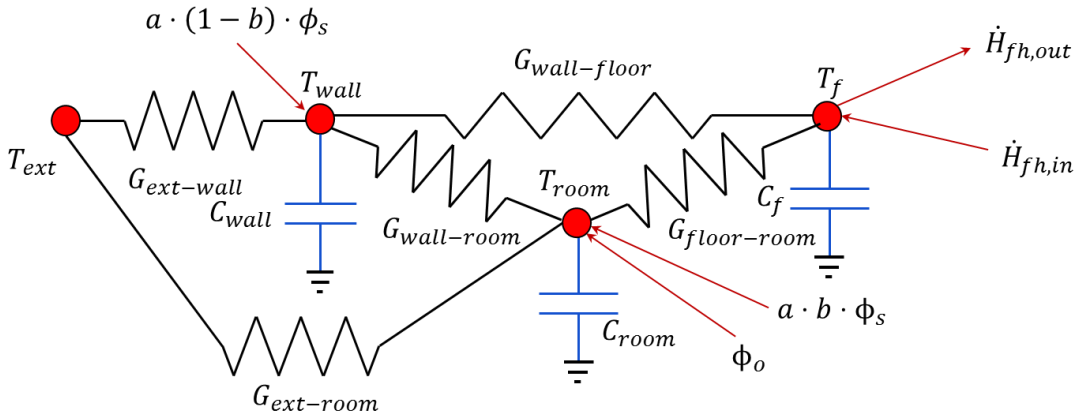

Figure 2.2.1 Building lumped parameters scheme

The model has one control variable the input enthalpy $\dot{H}_{fh,in}$ of water flowing in the floor heating system, $\dot{H}_{fh,out}$ is the enthalpy of water flowing out from the building. Three disturbances, the solar global irradiance, ϕ_r, the heat generation provided by the occupants and the internal supplies, ϕ_o, and the external temperature, T_{ext}.

There are three state variables, named T_r, T_f and T_w, which represent respectively the indoor air temperature, the floor temperature and the external walls temperature. Each state variable is associated with the corresponding heat capacity, namely C_r, C_f and C_w.

Each term G_{xy} represents the thermal conductance between temperatures T_x and T_y.

ϕ_o is the heat gain according to occupancy profile, and is based on a constant heat production coefficient per person according to the ISO 7730, the heat gain is reported in Figure 2.2.2.

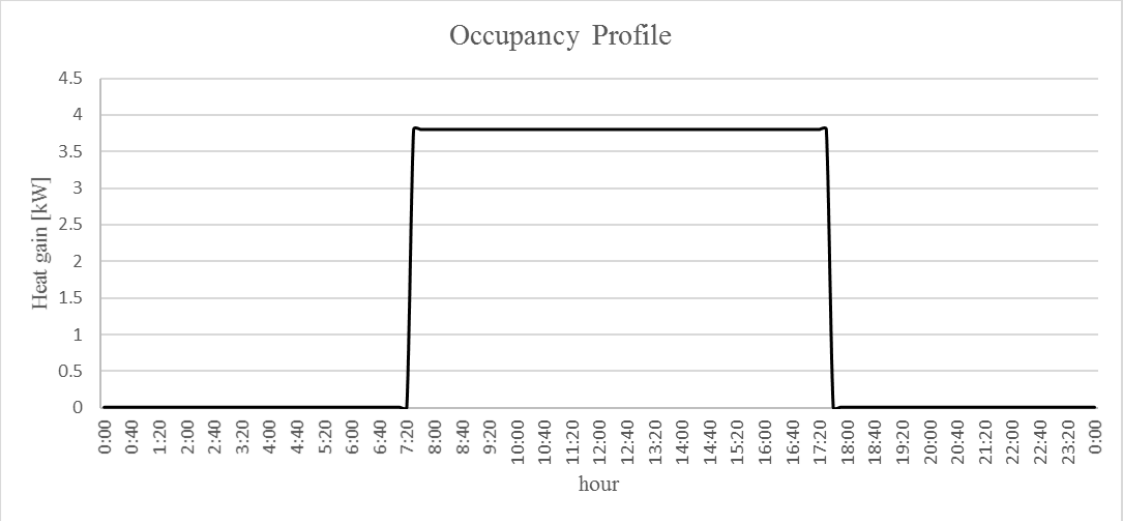

Figure 2.2.2 Occupancy profile

The parameter ***a*** is used to scale the solar radiation, taking into account the average shadowing and inclination of the sun during the day, while ***b*** divides the solar contribution between the wall and the room temperature. Ideally this parameter represents the portion of radiation passing through the windows heating up the room. The main assumption, which supports the last statement, is that the thermal input entering the windows, is completely reflected by the floor into the room space.

The net heat transfer rate flowing in the floor heating can be defined as the difference between inlet and outlet enthalpies as in ((2.4.1.1):

$$\dot{Q}_{fh,net} = \dot{H}_{fh,in} - \dot{H}_{fh,out} = \dot{m}_1 \cdot c_w \cdot (T_1 - T_2) \tag{2.4.1.1}$$

Where $c_w \left[\frac{kJ}{kg \cdot K}\right]$ is the water specific heat and $\dot{m}_1 \left[\frac{kg}{s}\right]$ is the total mass rate in the building given by the mass balance at the recirculation valve in (2.4.1.2):

$$\dot{m}_1 = \dot{m}_5 + \dot{m}_3 \tag{2.4.1.2}$$

It is worth mentioning that $\dot{m}_1 = 1.8 \left[\frac{kg}{s}\right]$ is a constant value defined by the size of the pipes in the floor heating system. T_1 can be also found from the energy balance at the recirculation valve under the hypothesis of constant water properties due to low operating temperature, obtaining the following expression (2.4.1.3):

$$T_1 = \frac{\dot{m}_5 T_5 + \dot{m}_3 T_2}{m_1} \tag{2.4.1.3}$$

Another important assumption, is the relation between T_2 and the other variables.

Under the assumption that the floor heating is working in a limited range of temperature and the flow inside the pipe is fully developed the following expression was derived:

$$T_2 = \alpha \cdot T_1 + (1 - \alpha) \cdot T_f \quad 0 < \alpha < 1 \tag{2.4.1.4}$$

As we already mentioned all the lumped parameters have been found using identification method [6]. They provide a good representation of the overall behavior of the building, but it is impossible to have detailed information about temperatures of single rooms or temperature distribution in the wall, in particular the temperatures considered are weighted averages of the real temperature distributions present in the building. It is also worth noticing that the model reflects the real dynamics of the building only for values of disturbances, states and controls similar to the experimental data used to train the parameters. Since the data belongs to a January two week period, the model should be valid for the heating season, but not for cooling. In Figure 2.2.3 are reported the temperature profiles from experimental data and the ones derived by the model for a two weeks period in March:

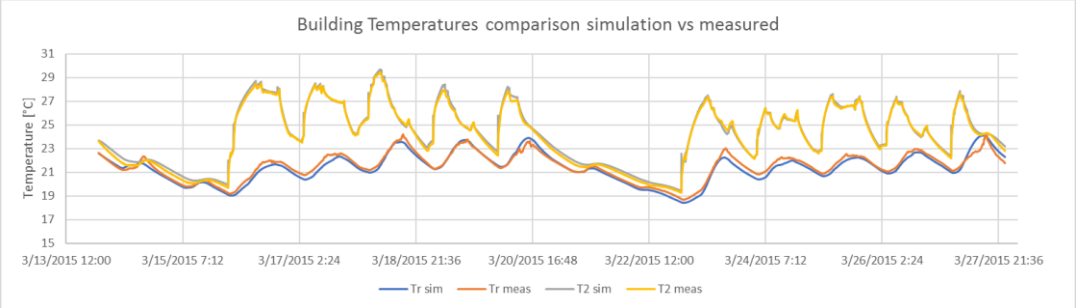

Figure 2.2.3 Building temperature profiles comparison simulation vs measured

After the model validation the dynamic states equations are reported:

$$C_f \frac{dT_f}{dt} = -\left(G_{fr} + G_{fw} + \dot{m}_{tot} c_w (1 - \alpha)\right) T_f + G_{fr} T_r + G_{fw} T_w + \dot{m}_{tot} c_w (1 - \alpha) T_1 \tag{2.4.1.5}$$

$$C_r \frac{dT_r}{dt} = -\left(G_{rf} + G_{rw} + G_{re}\right) T_r + G_{rf} T_f + G_{rw} T_w + \phi_o + ab\phi_r + G_{re} T_{ext} \tag{2.4.1.6}$$

$$C_w \frac{dT_w}{dt} = -\left(G_{wf} + G_{wf} + G_{we}\right) T_w + G_{wf} T_f + G_{wr} T_r + a(1 - b)\phi_r + G_{we} T_{ext} \tag{2.4.1.7}$$

The values of the constant parameters are reported in Table 2.4.1.1:

Table 2.4.1.1 Building parameters from identification

Parameters			Cr	120761.412	[kJ/K]
Gfr	2.578	[kW/K]	Cw	463441.674	[kJ/K]
Gfw	1.663	[kW/K]	a	0.727	\
Grw	4.131	[kW/K]	b	0.618	\
Gwe	1.241	[kW/K]	alpha	0.1759	\
Gre	0.612	[kW/K]	Area	500	m^2
Cf	73322.258	[kJ/K]	m1	1.8	[kg/s]

Considering the physical meaning of these parameters, it is important to remember that a lumped approach was used, so for example the heat capacity associated with the air in room can be affected by the mass of the building furniture. Furthermore is really difficult to estimate the interface between external wall and air, since composition and the temperature profile of the internal wall is unknown, therefore there could be a slight shift in the conductance G_{rw} and G_{we}.

2.3 Thermal Storage

The thermal energy storage allows to decouple the building energy demand from the heat pump and boiler. Thanks to this shift the heat pump can work when the COP is higher and when the price of electricity is lower to charge the thermal storage.
The most common way to model a thermal storage is by using a stratified approach [11], in Figure 2.3.1 a simple scheme for the stratified thermal storage is shown:

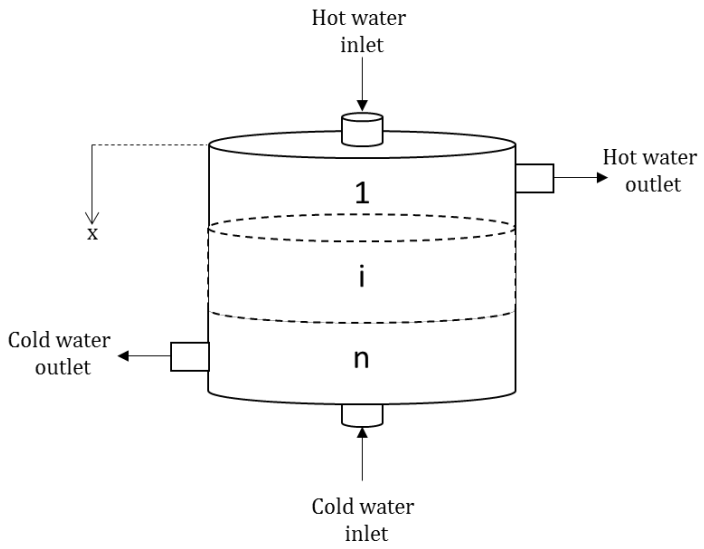

Figure 2.3.1 Stratified thermal storage tank scheme

Each layer represents a mass of water at constant temperature, increasing the number of layers allows to have a more accurate representation of the temperature profile inside the

thermal storage. This means increasing the number of dynamic states, for this application a trade off between number of states and accuracy of the model lead to a two layers model, in which the size of the layers is variable and based on the mass balance of the top and bottom portion of the storage. Since the temperature difference between inlet and outlet of the floor heating must be around $\Delta T_{in-out} \approx 10[°C]$, the ΔT inside the thermal storage will not be high. Because of this and because of the low mass flow rate $\dot{m}_5$ with respect to the total amount of water stored, the destratification due to mixing and natural convection between the two layers was neglected.

The heat loss to the surroundings was considered by using a global heat exchange coefficient that accounts also for the thermal bridges at inlets and outlets of the thermal storage. A schematic representation of the thermal storage is reported in Figure 2.3.2:

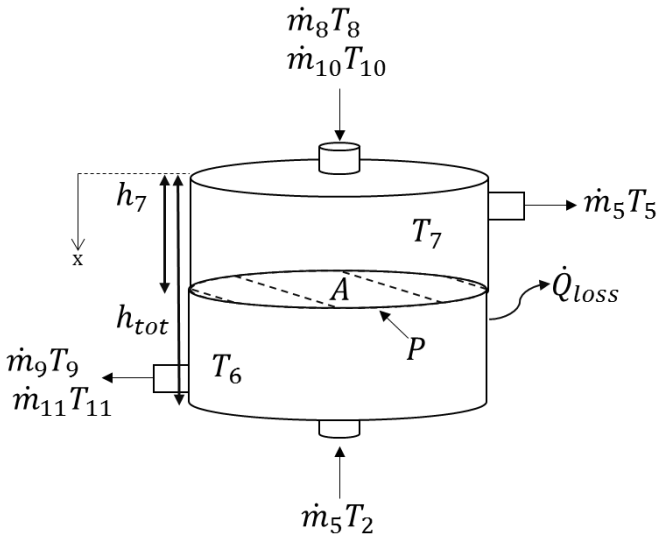

Figure 2.3.2 Schematic representation of the thermal storage with parameters

The dynamic states in this model are h_7,T_7 and T_6, which are respectively the height of the hot water stored in the tank, the temperature of the hot water in the tank and the temperature of the cold water in the tank.

$\dot{M}_9$and $\dot{m}_{11}$ are the outlet mass flow rates from the thermal storage to the boiler and the heat pump respectively, and they are equal to $\dot{m}_8$ and $\dot{m}_{10}$ for the mass balance.

T_9 and T_{11} are the cold outlet temperatures from the thermal storage to the boiler and heat pump, and in this case since there are just two layers, they are also equal. From (2.4.1.6) can be seen that T_9 and T_{11} are the result of the adiabatic mixing between cold water and hot water in the tank depending on the level of h_7. The same can be said for T_5 being the temperature of the hot water at the outlet of the thermal storage.

T_8 and T_{10} are the inlet temperature into hot part of the thermal storage. In order to keep the mathematical complexity as low as possible, the heat pump and boiler are assumed to operate at constant temperature difference $\Delta T = 10$ [°C], therefore T_8 and T_{10} can be defined as:

$$T_8 = T_{10} = T_9 + \Delta T \tag{2.4.1.1}$$

The reason behind this assumption is that in this way the thermal storage will operate with a ΔT of around 10 [°C] , However there is a limit on the maximum temperature allowed in the thermal storage $T_{7max} = 45$[°C].

Lastly the expression of $\dot{Q}_{loss}$ is reported in (2.4.1.2).

$$\dot{Q}_{loss} = UPh_7(T_7 - T_{amb}) + UP(h_{tot} - h_7)(T_6 - T_{amb}) \tag{2.4.1.2}$$

Where $U\left[\frac{kW}{m}\right]$ is the constant heat exchange coefficient, P[m] is the perimeter and h_{tot}[m] is the total height of the thermal storage and A[m^2] is the cross area of the thermal storage. These parameters were taken from ZANI SPA datasheet [12].

A further step to develop the model is to consider the outlets of the thermal storage in the two particular cases when the storage is nearly fully charged and nearly empty. In particular by taking a look at the Figure 2.3.3

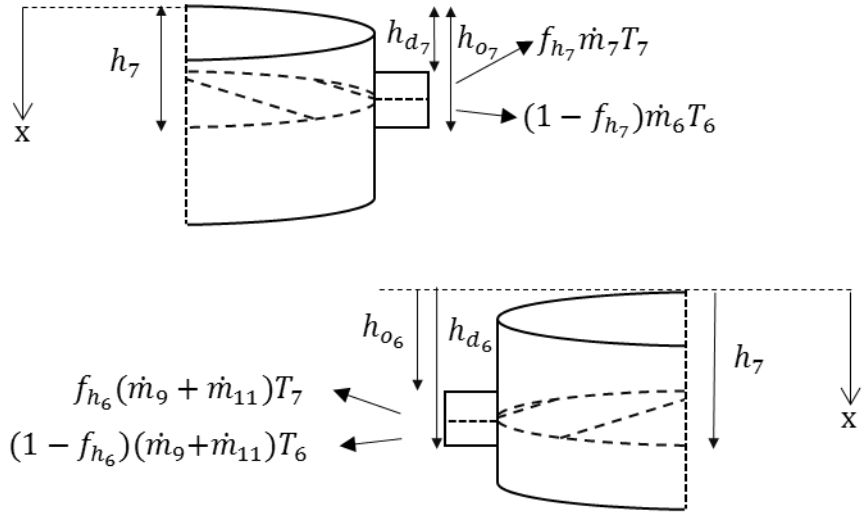

Figure 2.3.3 Detail of thermal storage outlets

The heights $h_{d_7}$and h_{o_7} represents respectively the height of dead volume and the height of the dead height plus the diameter of the outlet for the hot side. The height $h_{o_6}$and the difference between h_{d_6} and h_{tot} represent instead the dead height of cold water in the thermal storage and the distance between the top and the cold outlet. These parameters were taken from ZANI SPA datasheet [12].

When h_7 is lower than h_{d_7}, the storage is empty and therefore the outlet temperature is T_6, for $h_{d_7} < h_7 < h_{o_7}$ instead the outlet temperature is an adiabatic mixing between the mass flow rate of hot and cold water:

$$T_5 = \frac{f_{h_7} m_7 T_7 + (1 - f_{h_7}) m_6 T_6}{m_5} \tag{2.4.1.3}$$

The coefficient f_{h_7} is the fraction of hot water with respect to the total mass flow rate $\dot{m}_5$ flowing out through the hot outlet, in order to have smooth variation for the optimal controller, a sinusoidal profile described by (2.4.1.4 was chosen:

$$f_{h7} = \begin{cases} 1 & h_7 > h_{o_7} \\ f = \frac{1}{2} + \frac{1}{2}\sin\left(\frac{\pi}{h_{o_7} - h_{d_7}} * (h_7 - h_{d_7}) - \frac{\pi}{2}\right) & h_{d_7} \le h_7 \le h_{o_7} \\ 0 & h_7 < h_{d_7} \end{cases} \tag{2.4.1.4}$$

In Figure 2.3.4 is shown the trend of f_{h_7}

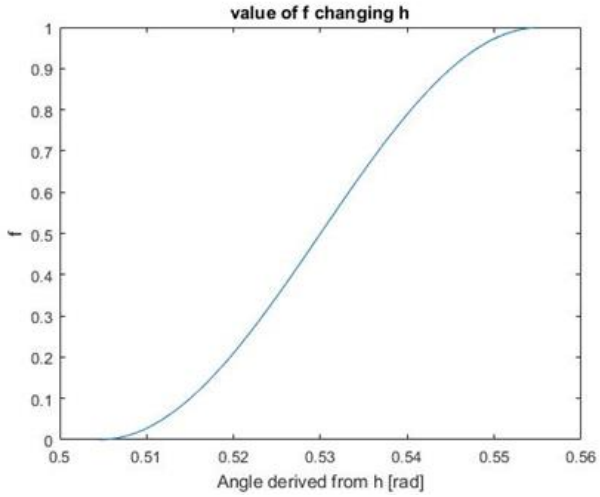

Figure 2.3.4 Trend of the mass flow rate repartition coefficient

The coefficient f_{h_6} is the fraction of hot water with respect to the total mass flow rate $\dot{m}_9 + \dot{m}_{11}$ flowing out through the cold outlet and is defined in a similar fashion to f_{h_7}, leading to the following expression:

$$f_{h6} = \begin{cases} 0 & h_7 < h_{o_6} \\ f = \frac{1}{2} + \frac{1}{2}\sin\left(\frac{\pi}{h_{d_6} - h_{o_6}} * (h_7 - DH_1) - \frac{\pi}{2}\right) & h_{0_6} \le h_7 \le h_{d_6} \\ 1 & h_7 > h_{d_6} \end{cases} \tag{2.4.1.5}$$

The outlet temperatures T_9 and T_{11} are defined according to the (2.4.1.6):

$$T_9 = T_{11} = \frac{f_{h6}(\dot{m}_{11} + \dot{m}_9) T_7 + (1 - f_{h6})(\dot{m}_{11} + \dot{m}_9) T_6}{\dot{m}_7} \tag{2.4.1.6}$$

Finally the equations describing the dynamic states are expressed as follows:

$$\rho_w c_w A_s \frac{dh_7}{dt} = \dot{m}_{10} + \dot{m}_8 - f_{h7}\dot{m}_7 - f_{h6}(\dot{m}_{11} + \dot{m}_9) \quad (2.4.1.7)$$

$$\begin{aligned} \rho_w c_w A_s h_7 \frac{dT_7}{dt} = {} & \dot{m}_8 c_w(T_8) + \dot{m}_{10} c_w(T_{10}) - f_{h7}\dot{m}_7 c_w T_7 \\ & - c_w\big(\dot{m}_{10} + \dot{m}_8 - f_{h7}\dot{m}_7 - f_{h6}(\dot{m}_{11} + \dot{m}_9)\big)T_7 - UPh_7(T_7 - T_{amb}) \\ & - f_{h6} c_w(\dot{m}_{11} + \dot{m}_9)T_7 \end{aligned} \quad (2.4.1.8)$$

$$\begin{aligned} \rho_w c_w A_s (h_{tot} - h_7) \frac{dT_6}{dt} = {} & \dot{m}_7 c_w(T_2) - ((1 - f_{h7})\dot{m}_7 T_6 - (1 - f_{h6})(\dot{m}_{11} + \dot{m}_9))c_w T_6 \\ & -UP(h_{tot} - h_7)(T_6 - T_{amb}) + c_w(\dot{m}_{10} + \dot{m}_8 - f_{h7}\dot{m}_7 \\ & - f_{h6} c\_w \ (\dot{m}_{11} + \dot{m}_9))T_6 \end{aligned} \quad (2.4.1.9)$$

The derivation of these equations can be found in A.1.1. The last important parameter to the define for the model of the thermal storage is the SOC "state of charge" of the thermal storage, it is a dimensionless parameter which gives information on the amount of heat available from the thermal storage with respect to a reference. However the definition is not as simple as in a battery, since heat stored depends on the reference temperature, and heat losses contribute lower this value even when the storage is at rest. Given these premises the SOC is defined in (2.4.1.10)

$$SOC = \frac{Q_{stored}}{Q_{max}} = \frac{\rho_w c_w A_s h_{stored} \Delta T_{stored}}{\rho_w c_w A_s h_{max} \Delta T_{max}} = \frac{\dfrac{h_7(T_7 - T_{ref}) + (h_{tot} - h_7)(T_6 - T_{ref})}{h_{tot}}}{h_{max}(T_{max} - T_{ref})} \quad (2.4.1.10)$$

Where $T_{ref} = 20$ [°C] is equal to the minimum comfort temperature in the building [13], and $T_{max} = 45$ [°C] is the maximum allowed temperature in the thermal storage.

2.4 Air source heat pump and Boiler

2.4.1 Air source heat pump

The heat pump is a key component of the heating system, and therefore its behavior should be modeled as close as possible to reality. In principle, two aspects of the heat pump behavior at different operating temperatures shall be considered: full load heating capacity and COP. However, to simplify the implementation of the control algorithm, a constant full load heating capacity is assumed, based on the consideration that, when a storage is present

in the system, the approximation introduced here does not have an important effect on the overall energy performance of the heat pump.

Therefore the main parameter becomes the COP of the heat pump, which is mainly a complex function of the external temperature T_{ext} and the feed temperature T_{10}, the latter being a function of a state as shown in (2.4.1.1) . With this formulation the cost function used in the optimization problem 3.1 will not be convex and more difficult to solve.

In [14] a comparison was done between simulations employing a $COP(T_{ext}, T_{10})$ and $COP(T_{ext}, \overline{T}_{feed})$ where $\overline{T}_{feed}$ is an average value, and the results show that the solutions are comparable, even if the solution with $COP(T_{ext}, \overline{T}_{feed})$ tends to overestimate the value of the COP in peak power points, so for a high ΔT_{10-11}. That will not be the case in this work, since the value of ΔT_{10-11} is fixed, leading to the decision of adopting a $COP(T_{ext}, \overline{T}_{feed})$, in order to have a convex cost function, with $\overline{T}_{feed} = 40$ [°C].

The expression was derived by extrapolation data from the AERMEC catalogue [15] for a 40[kW] heat pump, and approximated by a three digits polynomial function :

$$COP = COP_0 + a_1 T_{ext} + a_2 T_{ext}^2 + a_3 T_{ext}^3 \qquad (2.4.1.1)$$

In Figure 2.4.1 the measured value of the COP is reported:

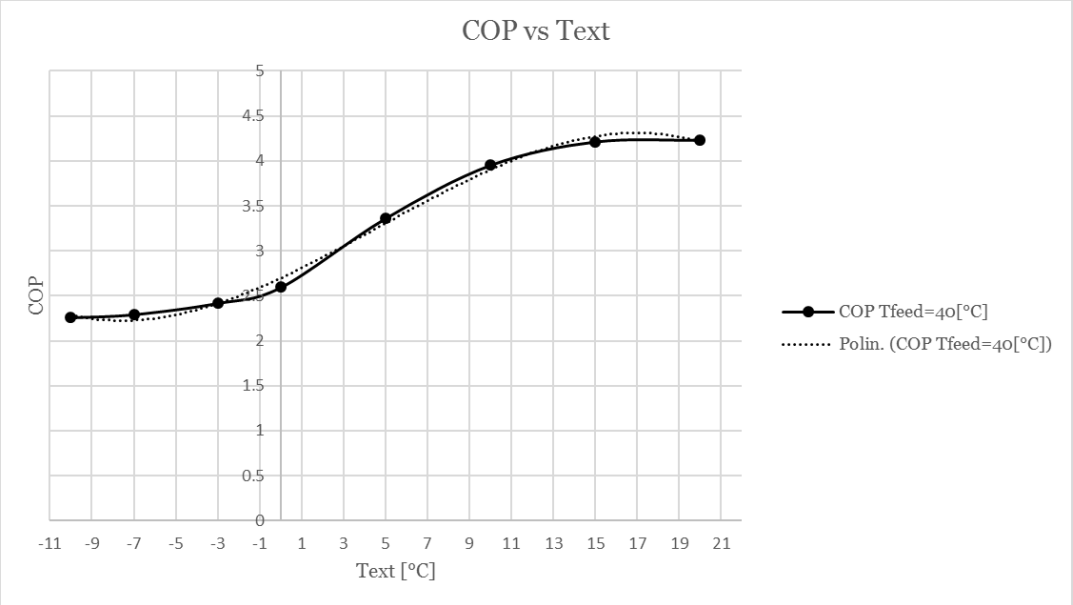

Figure 2.4.1 Plot of measured COP vs polynomial interpolation

2.4.2Boiler

The boiler model is simpler with respect to the heat pump, under the hypothesis of a given $\Delta T_{T_8-T_9} = 10\,[°C]$ an average value for the efficiency η_b was selected starting from the VIESSMAN catalogue [16]

2.5 Electrical configuration

In the cost function (2.6.2.2) appears the net electrical consumption of the building accounting for the consumption of lights, internal equipment, heat pump and the production of the photovoltaic. The electrical configuration in Figure 2.5.1 results trivial considering a steady state operation of the electrical components.

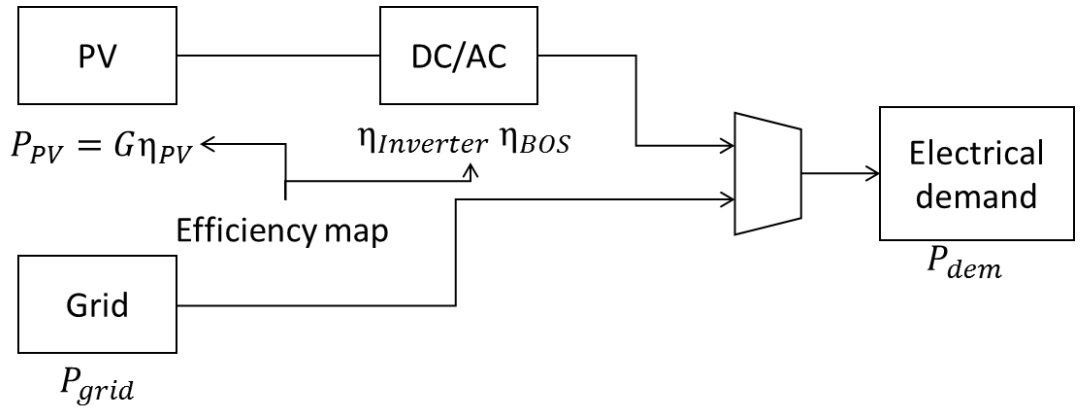

Figure 2.5.1 Electrical configuration

Where P_{PV} is the power generated by the photovoltaic system, η_{PV} its efficiency, $\eta_{Inverter}$ and η_{BOS} the efficiencies of the inverter and balance of system, P_{grid} is the power absorbed from the grid and P_{dem} is the power demand:

$$P_{dem} = \frac{m_{10} c_w \Delta T_{T_{10-11}}}{COP} + P_{build} \qquad (2.4.2.1)$$

Where the first contribution is the electrical power absorbed by the heat pump and the second due to lights and appliances in the building which is modeled after a case study done on north Italian schools [17]. The profiles for a typical working day for different months and a typical weekend are shown in the plot below:

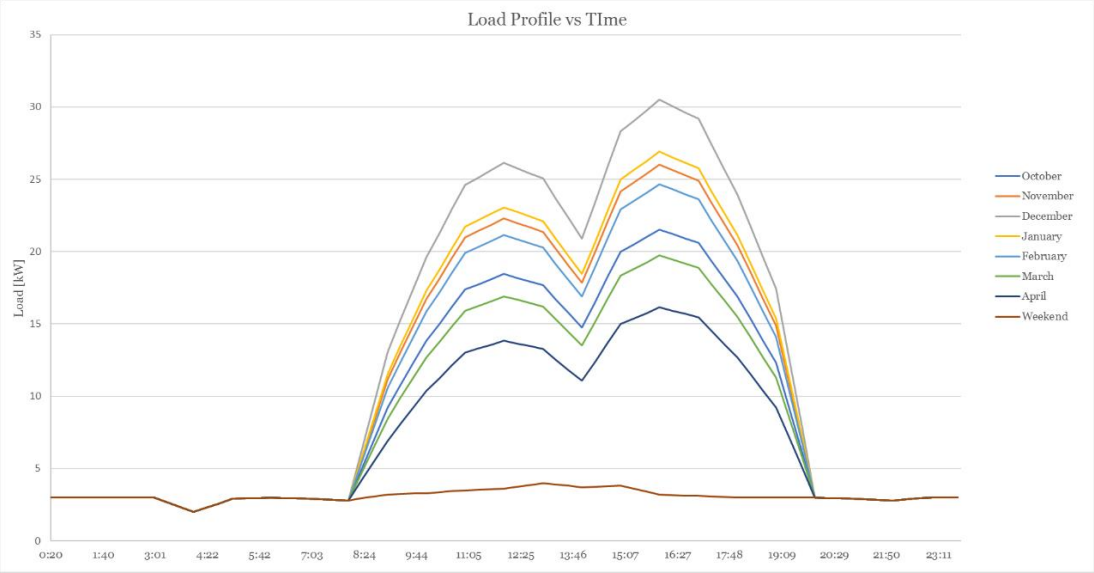

Figure 2.5.2 School lights and appliances load profile

The equation for the electrical balance will be:

$$P_{grid} = P_{dem} - \eta_{Inverter}\eta_{BOS}P_{PV} \qquad (2.4.2.2)$$

It's worth mentioning that P_{grid} can be also negative if the PV power is higher than the demand, meaning that energy is sold to the grid.

2.6 Photovoltaic system

The main component of the PV model are the photovoltaic modules, in particular the Waris WRS250ST60F [18] , with a nominal power of 250[W]. The total nominal power of the PV plant is 35 [kW], sized to fit the peak energy demand of the building lights, internal equipment and heat pump. Consequently a suitable 35 [kW] inverter from Adavanced Energy [19] was chosen.

2.6.1 Roof orientation and solar radiation

By taking a look at the school blueprint, only a portion of the roof is south oriented and suitable for installing the modules.

Accounting for environmental factors, the shadowing from landscape obstructions can be neglected during the whole year since in front of the roof is present a park and farm fields. The value of albedo is strongly affected by the environment nearby the installation site, in this case

the school is located close to the countryside and accordingly with the regulation UNI 8477, an average value of 0.15 was chosen.
In Figure 2.6.1 the average daily irradiation for the heating season is reported, the global horizontal radiation was taken from Arpa Lombardia website [20], and all the sun coordinates, δ, En, ts, ω, ϑsz, γs, ψs, θs, where calculated with a timespan of 20 minutes.

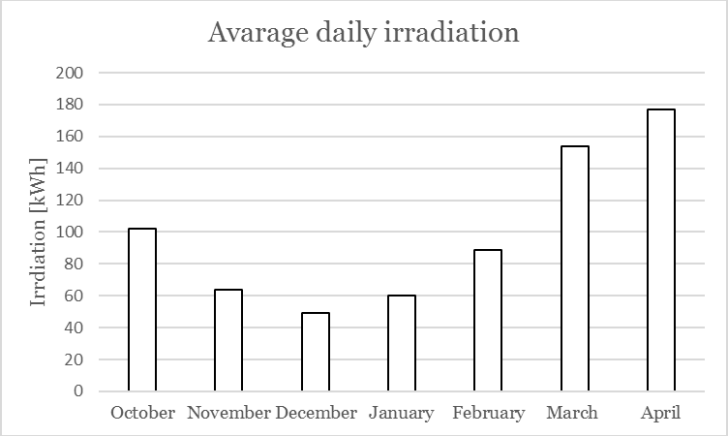

Figure 2.6.1 Average daily irradiation

2.6.2Modules and Inverter

As shown in Figure 2.6.1 the average irradiation in Zibido is not very high, this lead to the choice of the modules [18] that have an average efficiency but are cheaper. According to the measures of the roof, and the nominal power required a total of 140 modules were considered couple with the inverter reported in [19]. Once defined the inverter, the matching analysis was performed in order to check if all the voltage and current limits were respected. Assuming a minimum cell temperature of -10°C and a maximum one of 70°C, according with the regulations, the corrected parameters in terms of V_{oc}, open circuit voltage, I_{sc} , short circuit current e V_{mpp}, maximum power point voltage, have been calculated, through these equations

$$\begin{aligned} Voc\ (Tc,min) &= Voc,ref + [(Tc,min - Tc,ref) \cdot \beta] \\ V_{MPP}\ (Tc,min) &= V_{MPP,ref} + [(Tc,min - Tc,ref) \cdot \beta] \\ V_{MPP}\ (Tc,max) &= V_{MPP,ref} + [(Tc,max - Tc,ref) \cdot \beta] \\ Isc\ (Tc,max) &= Isc,ref + [(Tc,max - Tc,ref) \cdot \alpha] \end{aligned} \qquad (2.6.2.1)$$

Where X_{ref} stands for the reference value X_{min} stands for the minimum value and X_{max} stand for the maximum value. The parameters $\beta \left[\frac{A}{°C}\right]$ and $\alpha \left[\frac{A}{°C}\right]$ are the coefficients of temperature for the voltage and current respectively taken from Waris datasheet [18].
The power of the inverter must be in the range of 80%-110% of the PV system, in this case the two nominal powers are exactly the same, then the number of strings in parallel and the number of modules in series in each string was checked.

For the maximum number of strings in parallel, the limiting parameters is the maximum current acceptable by the MPPT system, because the overall currant is the sum of the currents flowing in each string and the test is done considering the maximum current flowing in every string, which is the I_{sc} when the temperature is the highest:

$$Max\ n°\ of\ strings\ for\ each\ MPPT = \frac{Imax, inv_{(MPPT)}}{Isc\ (Tc, max)} = 14 \qquad (2.6.2.2)$$

For the maximum number of modules in each string, the limiting parameter is the maximum voltage acceptable by the inverter, because, for the series disposition, the overall voltage is the sum of the voltages of each module and the test is done considering the maximum voltage on the module, which is V_{oc} when the temperature is the lowest

$$Max\ n°\ of\ modules\ per\ string = \frac{Vmax, inv}{Voc\ (Tc, min)} = 13 \qquad (2.6.2.3)$$

The extreme MPPT values represent the range of useful voltage and current in order to make the system able to seek the maximum power operating point, so it is important for the maximum power point voltage and current to be in this range:

$$\begin{aligned} V_{OC}(Tc, min)_{str} &= V_{OC}\ (Tc, min) \cdot n°_{mod\ x\ string} \leq V_{max,inv} \\ I_{SC}(Tc, max)_{inv} &= I_{SC}\ (Tc, max) \cdot n°_{strings} \leq I_{max,inv} \end{aligned} \qquad (2.6.2.4)$$

In this case 14 modules per string and 10 strings were chosen in order to achieve 35[kW] of nominal power. In the Table 2.6.2.1 are reported the final values for the calculations and every checked parameter results in within the appropriate range.

Table 2.6.2.1 Inverter-photovoltaic matching check

Vmax_string (-10°C) [V]	482.6892	<595
Vmin_string (70°C) [V]	335.8796	> 295
Vmax_open circuit (-10°C) [V]	590.9092	< 600
Imax [A]	92.3635	< 125

3 OPTIMAL CONTROL PROBLEM

3.1 Optimal control problem formulation

Optimal control deals with problems in which a time variable control u(t) is chosen for a dynamic system x(t) such that a certain optimality criterion is met under certain boundary conditions and constraints on dynamic states and controls. The criterion is the cost function J associated with the optimal control problem. The general formulation for J can be expressed as in

$$J(t) = h(x(t), t) + \int_{t_0}^{t_f} g(x(t), u(t), t)\, dt \tag{2.6.2.1}$$

Where g(x(t), u(t), t) is a function of states and controls and h(x(t), t) is the terminal cost.
The objective of the optimal controller in this problem is to minimize the energy consumption of the building while ensuring a minimum level of thermal comfort inside the building. In [14] is reported a way to put together the energy consumption and the discomfort, by starting from that formulation and adapting it to this case we obtain the two cost functions:

$$J_{en}(t) = C_{elec}(t) \cdot \left(\frac{\dot{m}_{hp} \cdot c_w \cdot (\Delta T)}{COP(T_{ext})} + P_{building} - P_{pv} \right)^{+} + C_{feed_{in}} \cdot \left(\frac{\dot{m}_{hp} \cdot c_w \cdot (\Delta T)}{COP(T_{ext})} + P_{building} - P_{pv} \right)^{-} + \frac{C_{ng} \cdot \dot{m}_b \cdot c_w \cdot (\Delta T)}{\eta_{th}} \tag{2.6.2.2}$$

Where the first term represents the maximum between zero and the electrical balance of the building multiplied by the cost of the electricity C_{elec} $\left[\frac{€}{kWh}\right]$, the second term represents the minimum between zero and the electric balance of the building multiplied by the feed-in tariff $C_{feed_{in}}$ $\left[\frac{€}{kWh}\right]$ and the last term represents the boiler power multiplied by the cost of natural gas C_{ng}. A better explanation for this prices is shown in B.1.1.
The discomfort cost function instead is defined as:

$$J_{dis}(t) = W_{en-dis}\left(\frac{\phi_o(t)}{\phi_{o_n}}\right)\left(T_r - T_{ref}\right)^2 \quad (2.6.2.3)$$

Where T_r is the room temperature, $T_{ref} = 21$ [°C] is the room reference temperature, $\left(\frac{\phi_o(t)}{\phi_{o_n}}\right)$ is the ratio between the occupancy heat gain rate and it's nominal value of 3.8 [kW] and W_{en-dis} is a constant weight that converts the units of the discomfort [K^2h] in price units [€], an explanation on the derivation of this parameter can be found in A.1.2.

Finally the expression for the total cost function is shown:

$$min\, J_{tot}(t) = \int_{t_0}^{t_f} [kJ_{en}(t) + (1-k)J_{dis}(t)]dt \quad (2.6.2.4)$$

k is a parameter which ranges $0 < k < 1$ that expresses how much the cost function accounts for the energy contribution and the discomfort contribution, for $k = 1$, the cost function minimizes just the energy consumption, while for $k = 0$ only the discomfort will be minimized. Secondly the boundaries and the constraints on the states and control must be introduced:

$$\begin{aligned}
&\overline{h_7}(t_0) = \overline{h_7}(t_f)\\
&0.15\ [m] = h_{7_{min}} < h_7 < h_{7_{max}} = 2.7\ [m]\\
&0 < m_5 < m_1 = 1.8\ \left[\frac{kg}{s}\right]\\
&0 < m_{hp} < m_{hp_{max}} = 0.9\left[\frac{kg}{s}\right]\\
&0 < m_b < m_{b_{max}} = 0.9\left[\frac{kg}{s}\right]\\
&0 < T_7 < T_{7_{max}} = 45\ [°C]\\
&0 < T_6 < T_{6_{max}} = 35\ [°C]
\end{aligned} \quad (2.6.2.5)$$

The only boundary condition on this problem is set on the height h_7 where the initial value should be equal to the final value. The values of the parameters are determined from the physical model, in particular $\dot{m}_5$ can not be higher than the maximum mass flow rate in the building, the maximum mass flow rates of the heat pump $\dot{m}_{hp}$ and boiler $\dot{m}_{b_{max}}$ are calculated based on the maximum power of the boiler and the heat pump accordingly with the physical model and the height has to stay between the dead volumes of the thermal storage.

3.2 Optimal control problem solving

Once the dynamic system, the cost function, boundaries and constraints are defined, a suitable methodology to solve the optimal control problem in a reasonable amount of time has

to be applied. Many approaches are possible, for example DP “Dynamic Programming”, PMP “Pontryagin’s Minimum Principle” and converting the optimal control problem into a CNLP “Constrained Non Linear Programming” problem.

Dynamic programming guarantees the global optimum, however is subjected to Bellman’s curse of dimensionality, meaning that the computational time increases exponentially with the number of states in the dynamic system.

PMP converts the optimal control problem from the dynamic system, cost function and constraints form into a boundary value problem, with this mathematical formulation is possible to express a necessary condition for optimality on the controls allowing a faster speed convergence with respect to DP, however is not trivial to apply constraints on the controls using this approach, find the guesses for parameters which are not physical and the global optimum is not guaranteed.

The last and chosen method belongs to the so called “direct” methods, there are many ways to convert an optimal control problem into a CNLP problem, in TOMLAB PROPT [21] environment for MATLAB, Chebyshev [22] pseudo spectral collocation method is employed. The general approach of a pseudo spectral technique consists of converting the time continuous optimal control problem into a discrete time problem, a more detailed description is given in A.1.3. Once the optimal control problem is converted to a CNLP problem, PROPT uses the solver SNOPT [23] , which uses a SQP “Sequential Quadratic Programming” method to solve the CNLP problem, a more detailed explanation is reported in A.1.4.

Using this approach does not guarantee the global optimum unless the optimizing function is quite smooth in the first derivative, in the considered problem it can not be ensured that the function is smooth, however the solution found will be reasonably close to the optimal solution, furthermore usually to check if the global optimum is reached different initial conditions for the same problem should be tested. However in the considered problem, changing the initial conditions will change the nature of the problem, starting for example from a high SOC “State Of Charge” or a low SOC of the thermal storage will affect the way the controller has to operate the heat pump and the boiler in order to achieve the minimum thermal discomfort, leading to a different energy performance.

To keep in check this possibility the solution trends by changing the parameter k were checked and see if they respected what was expected.

3.3 Rule based controller design

In order to the have a reference for the solution obtained by the optimal controller a simple rule based controller was designed. The main objective of the rule base controller is to ensure thermal comfort to the people inside the building. To do so the dynamic model of the building, the heating system and the controller were designed in MATLAB environment.

3.3.1 Measures and set points

Considering the heating system reported in and the building scheme in Figure 2.2.1 the controller will have to check the temperature of the room T_r and the mean temperature in thermal storage T_m which is defined as:

$$T_m = \frac{T_7 h_7 + T_6(h_{tot} - h_7)}{h_{tot}} \tag{3.3.1.1}$$

Which is equivalent to the adiabatic mixing temperature inside the thermal storage.
The set-point of T_r is defined as in the following figure:

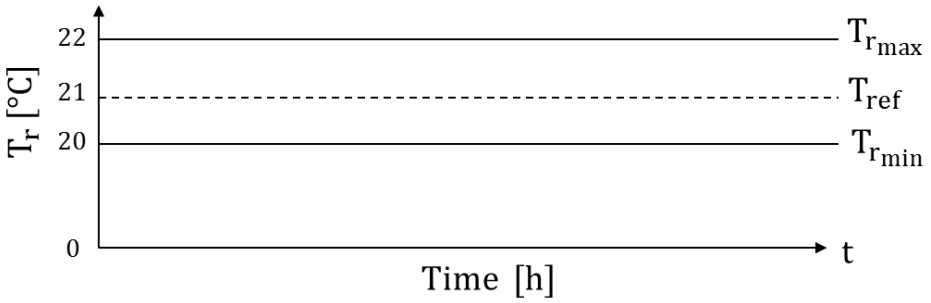

Figure 3.3.1 Room set point temperature definition

The set point will be $T_{ref} \pm \Delta T_r$ where $\Delta T_r = 1$ [°C], in accordance with the regulations [13] and [24], furthermore depending on the month considered, when there are no people in the building a set point on $T_{r_{min}} \pm \Delta T_r$ was introduced, to prevent the room temperature from dropping during the night or in the weekends, the values are reported in Table 3.3.3.1 .
The temperature T_m instead has to stay in between the minimum $T_{m_{min}}$ and maximum $T_{m_{max}}$ allowed temperatures in the storage, which are defined as:

$$T_{m_{min}} = \frac{T_{7_{min}} h_{7_{min}} + T_{6_{min}}(h_{tot} - h_{7_{min}})}{h_{tot}} \tag{3.3.1.2}$$

$$T_{m_{max}} = \frac{T_{7_{max}} h_{7_{max}} + T_{6_{max}}(h_{tot} - h_{7_{max}})}{h_{tot}}$$

Where the heights limits $h_{7_{min}}$ and $h_{7_{max}}$ are the physical limits for the dead volumes inside the thermal storage, while $T_{7_{min}} = 35[°C]$ and $T_{7_{max}} = 45[°C]$ are the minimum and maximum temperature allowed in the thermal storage, $T_{6_{min}} = 25[°C]$ and $T_{6_{max}} = 35[°C]$.$T_{m_{max}}$ was however slightly changed depending on the considered month, to avoid excessive recirculation of hot water in the thermal storage in the heat pump and boiler.

3.3.2 Controls and control actions

Considering the heating system reported in chapter 2, in order to satisfy the set points the controller will have to control the inlet temperature in the building T_1 for the room temperature, the heat pump and boiler mass flow rates $\dot{m}_{10}$ and $\dot{m}_8$ to charge the thermal storage tank.

The control of T_1 defined in (2.4.1.3) is determined by the opening of the three way valve v_1, where there is an adiabatic mixing between the hot water $\dot{m}_5$ at T_5 defined in (2.4.1.3) coming from thermal storage and the recirculation cold water $\dot{m}_2$ at T_2 defined in (2.4.1.4) from the floor heating outlet. A climatic curve is used to determine the value of T_1 depending on the value of the external temperature, which is reported in Figure 3.3.2

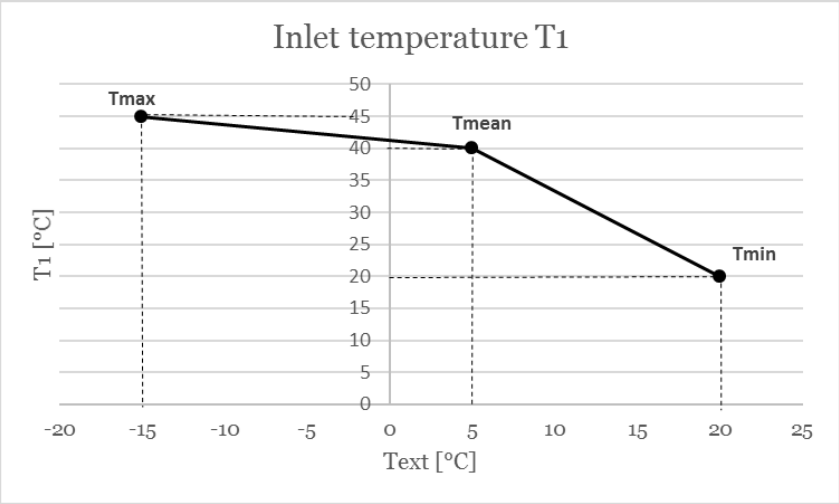

Figure 3.3.2 Climatic curve rule based controller

The maximum temperature T_{max} was determined by considering no recirculation from the building outlet, $\dot{m}_5 = \dot{m}_1$ and the maximum temperature allowed in thermal storage for the coldest day of the year. T_{min} corresponds to the value at which the heating system stops working, when $T_{ext} = 20$ [°C] equal to the minimum thermal comfort temperature. T_{mean} was

determined by tuning the rule based controller during the heating season, by finding a trade off between the discomfort due to the temperatures lower than $T_{r_{min}}$ in the colder months and discomfort due to the temperatures higher than $T_{r_{max}}$ in the hotter months. Moreover to achieve thermal comfort in the occupied period from 7:30 to 17:30, the heating system has to start working earlier, especially on Monday morning after the weekend, depending on the month considered the controller was properly tuned, starting earlier in colder months and later in hotter ones.

The control of the heat pump and boiler, acts on the inverter of the respective circulating pumps to change the values of $\dot{m}_{10}$ and $\dot{m}_{8}$, while the temperature T_{10} and T_{8} are determined as described in 2.4. However since the heating demand from the building is decoupled by the thermal storage, the heat pump and boiler will always work at their nominal powers to charge the thermal storage. Two control strategies for heat pump and boiler were tested, the first one consists of not giving priority to heat pump and boiler, so they will both work at their nominal power to fill the thermal storage, in the second operating mode priority is given to the heat pump and the boiler is switched on only if T_{mean} goes below a certain threshold plus a certain $\Delta T_{mean} = 2[°C]$.

3.3.3 Controller tuning and results

The parameters that needed to be tuned and the relative values are reported in
Table 3.3.3.1

Table 3.3.3.1 Tuning parameters rule based controller

	RBC			**RBCseq**			
	adv-work [h]	adv-weekend [h]	Tmin [°C]	adv-work [h]	adv-weekend [h]	Tmin [°C]	Tmean boiler [°C]
October	3	7	17.5	3	7	17.5	35
November	5	7	18	5	7	18	35
December	5	7	18.5	5	7	18.5	37
January	5	7	18.5	5	7	18.5	37
February	5	7	18	5	7	18.5	37
March	4	7	18	4	7	18	35
April	3	7	17.5	3	7	17.5	35

The first columns of each controller represent how many hours earlier the heating system will be started before people will are in the building, the second columns report the same anticipation but for Monday. The third columns show the minimum temperature at which the building is kept throughout the week to achieve thermal comfort. The fourth column $T_{mean_{boiler}}$ shows the temperature at which the boiler starts to charge the storage in the case of the sequential rule based controller.

To further check the good operating conditions of the rule based controller from a thermal comfort perspective, the scatter plot reported in Figure 3.3.3 for the normal RBC and Figure

3.3.4 for the sequential RBC show the trend of the room temperature depending on external temperature T_{ext} [°C] and the solar radiation hitting the building $G\ \left[\frac{kW}{m^2}\right]$ throughout the whole heating season. Plots for each temperature band are available in appendix C.1.1.

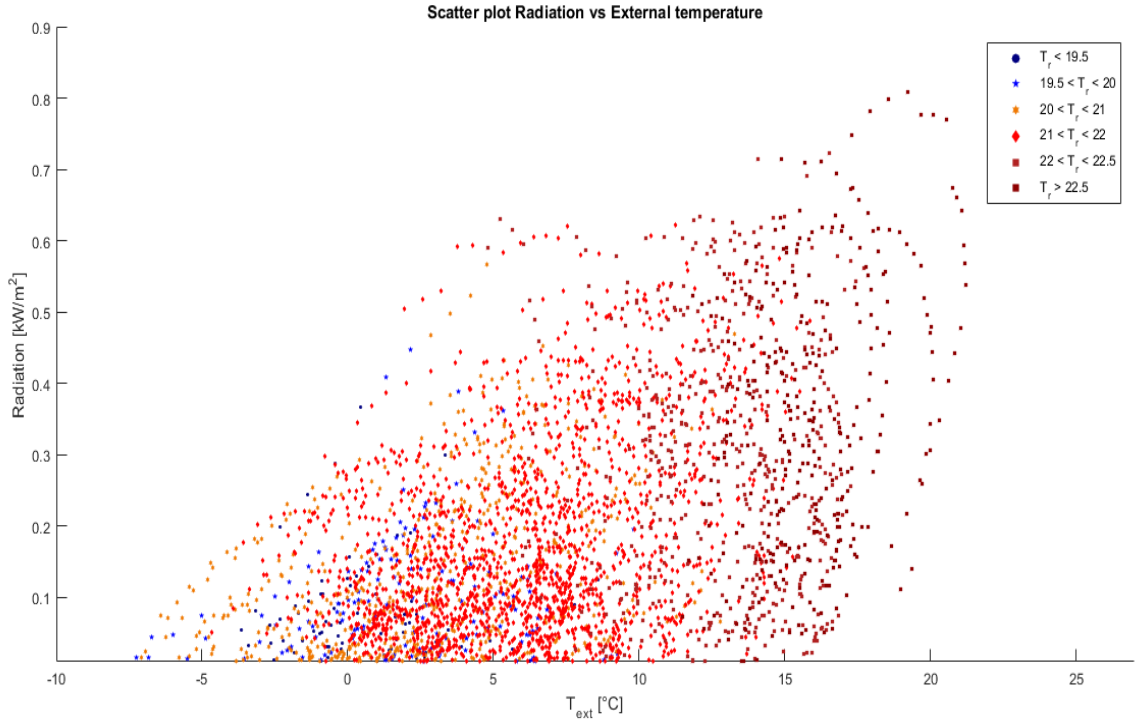

Figure 3.3.3 Rule based control scatter plot

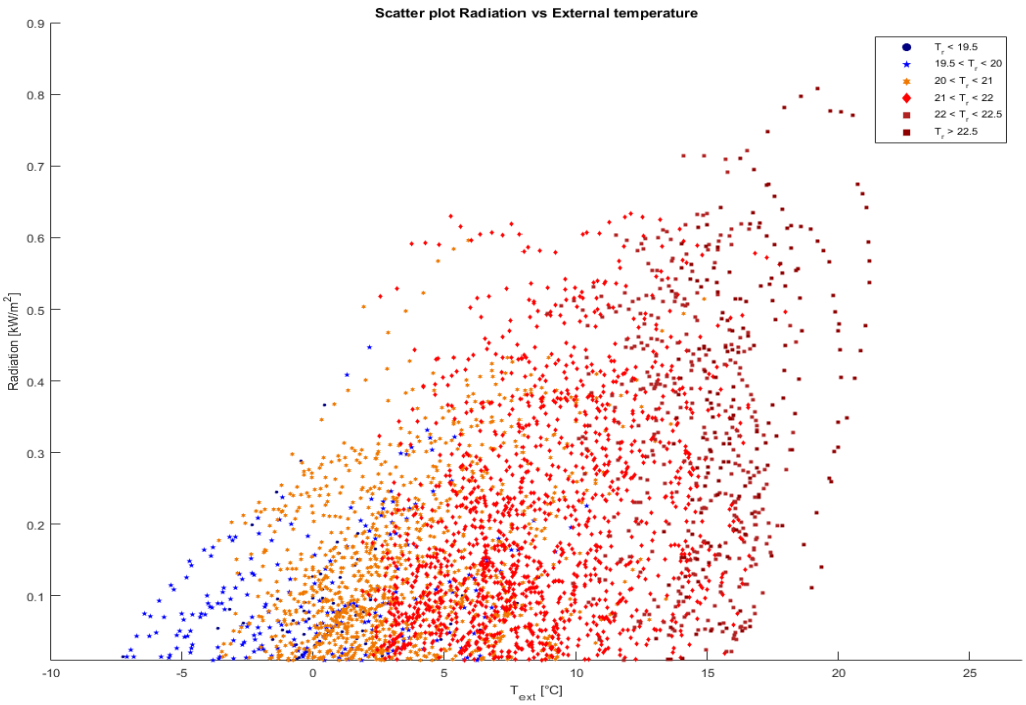

Figure 3.3.4 Sequential rule based controller scatter plot

In Table 3.3.3.2 the results for each room temperature level considering all the working hours of the heating season are reported

Table 3.3.3.2 Room temperatures levels

Room Temperature [°C]	[h] RBC	%	[h] RBCseq	%
Tr < 19.5	27	2%	21	2%
19.5 < Tr < 20	56	5%	85	7%
20 < Tr <21	230	19%	429	35%
21 < Tr < 22	622	51%	504	41%
22 < Tr < 22.5	175	14%	120	10%
Tr > 22.5	113	9%	63	5%
Total working hours	1223	100%	1223	100%

In the Table 3.3.3.2 and the Figure 3.3.3 can be observed that the winter thermal discomfort due to low temperature is very limited, in fact only the 7% of the total working hours is under 20 [°C] and the 2% under 19.5 [°C]. That is not the case for thermal discomfort due to higher temperature than the threshold 22 [°C] during the warmer days of the heating season in fact up to 23% of the working hours are above the maximum comfort temperature and 9% higher than 22.5 [°C] for the normal RBC. Instead the sequential RBC has a slightly worse performance in winter, due to the fact the average inlet temperature in the building is lower in early morning as shown in Figure 4.1.3, but this grants a slightly better performance in the hotter months, preventing the building from overheating.

However both RBCs have the issue of overheating and the reason is that the rule based controller is not able to predict the weather condition for the incoming day, therefore it will switch on the heating system in the morning while measuring a room temperature level lower than the minimum threshold, and when the external temperature and solar radiation increase throughout the day, the building will be heated up above the thermal comfort zone.

Meanwhile the optimal controller has as input disturbances the weather data, and is able to consequently adjust the heat input into the building preventing the room temperature to reach the thermal discomfort as shown in 4.3.2.

4 RESULTS

4.1 Rule based controller results

In this paragraph the results on the performance of the rule based controller and sequential rule based controller for two sample months April and January are reported considering different plots, the other months are available in C.1.3 and C.1.4.
In the first plot the floor temperature T_{floor} , the room temperature T_{room} and the external wall temperature T_{wall} are plotted against the thermal comfort band defined in paragraph 3.3.1, and the occupation heat gain defined in paragraph 2.2. In the second plot the hot and cold temperatures in the storage T_7 and T_6 are reported against the SOC "State of charge" of the thermal storage, defined in (2.4.1.10), and in the fourth plot $\dot{Q}_{in} = G_{fr}(T_f - T_r)$ which is the heat rate provided by the floor heating system to the room, $\dot{Q}_{hp}$ the heat rate provided by the heat pump and $\dot{Q}_b$ the heat rate provided boiler along with the occupation heat gain.

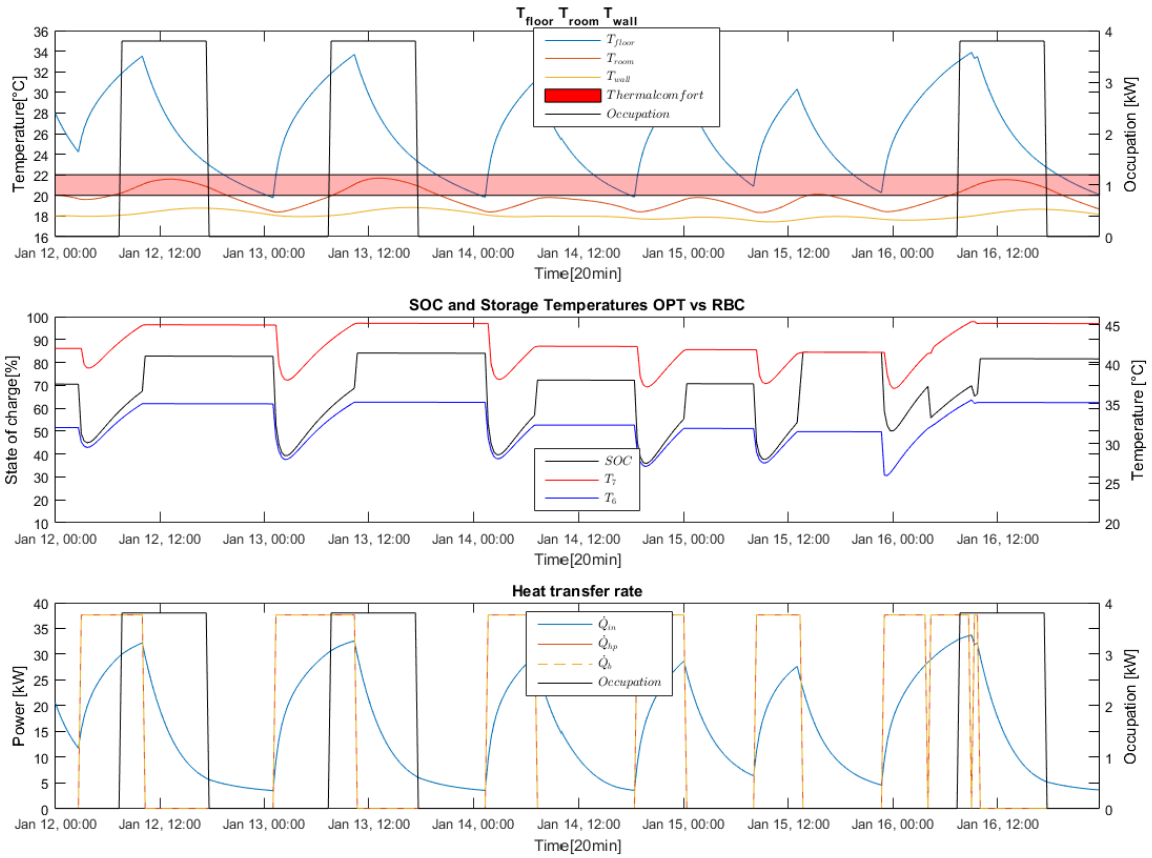

Figure 4.1.1 January results for RBC, 1) T_{floor}, T_{room} and T_{wall} vs ϕ_o
2) T_7 and T_6 vs State of charge 3) $\dot{Q}_{in}$, $\dot{Q}_{hp}$ and $\dot{Q}_b$ vs ϕ_o

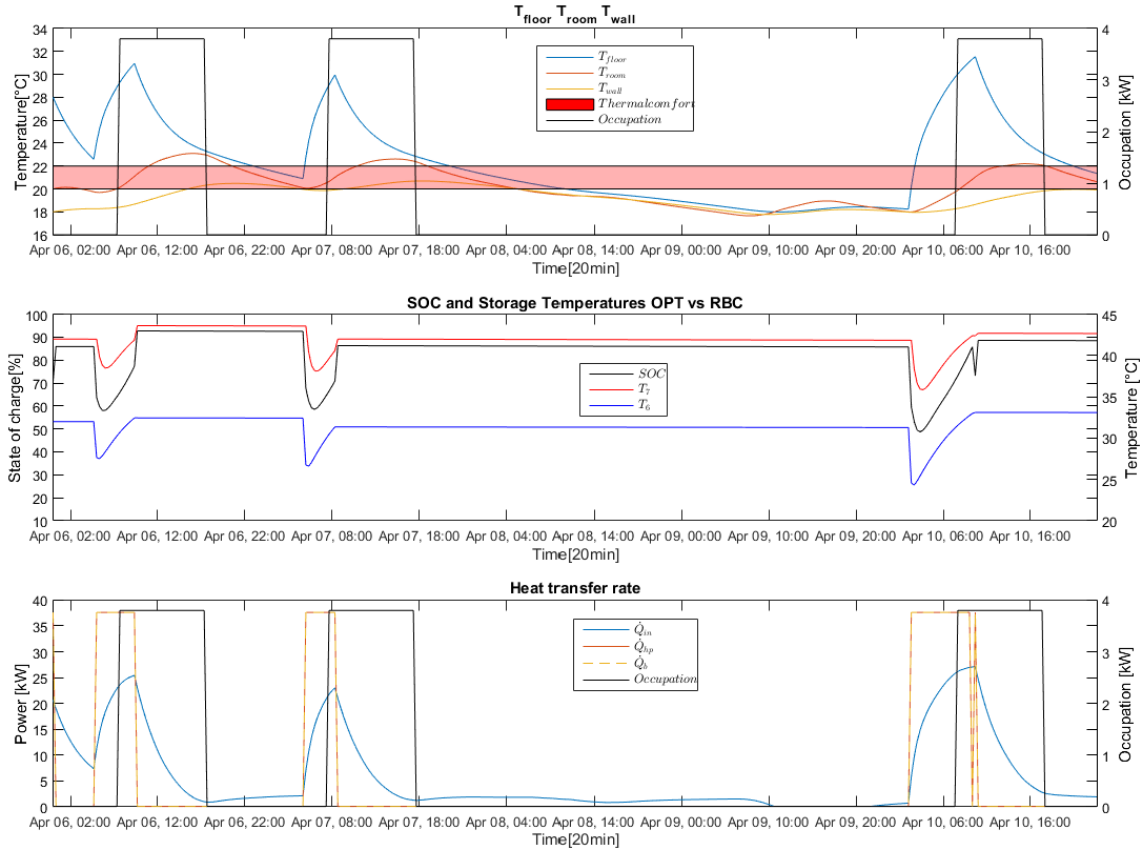

Figure 4.1.2 April results for RBC 1) T_{floor}, T_{room}, and T_{wall} vs ϕ_o
2) T_7 and T_6 State of charge 3) $\dot{Q}_{in}$, $\dot{Q}_{hp}$ and $\dot{Q}_b$ vs ϕ_o

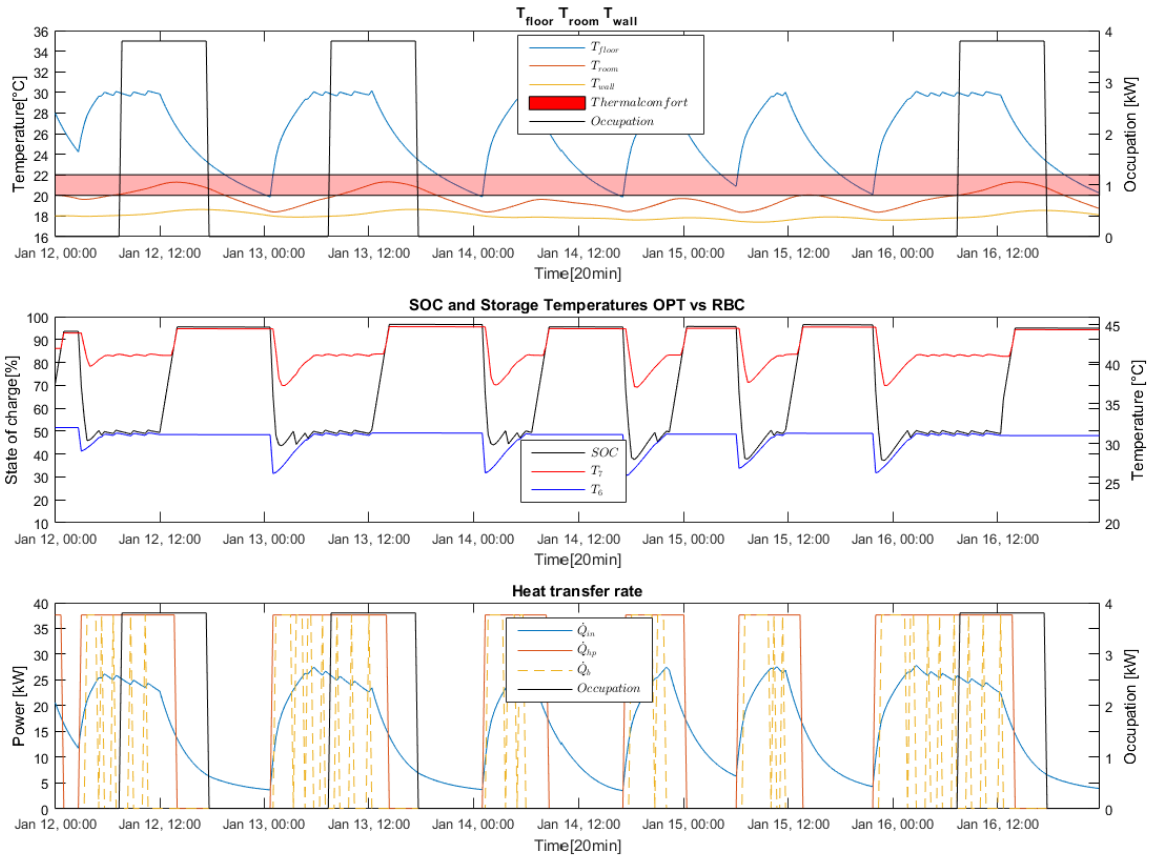

Figure 4.1.3 January results for sequential RBC, 1) T_{floor} , T_{room} and T_{wall} vs ϕ_o 2) T_7 and T_6 vs State of charge 3) $\dot{Q}_{in}$, $\dot{Q}_{hp}$ and $\dot{Q}_b$ vs ϕ_o

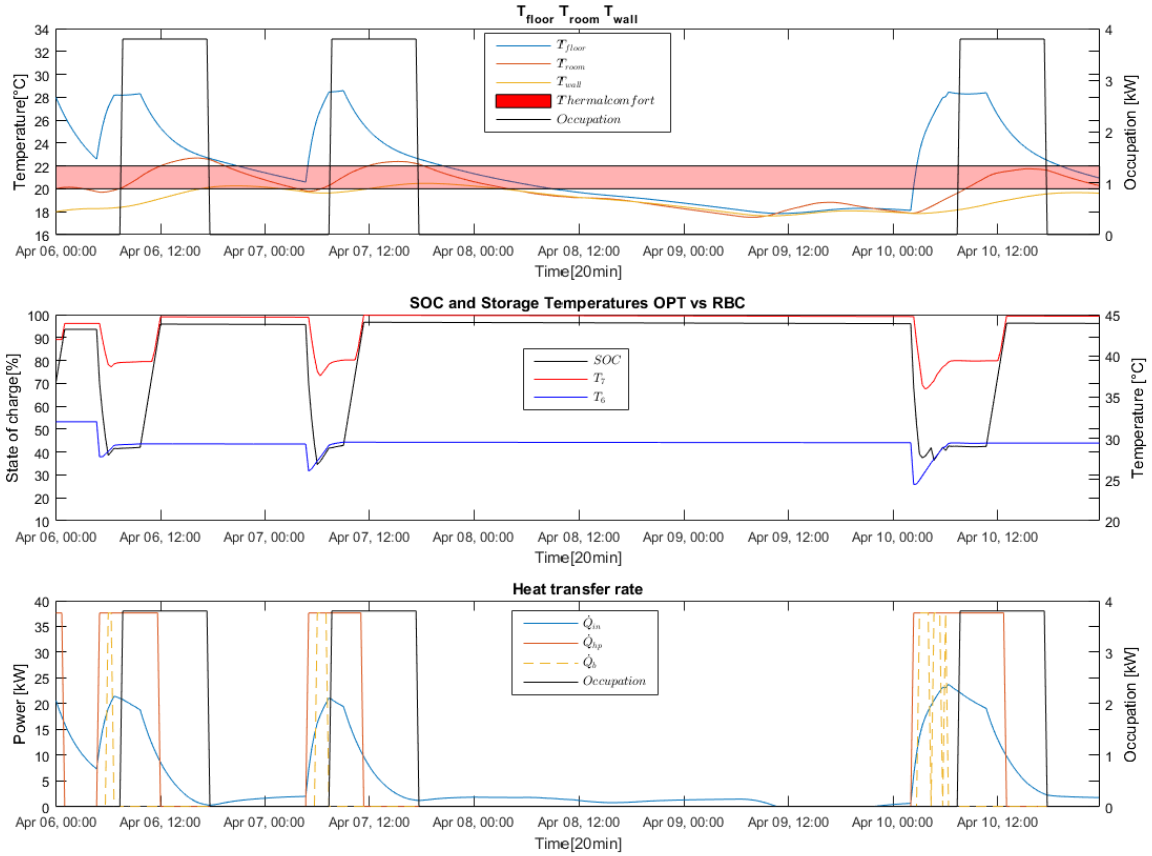

Figure 4.1.4 April results for sequential RBC, 1) T_{floor} , T_{room} and T_{wall} vs ϕ_o 2) T_7 and T_6 vs State of charge 3) $\dot{Q}_{in}$, $\dot{Q}_{hp}$ and $\dot{Q}_b$ vs ϕ_o

Doing a general discussion valid for the RBC and sequential RBC, by comparing the first plot 1) for each month, it can be noticed that in spring and autumn the temperature rises above the thermal comfort band, because as stated before the RBC is not able to predict the radiation throughout the day overestimating the building heating demand. It's also interesting to notice what reported in Table 3.3.3.1

Table 3.3.3.1, during normal working days the heating system will start some hours before people arrive in the building and after the weekend it needs to start even sooner to reach the minimum allowed temperature. Furthermore a minimum temperature has to be kept also during the weekends, because with a fixed starting hour, if the building is left to cool down especially during the colder months, the room temperature will not be able to reach the thermal comfort band on time. This brings wasteful consumption of energy that could be avoided when implementing an optimal controller, since it is able to check the weather prediction and act in accordance.

From plot 2) can be seen that the RBCs respect the control imposed on the storage mean temperature, however in this way, the RBCs will always try to fill the thermal storage without being able to exploit the decoupling between the thermal storage, the heat pump and the boiler. Meanwhile in and can be seen that the optimal controller exploits the thermal storage, charging it only when it is most economically convenient.

In the last plot 3) the RBC uses the heat pump and boiler at nominal power to charge the thermal storage and the total heat provided is the same for the RBC and priority is given to the heat pump in the sequential RBC, leading to a better performance overall with respect to the other RBC, but letting the heat pump working in inefficient conditions in winter, while in Figure 4.2.1 is shown that optimal controller prioritize the cheaper option to charge the thermal storage.

4.2 Optimal controller results

In this paragraph the results on the performance of the optimal controller for two sample months April and January are reported considering different plots, the other months are available in C.1.5, only the results with the best k are reported, where the best value of k was chosen based on the average discomfort taking as a reference the sequential rule based controller, more details in paragraph 4.3.

In the first plot the floor temperature T_{floor}, the room temperature T_{room}, and the external wall temperature T_{wall} are plotted against the thermal comfort band defined in paragraph 3.3.1, and the occupation heat gain defined in paragraph 2.2. In the second plot the hot and cold temperatures in the storage T_7 and T_6 are reported against the SOC "State of charge" of the thermal storage, defined in (2.4.1.10) and in the fourth plot $\dot{Q}_{in} = G_{fr}(T_f - T_r)$ which is the heat rate provided by the floor heating system to the room, $\dot{Q}_{hp}$ the heat rate provided by the heat pump and $\dot{Q}_b$ the heat rate provided boiler along with the occupation heat gain.

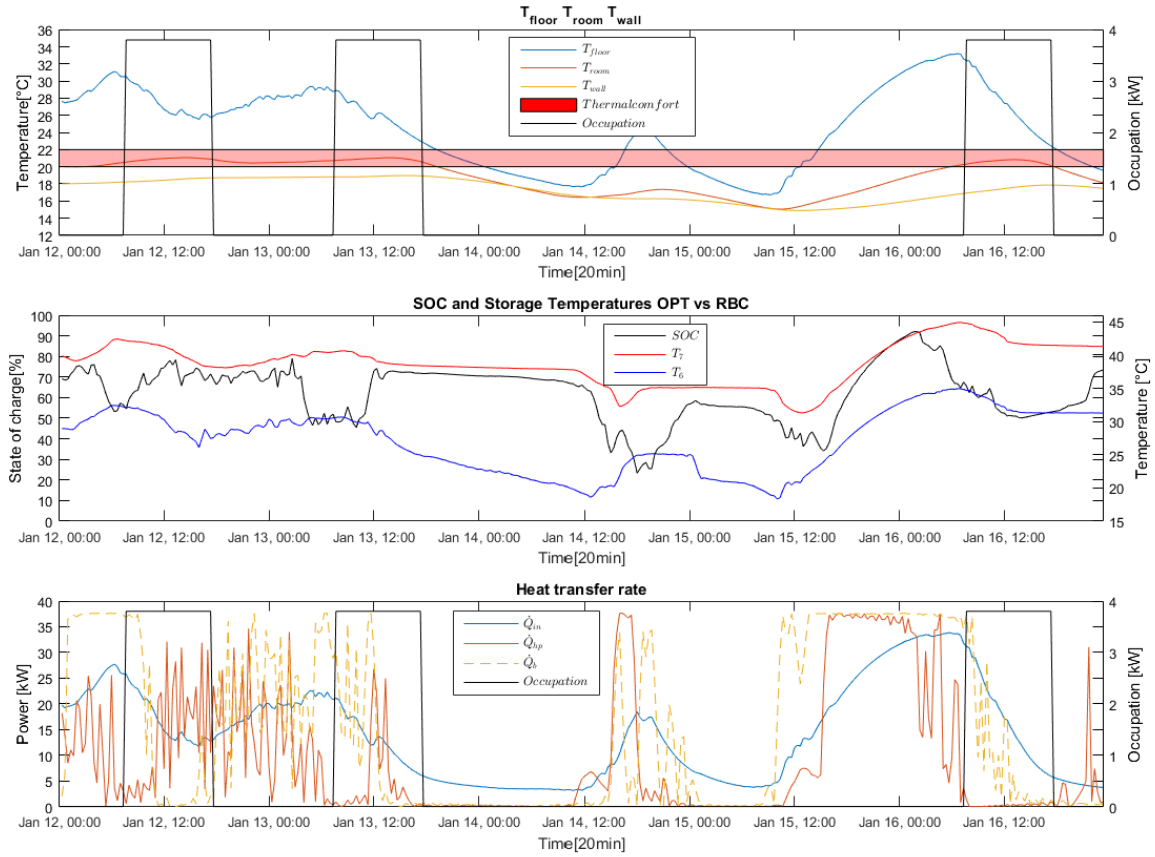

Figure 4.2.1 January results for optimal controller, 1) T_{floor}, T_{room} and T_{wall} vs ϕ_o 2) T_7 and T_6 vs State of charge 3) $\dot{Q}_{in}$, $\dot{Q}_{hp}$ and $\dot{Q}_b$ vs ϕ_o

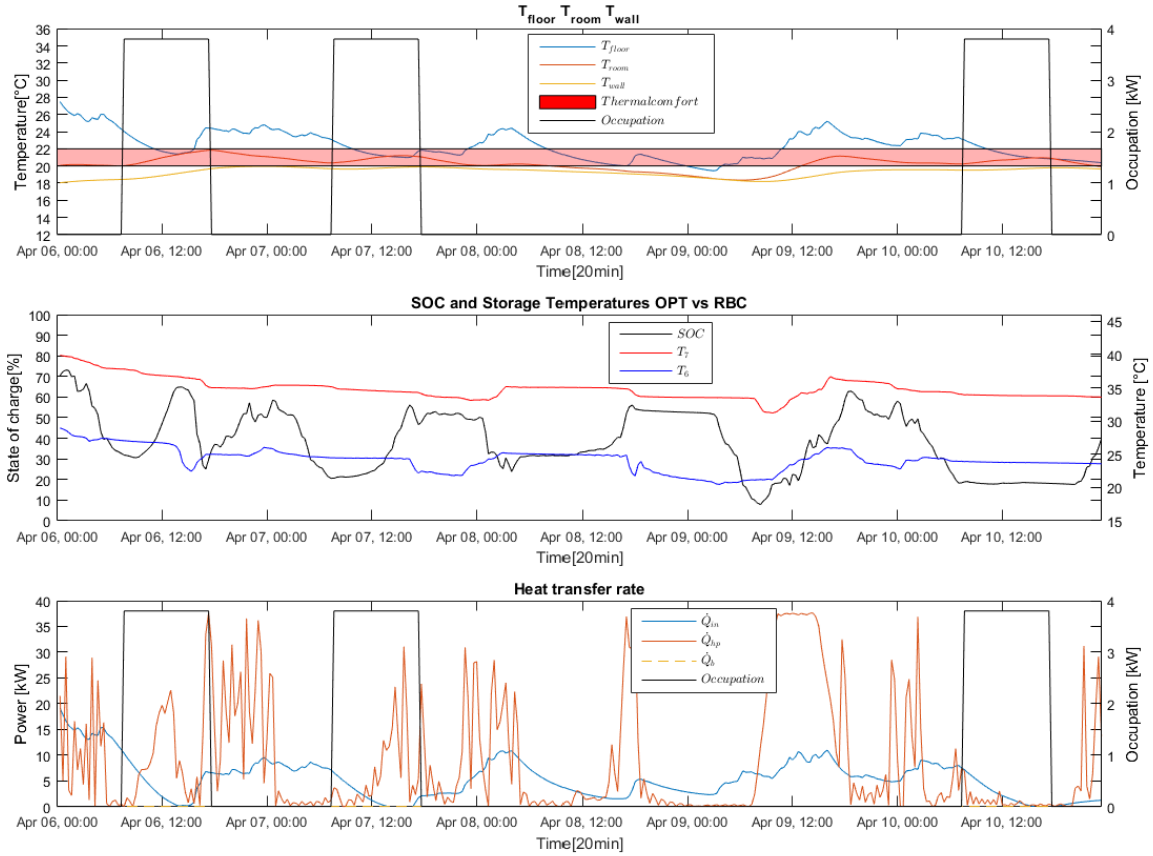

Figure 4.2.2 April results for optimal controller, 1) T_{floor}, T_{room} and T_{wall} vs ϕ_o 2) T_7 and T_6 vs State of charge 3) $\dot{Q}_{in}$, $\dot{Q}_{hp}$ and $\dot{Q}_b$ vs ϕ_o

From the optimal control monthly plots a few things can be shown, starting with plot 1) the average temperature of the floor T_f is lower in spring and autumn, and higher in the colder winter months, in this way the optimal controller is able to provide heat to the building without overheating in warmer seasons and achieve thermal comfort during colder ones.

From plot 2) can be noticed that the optimal controller is able to exploit better the thermal storage with respect to the RBCs, in fact the ΔSOC is way higher than in the RBCs, furthermore during the weekend we have a rapid drop of the thermal storage temperatures T_7 and T_6, due to the fact that the building is let to cool down during the weekend, however by starting before the RBCs, the optimal controller is able to guarantee thermal comfort during Monday by starting to heat up the building before the RBCs.

In the last plot 3) is shown how the optimal controller choses to use the heat pump during warmer seasons, reducing the consumption of the boiler to zero, while in colder seasons the boiler is preferred to heat pump to charge the thermal storage.

4.3 Rule based controllers comparison with optimal controller

In the previous paragraphs a view on the behavior of the RBCs and optimal controller was shown. In this paragraph the detailed comparison between the three controllers will be shown for each five sample days from Thursday to Monday, for the whole heating season.

First a view on the general performance is shown, comparing the RBCs and the optimal controller for the whole heating season at different values of k, by taking a look at the total heat provided by the heat pump and boiler Q [kWh], the total Energy cost [€], the total Primary energy [kWh_f] consumption and Emissions [$kgCO_2$] as defined in appendix B.1.2 and the B.1.2.

Second the same quantities are shown for the whole heating season considering the two RBCs and the optimal controller for the best value of k, defined as the cheaper option with an adequate thermal comfort.

Lastly is shown a more detailed comparison between the sequential RBC and the optimal controller is shown analyzing the daily trend of the important variables for two sample months, January and April, the plots for the other months can be found in C.1.6.

4.3.1 Lumped parameters comparison RBCs vs optimal controller

In Figure 4.3.1 the trend of the controllers is shown by putting on the x-axis the total heat provided by heat pump and boiler to the storage Q [kWh] and on y-axis the error with respect to the set point temperature as defined in the cost function in paragraph 3.1 divided by the total number of occupied hours during the five days considered, so that it represents the average quadratic hourly error with respect to the set point temperature $T_{set-point} = 21$ [°C].

It is worth mentioning that to do a fair comparison, the difference between initial and final SOC $SOC_f - SOC_{in}$ and therefore the difference in energy stored in the thermal storage, was taken into consideration for the calculation of the lumped parameters.

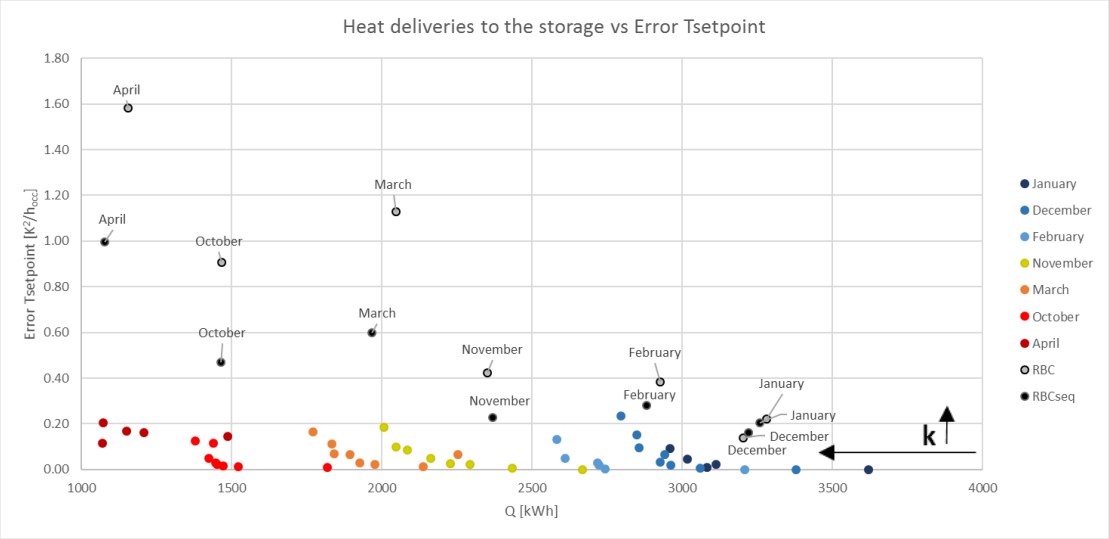

Figure 4.3.1 Heat deliveries to storage vs Error $T_{set-point}$ for each month

In Figure 4.3.2 the trend of the controllers is shown by putting on the x-axis the total Energy cost [€] and on y-axis the error with respect to the set point temperature.

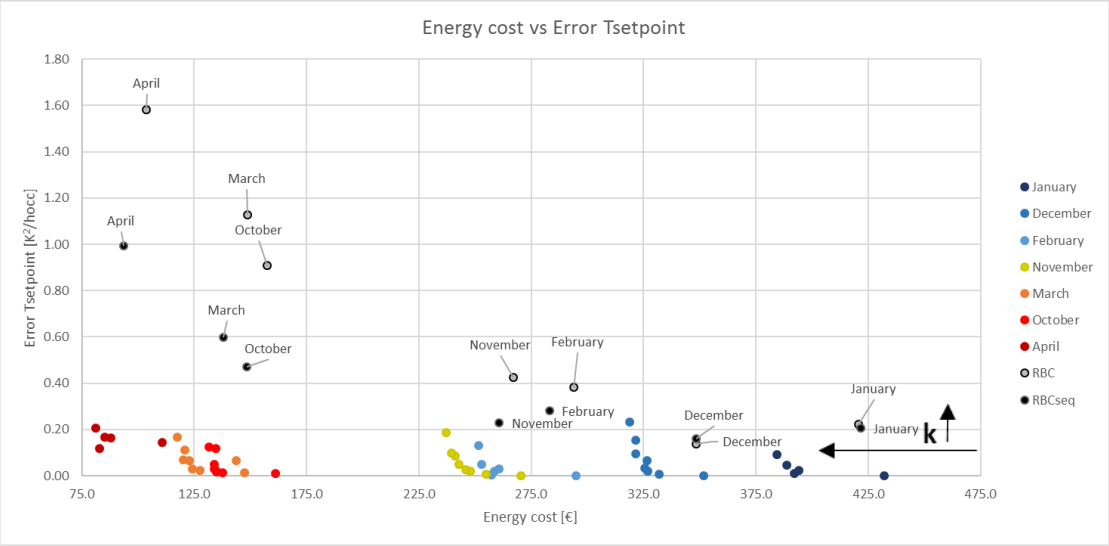

Figure 4.3.2 Energy cost vs Error $T_{set-point}$ for each month

In Figure 4.3.3 the trend of the controllers is shown by putting on the x-axis the total Primary energy [kWh_f] consumption and on y-axis the error with respect to the set point temperature.

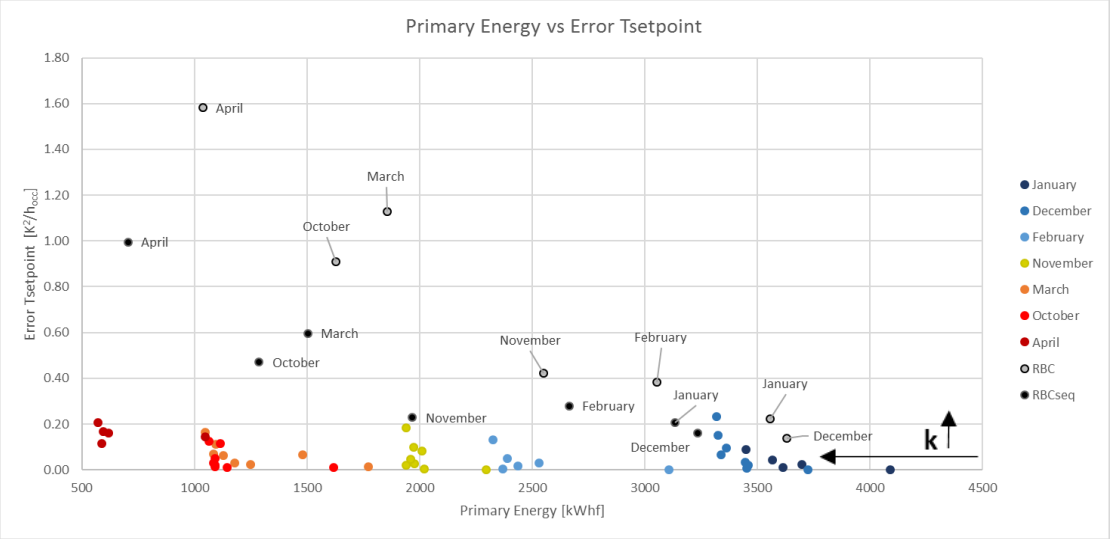

Figure 4.3.3 Primary energy vs Error $T_{set-point}$ for each month

In Figure 4.3.4 the trend of the controllers is shown by putting on the x-axis the total Emissions [$kgCO_2$] and on y-axis the error with respect to the set point temperature.

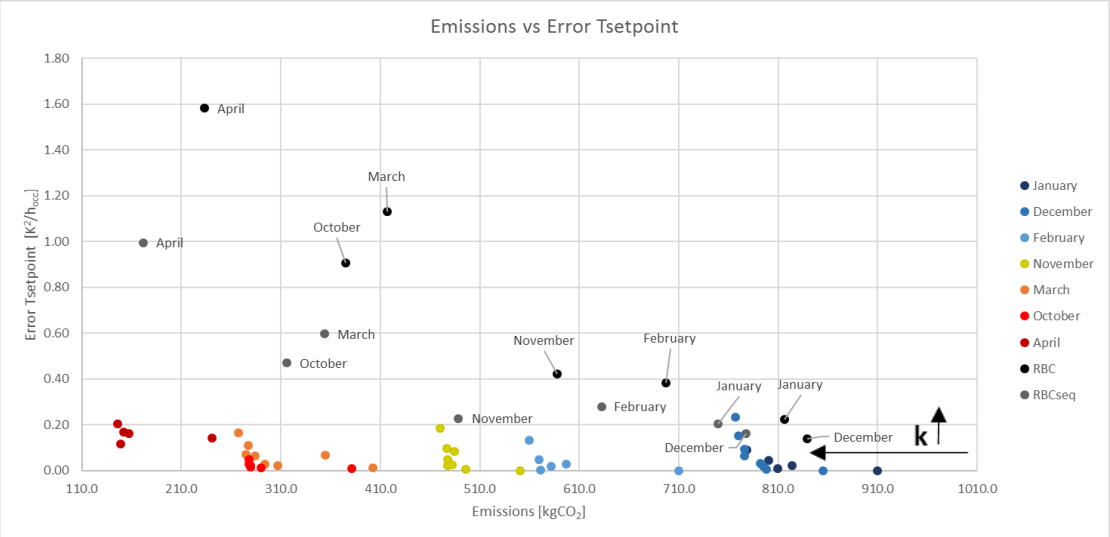

Figure 4.3.4 Emissions vs Error $T_{set-point}$ for each month

The first thing worth mentioning is the expected trend of the optimal controller results by increasing the value of k for all months, as the parameter k increases the heat consumption reduces while the error increases, meaning that the solver is behaving according to what expected.

Secondly is clear how the sequential RBC outperforms the other RBC in terms error on the set point, heat input and energy cost apart from the coldest months in which the two controllers perform in a similar fashion, therefore for the detailed analysis only the sequential RBC is considered.

The optimal controller has an average lower error on the set point with respect to the RBCs and a lower heat consumption apart from April and October in which the heat provided is similar, due to a lower demand in general, but taking a look at the energy cost in Figure 4.3.2, the energy cost is lower due to the fact that the optimal controller is able to produce heat when is cheaper.

However this causes an increase in Primary energy consumption and CO_2 emissions in the colder months, because the cheapest way to produce heat is to burn natural gas in the boiler.

Considering just the results of the optimal controller for the best k and comparing the same parameters as before, more conclusions can be derived.

In Figure 4.3.5 the heat delivered to the storage Q[kWh] plotted against the months is reported, it is worth mentioning than for the mean value, October and April were considered by only half in the weighted average, since the heating season starts on the 15th of October and ends on the 15th of April.

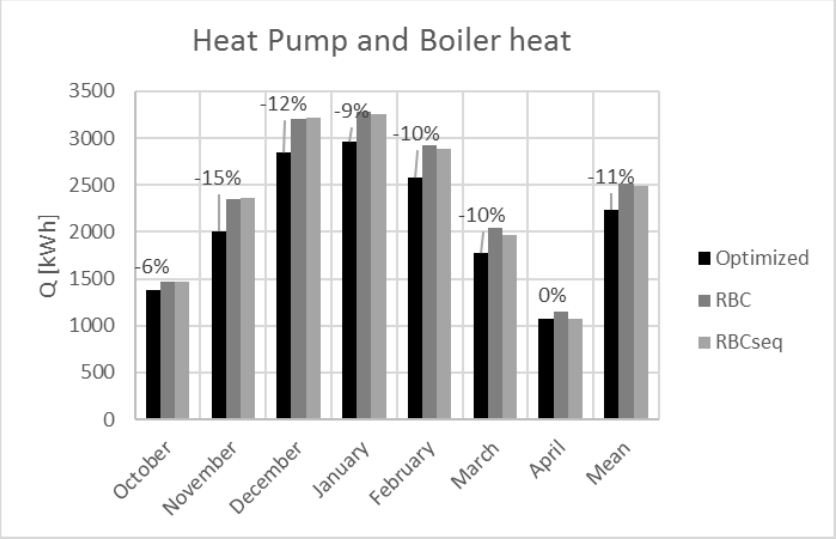

Figure 4.3.5 Heat input vs Months

In Figure 4.3.6 the Energy cost [€] plotted against the months is reported

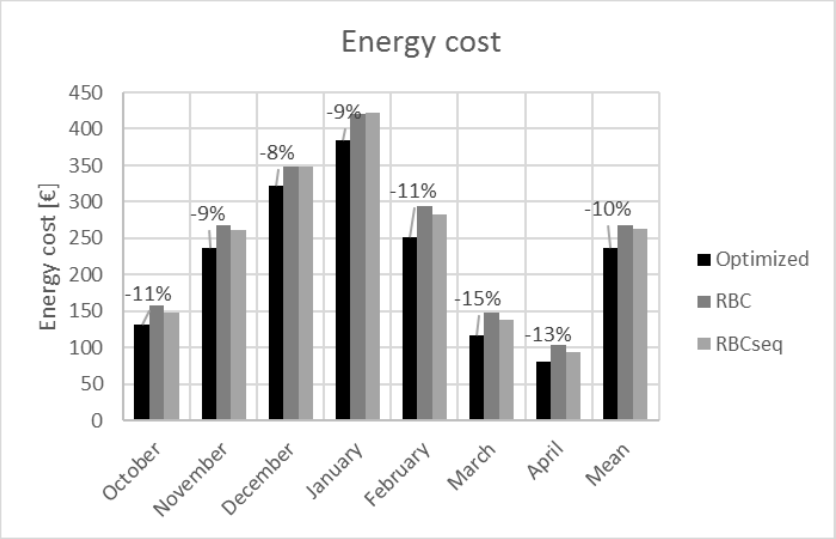

Figure 4.3.6 Energy cost vs Months

From the first plot it is clear that during colder months the optimal controller tends to provide less heat with respect to the RBCs while in Autumn and Spring the heat consumption is quite similar. However considering the energy cost there are higher savings in Spring and Autumn with respect to the colder months. This is due to the lower cost of electricity, higher COP of the heat pump and the ability of the optimal controller to exploit the thermal storage, in fact only the heat pump is used to produce heat, despite the fact the heat pump nominal power is lower than the building energy demand, while in colder months average price of the heat provided by the heat pump and boiler is similar Figure 4.3.14, not allowing the optimal controller to greatly outperform the RBCs.

Considering the mean values, the optimal controller is able to save up to the 11% of the heat provided by the heat pump and boiler and 10% of the energy cost throughout the whole heating season, which is a promising result, considering that it can not be taken for granted that the solution of the optimal controller is a global optimum, leaving the possibility to further improve these numbers.

In Figure 4.3.7 the Error on $T_{set-point}$ $\left[\frac{K^2}{h_{occ}}\right]$ against the months is reported

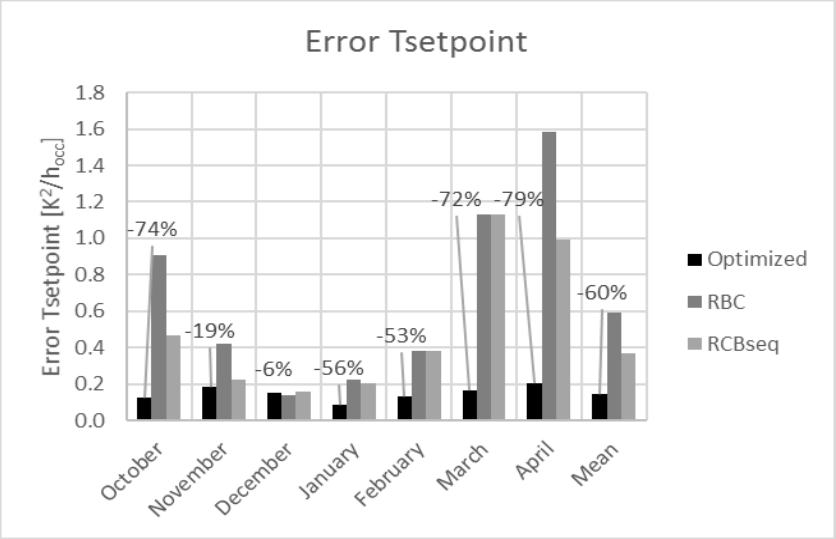

Figure 4.3.7 Error $T_{set-point}$ vs Months

As expected the optimal controller, having the ability to predict the external temperature and solar radiation, outperforms the RBCs, especially in Spring and Autumn when the RBCs overheat the building because the solar contribution is not negligible.

In Figure 4.3.8 and Figure 4.3.9 the Primary energy [kWh_f] consumption and the Emissions [$kgCO_2$] against the months are reported

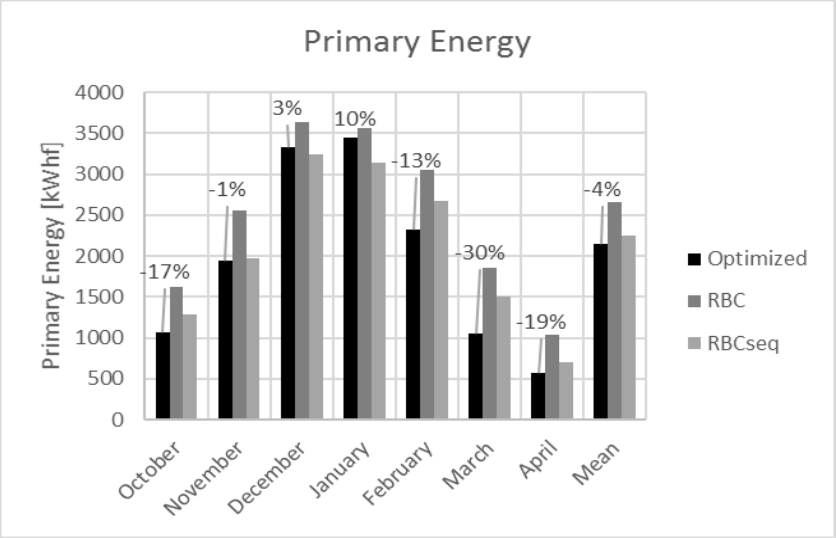

Figure 4.3.8 Primary Energy vs Months

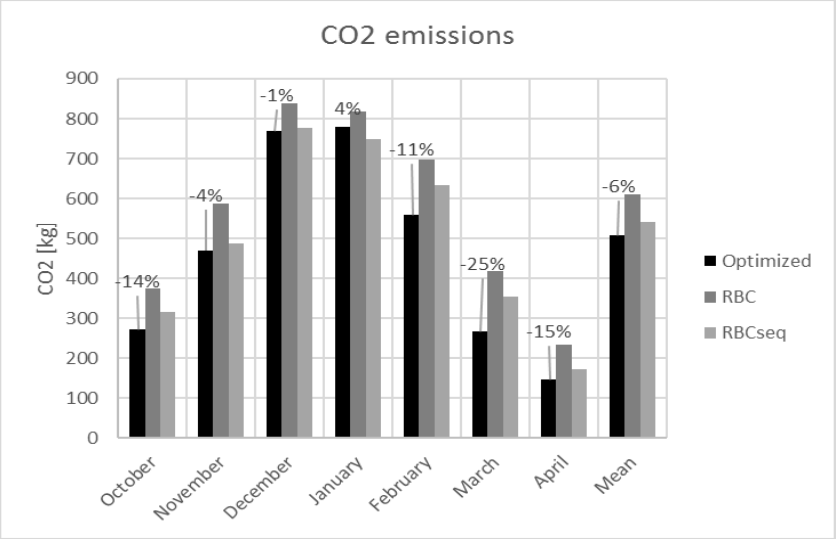

Figure 4.3.9 Emissions vs Months

As mentioned before, the Primary energy and Emissions savings are not remarkable, because even if in Spring and Autumn the optimal controller manages to the reduce the Primary energy consumption and the Emissions, in the colder months the optimal controller privileges the boiler over the heat pump, because it is cheaper.

4.3.2 Daily comparison optimal controller vs sequential RBC

In this paragraph is shown the daily comparison between the performance of the optimal controller in the case of the best k and the sequential RBC, for the two sample months of January and April, the results for the other months are reported in C.1.6.

In Figure 4.3.10 and Figure 4.3.11 the trends of the time step and cumulative cost functions are reported with respect to the time, on the left y-axis the Time step cost function [€] and on the right y-axis the cumulative cost function [€]

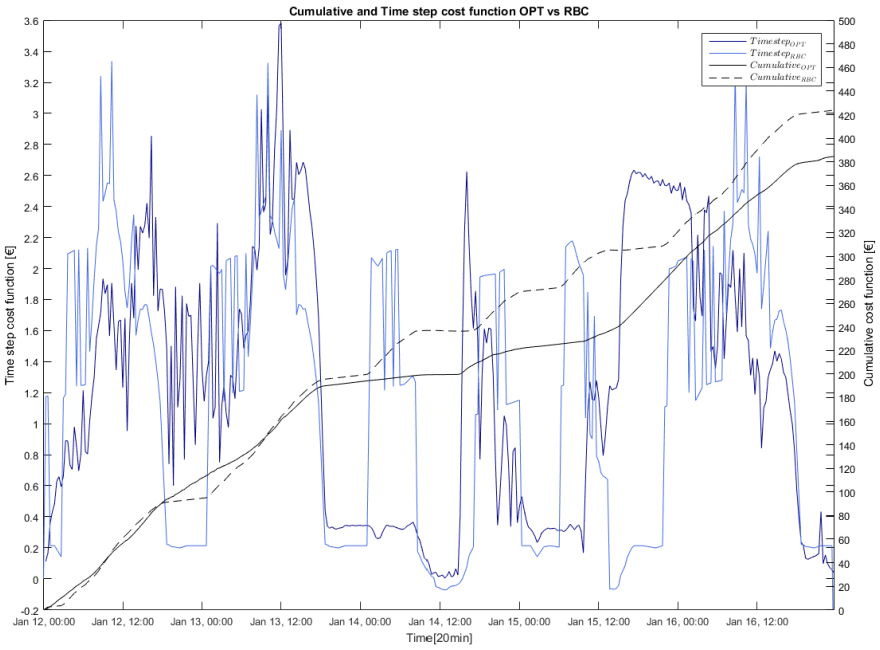

Figure 4.3.10 January time step cost function and cumulative cost function vs time

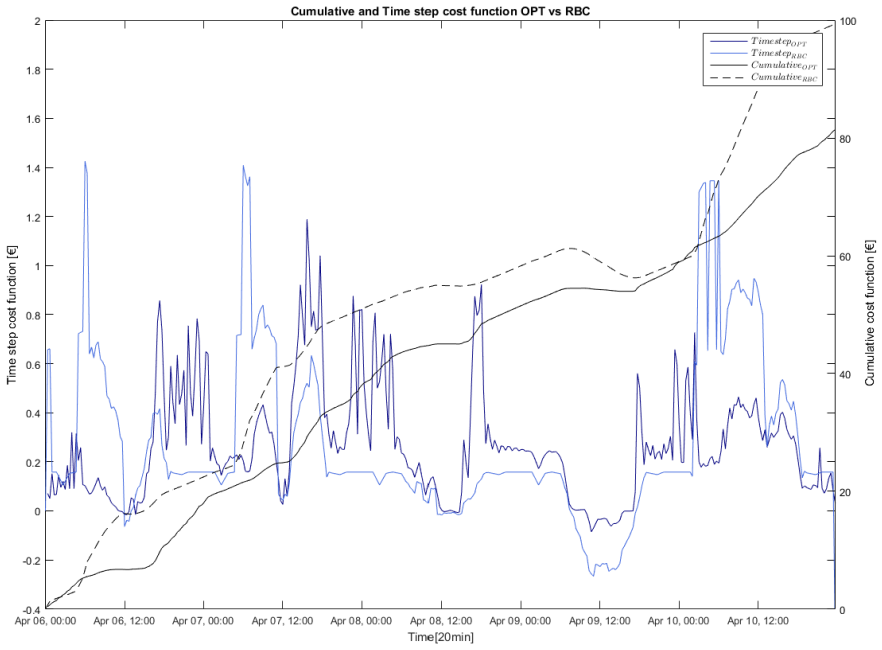

Figure 4.3.11 April time step cost function and cumulative cost function vs time

By comparing the optimal controller with the sequential RBC, how in January the two cumulative functions show similar trends for Thursday the 12th and Friday the 13th , due to the fact that the price of producing heat with the heat pump and the boiler are similar, therefore

the optimal controller does not have a lot of room for improvement. However the RBC cumulative cost has a higher slope during the weekend, January the 14th and January the 15th, because it has to maintain a minimum temperature to guarantee thermal comfort on Monday. A different conclusion instead is derived by taking a look at April, in fact the optimal controller outperforms the RBC during the working days, because it has more freedom in exploiting the thermal storage using the heat pump at high efficiencies, but in the weekend the RBC cumulative cost can achieve a negative slope, because the photovoltaic system is producing more energy than required and selling it to the grid, this is true also for the optimal controller, but in a smaller fashion, because it uses the energy produced by the photovoltaic system to charge the storage with the heat pump. This is probably due to a suboptimal solution, where a local minimum was found by the optimal controller, because by taking a look at Table 4.3.2.1 where a comparison is made between the price at which the excess energy from the PV system is sold, PUN + CUSf and the maximum cost at which the heat pump produces heat, it is clear that, if excess energy is produced it should be sold to the grid to have the highest profit.

Table 4.3.2.1 Comparison PUN+CUSf vs cost of heat production from heat pump

	Pun+Cusf [€/kWh]	max Cel/COP [€/kWhth]
October	0.079	0.052
November	0.084	0.061
December	0.082	0.070
January	0.097	0.092
February	0.080	0.067
March	0.069	0.048
April	0.068	0.047

In the Figure 4.3.12 and Figure 4.3.13 three plots are reported, in the first one a comparison between the room temperatures T_r [°C] and the Occupation heat gain, in the second plot the heat transferred from the floor to the room $\dot{Q}_{in} = G_{fr}(T_f - T_r)$ [kW] and the net power difference between the electricity demand due to appliances P_b [kW] and the power produced by the PV system P_{pv} [kW] against the inlet temperature in the floor heating T_1. In the third plot are reported the total electricity power demand and natural gas heat demand against the cost at which heat is produced by the heat pump $\frac{C_{el}}{COP}\left[\frac{€}{kWh_{th}}\right]$. the plots for the other months are reported in C.1.6.

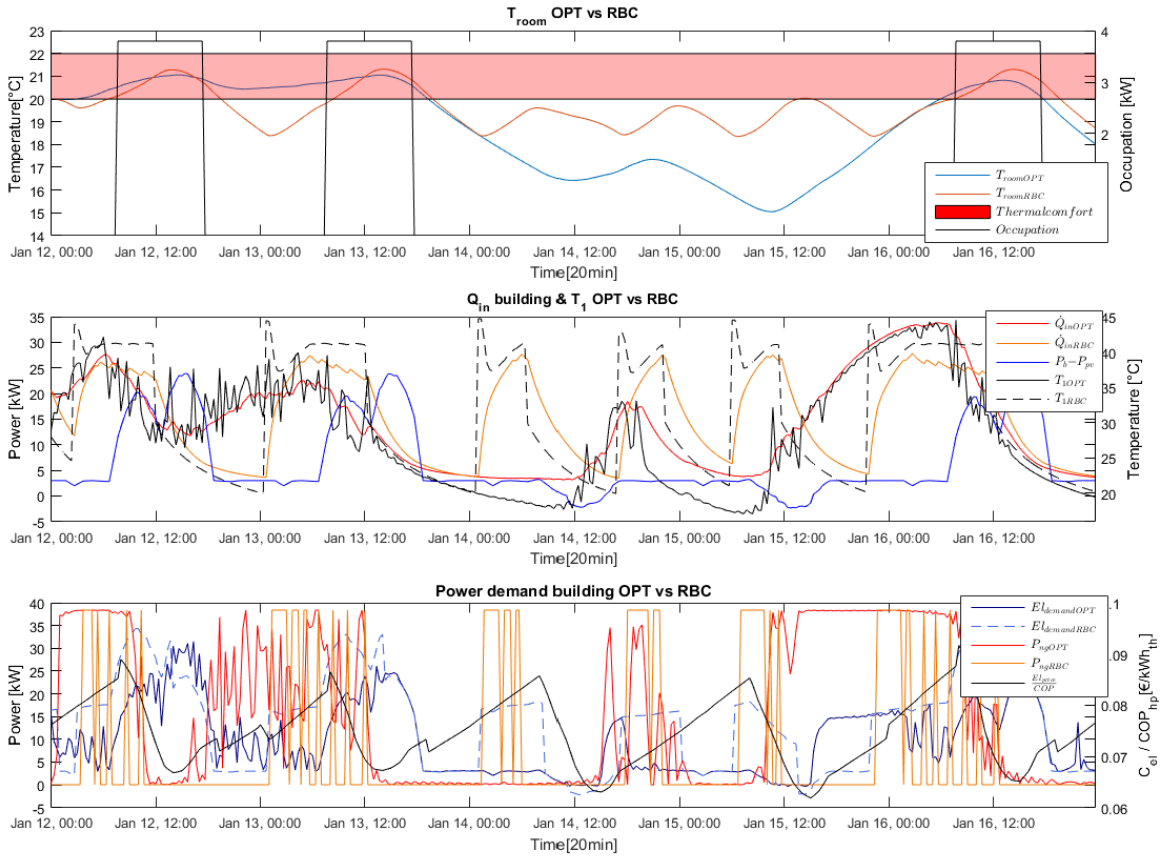

Figure 4.3.12 January OPT vs RBC 1) T_{room} vs Occupation heat gain, 2) $\dot{Q}_{in} = G_{fr}(T_f - T_r)$, $P_b - P_v$ vs T_1 3) Electricity demand, P_{ng} vs $\frac{C_{el}}{COP}$

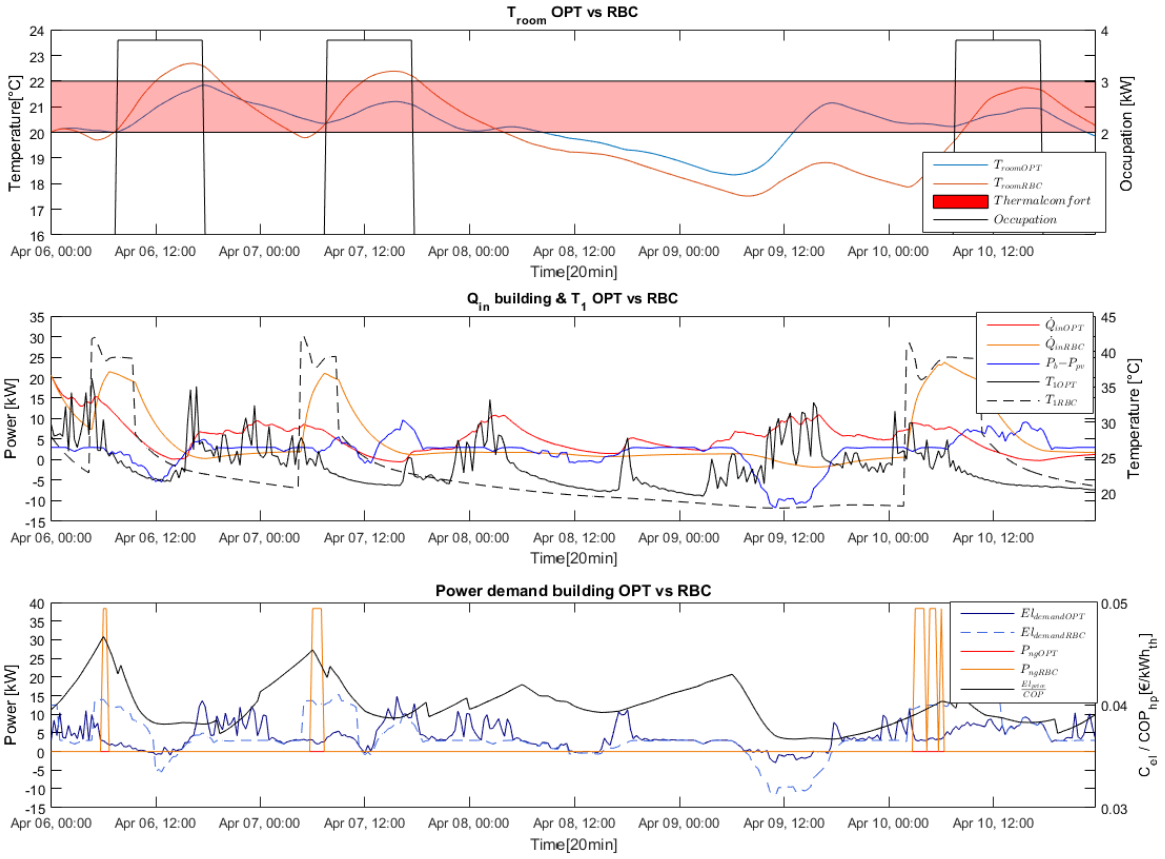

Figure 4.3.13 April OPT vs RBC 1) T_{room} vs Occupation heat gain, 2) $\dot{Q}_{in} = G_{fr}(T_f - T_r)$, $P_b - P_v$ vs T_1 3) Electricity demand, P_{ng} vs $\frac{C_{el}}{COP}$

By taking a look at the first plot 1) it is clear how during January the optimal controller let the building cool down, while during April the optimal controller tends to exploit the excess power from the PV system to charge the storage and heat up the building, leading to an higher room temperature with respect to the sequential RBC. It is also interesting to notice that the room temperature of the RBC tends to have a parabolic shape during the occupied hours having a peak around noon, and this leads to overheating in April, while the optimal controller room temperature has a flatter profile close to the set point, preventing overheating in April, and overall granting thermal comfort while using less heat.
From the second plot 2) it can be noticed how the optimal controller manages to have a flatter temperature profile, for April because the average inlet temperature T_1 is lower in the case of the optimal controller, in this way the heat rate $\dot{Q}_{in}$ has a lower value, since if T_1 is lower T_{floor} will be lower, reducing the average heat rate allows the storage to be charged by using just the heat pump in April.

In January the average inlet temperature is similar, even tough it is lower during the working days and higher in the weekend to allow the optimal controller to reach thermal comfort during Monday despite the building temperature drop during the weekend for the optimal controller, the same can be said for the inlet heat transfer rate even tough in January the optimal controller uses both the heat pump and the boiler.
In fact in plot 3) is shown how, in January the electrical demand of the optimal controller is slightly lower than the RBC and the natural gas demand especially before Monday is way higher because of the high cost of producing heat with the heat pump, due to higher electricity cost and lower COP because of a low external temperature. It is also worth noticing how the optimal controller tries to use the excess power from the PV as said before, in fact the negative peak of the electrical demand is way lower in the optimal controller case.

In Figure 4.3.14 and Figure 4.3.15 is shown a detail on the thermal storage variables and the system controls for January and April. In the first plot the thermal storage SOC [%] against the temperatures T_7 [°C] and T_6[°C] are reported. In the second plot the control mass flow rates $\dot{m}_{10}$ $\left[\frac{kg}{s}\right]$ and $\dot{m}_8$ $\left[\frac{kg}{s}\right]$, respectivly the mass flow rate of the heat pump and the boiler are shown against the cost of the natural gas divided by the boiler efficiency C_{ng} $\left[\frac{€}{kWh_f}\right]$ and the cost producing heat from the heat pump $\frac{C_{el}}{COP}\left[\frac{€}{kWh_{th}}\right]$. Similarly in the last plot the heat transfer rates of heat pump and boiler are reported instead.

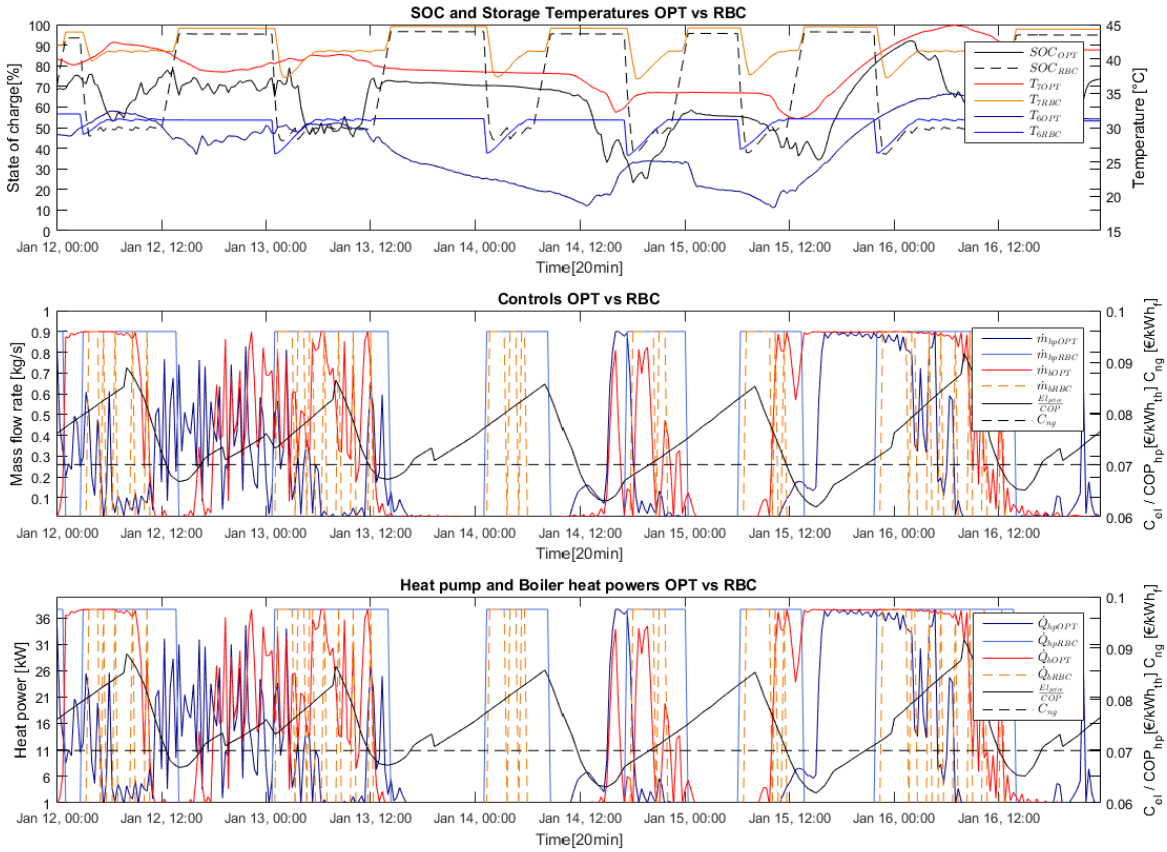

Figure 4.3.14 January OPT vs RBC 1) SOC vs T_7 and T_6,

2) $\dot{m}_{10}$ and $\dot{m}_8$ vs C_{ng} and $\frac{C_{el}}{COP}$, 3) $\dot{Q}_{hp}$ and $\dot{Q}_b$ vs C_{ng} and $\frac{C_{el}}{COP}$

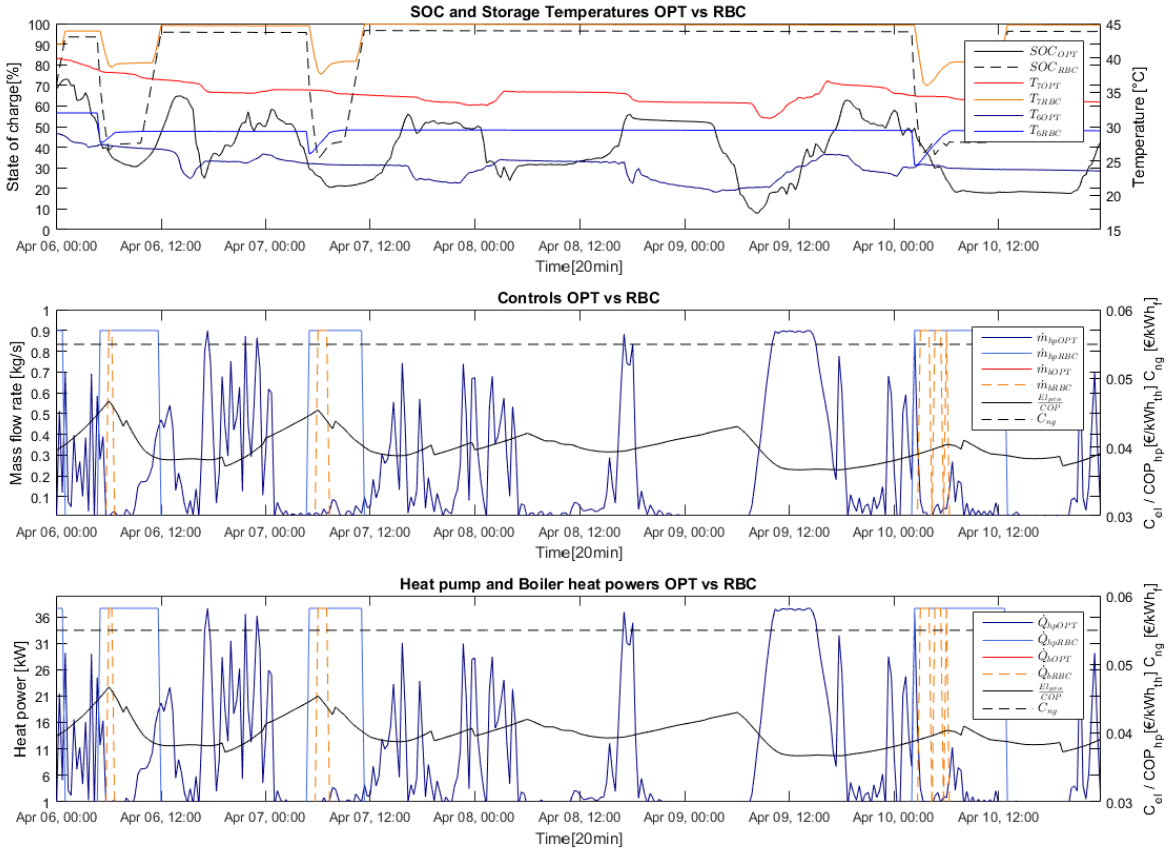

Figure 4.3.15 April OPT vs RBC 1) SOC vs T_7 and T_6,

2) $\dot{m}_{10}$ and $\dot{m}_8$ vs C_{ng} and $\frac{C_{el}}{COP}$, 3) $\dot{Q}_{hp}$ and $\dot{Q}_b$ vs C_{ng} and $\frac{C_{el}}{COP}$

In the first plot 1) is shown how both in January and April, the SOC of the RBC is always kept at very high values, because the controller is programmed to charge the thermal storage as soon as the it starts to be depleted, while SOC in the optimal controller undergoes a lot of swings and on average is lower. This is also due to the fact that the average temperature in storage is lower in the optimal case, beside in the night before January's Monday to allow the controller to reach thermal comfort.

From plots 2) and 3), is shown how in winter the cost of producing heat with the boiler is almost always lower than the one of the heat pump, leading the optimal controller to prefer using the boiler most the times, while the sequential RBC always prioritize the heat pump. In April instead the opposite happens since producing heat with the heat pump is always cheaper.

4.4 Conclusions

In this study it was demonstrated:

1. The designed dynamic system model of the hybrid heating system with thermal storage and the building model, even though simplistic, is able to represent the general thermal behavior of the building and of the heating system in a realistic way.
2. The rule based controllers were designed as a reference, and the sequential rule based controller, by giving priority to the heat pump, resulted in an overall better performance with respect to the other rule based controller. However all the problems highlighted in the introduction, overheating in Spring and Autumn, not exploiting the thermal storage and maintaining a minimum temperature even when there are no people in the building still remain.
3. The formulated optimal control problem, the constraints and the time horizon were obtained by tuning all the involved parameters. Different values of the parameter k and the weight parameter W_{en-dis} were tried to find the right equilibrium between the energy cost function and the thermal discomfort cost function. Various constraints, in particular on the storage temperatures were tried, in order to prevent the optimal controller to give unrealistic solutions. Lastly different times horizon and time steps were applied to obtain a trade off between the computational time and realistic results, which can be safely extended for the whole heating season.
4. The results of the optimal controller, show how it is possible to overcome the problems presented in the rule based controllers, for example to prevent overheating in the warmer season, the average inlet temperature T_1 is lower with respect to the RBC case, but starting heating up the building earlier, especially in the weekend. This allows also the building temperature to drop during the weekend while still achieving thermal comfort in Monday morning. Finally the optimal controller exploited the storage system to supply the energy demand to the building, while charging it using the cheaper alternative between the heat pump and the boiler depending on the weather conditions and the price of electricity.
5. These results lead the optimal controller to outperform the rule based controller, leading to an average 10% economic saving and a 11% in heat delivered by the heat pump and the boiler to the thermal storage. Instead the primary energy consumption and the emissions are not significantly lower, because in winter the optimal controller tends to favor the use of the boiler since is the cheaper option, while the sequential RBC always favors the heat pump.
6. However the solution of the optimal controller presents an issue with dealing with the photovoltaic system, as discussed in paragraph 4.3.2. Furthermore the optimal

controller does not account for the degradation of the actuators, the circulation pumps or inefficiencies due to very low partial load, because there is not a term in the cost function that accounts for them, leading the overall solution to be a suboptimal solution with margin for improvement. Further studies can be conducted in this sense, considering also a more complex model for the heat pump and the boiler control, the losses due the circulation pumps and the degradation of the components.

7. The solution from the optimal controller can be used to design an optimized rule based controller or simpler MPC formulation for real time applications. Also design studies can be conducted employing the optimal controller and changing key parameters such as the temperature difference across the heat pump and boiler, or the size of the thermal storage, to see how these affect the performance of the system.

Bibliography

[1] D. Kolokotsa, D. Rovas, E. Kosmatopoulos, and K. Kalaitzakis, “A roadmap towards intelligent net zero- and positive-energy buildings,” *Sol. Energy*, vol. 85, no. 12, pp. 3067–3084, 2011.

[2] K. Holmström, A. O. Göran, and M. M. Edvall, “User’s guide for TOMLAB 7,” p. 268, 2010.

[3] J. Drexhage, D. Murphy, O. Brown, A. Cosbey, P. Dickey, J. Parry, J. Van Ham, R. Tarasofsky, and B. Darkin, *Climate Change*. .

[4] M. W. Ahmad, M. Mourshed, B. Yuce, and Y. Rezgui, “Computational intelligence techniques for HVAC systems : A review,” pp. 359–398, 2016.

[5] S. Prívara, Z. Váňa, E. Žáčeková, and J. Cigler, “Building modeling: Selection of the most appropriate model for predictive control,” *Energy Build.*, vol. 55, pp. 341–350, 2012.

[6] E. Zavaglio, R. Scoccia, and M. Motta, “RC building modelling for control purposes : a case study,” 2016.

[7] R. Baccoli, C. Mastino, and G. Rodriguez, “Energy and exergy analysis of a geothermal heat pump air conditioning system,” *Appl. Therm. Eng.*, vol. 86, pp. 333–347, 2015.

[8] A. Parisio, L. Fabietti, M. Molinari, D. Varagnolo, and K. H. Johansson, “Control of HVAC Systems via Scenario-based Explicit MPC,” pp. 5201–5207, 2014.

[9] V. De Oliveira and J. Johannes, “Dynamic online optimization of a house heating system in a fluctuating energy price scenario,” 2013.

[10] F. Amara, K. Agbossou, A. Cardenas, Y. Dubé, and S. Kelouwani, “Comparison and Simulation of Building Thermal Models for Effective Energy Management,” *Smart Grid Renew. Energy*, vol. 6, no. 4, pp. 95–112, 2015.

[11] A. Rahman, A. D. Smith, and N. Fumo, “Performance modeling and parametric study of a stratified water thermal storage tank,” *Appl. Therm. Eng.*, vol. 100, pp. 668–679, 2016.

[12] ZANI SPA, “Listino tecnico commerciale,” *ZANI SPA*, 2012.

[13] *D.P.R 26 AGOSTO 1993, N.412*. 1993.

[14] C. Verhelst, F. Logist, J. Van Impe, and L. Helsen, “Study of the optimal control problem formulation for air-to-water heat pump systems,” pp. 43–46, 2012.

[15] AERMEC, *Anli 020-100 h|hp|hx*. .

[16] VIESSMAN, “VITODENS 222-W Foglio dati tecnici,” 2007.

[17] C. Delmastro, G. Mutani, and S. Perassi, “In Use Monitoring of Public Buildings . Case Study in North Italy,” *Int. J. Heat Technol.*, vol. 34, no. 2, pp. 266–276, 2016.

[18] WARIS, “WARIS datasheet.” pp. 1–2, 2005.

[19] Advanced Energy, “PVP35kW and PVP50kW,” 2011.

[20] R. Lombardia, “www.arpalombardia.it,” 2015. [Online]. Available: http://www.arpalombardia.it/Pages/ARPA_Home_Page.aspx.

[21] P. E. Rutquist and M. M. Edvall, “PROPT - Matlab Optimal Control Software,” 2010.

[22] M. A. Kazemi, “Pseudospectral Chebyshev Optimal Control of Constrained Nonlinear Dynamical Systems,” vol. 217, pp. 195–217, 1998.

[23] P. E. Gill, W. Murray, M. A. Saunders, and P. E. Gilit, “SNOPT : An SQP Algorithm for Large-Scale Constrained Optimiz,” vol. 47, no. 1, pp. 99–131, 2017.

[24] “DECRETO LEGISLATIVO 29 dicembre 2006, n.311,” 2006.

[25] L. Fox and I. B. Parker, *Chebyshev Polynomials in Numerical Analysis*. 1972.

[26] J. Vlassenbroeck and R. V. A. N. Dooren, “A Cheby shev Technique for Solving Nonlinear Optimal Control Problems,” vol. 33, no. 4, 1988.

[27] GSE, “Electricity and Natural gas prices.” [Online]. Available: http://www.mercatoelettrico.org/it/.

[28] Autorità per l’ernergia elettrica e il gas, *SCAMBIO SUL POSTO : AGGIORNAMENTO DEL LIMITE MASSIMO PER LA RESTITUZIONE DEGLI ONERI GENERALI DI SISTEMA NEL CASO*. 2013.

[29] “www.energialombardia.eu.” [Online]. Available: http://www.energialombardia.eu/produzione_energia_elettrica.

A. APPENDIX EQUATIONS

A.1.1 Thermal storage model equations

Starting from the energy and mass balance across the thermal storage in Figure 2.3.2, we obtain the following equations

$$\rho_w c_w A_s \frac{d(h_7 T_7)}{dt} = \dot{m}_8 c_w (T_8) + \dot{m}_{10} c_w (T_{10}) - f_{h7} \dot{m}_5 c_w T_7 - UP h_7 (T_7 - T_{amb}) - f_{h6}(\dot{m}_{11} + \dot{m}_9) T_7 \quad \text{(A.1.1)}$$

$$\rho_w c_w A_s \frac{d((h_{tot} - h_7) T_6)}{dt} = \dot{m}_5 c_w T_2 - (1 - f_{h7}) \dot{m}_5 T_6 + (1 - f_{h6})(\dot{m}_{11} + \dot{m}_9) c_w T_6 - UP(h_{tot} - h_7)(T_6 - T_{amb}) \quad \text{(A.1.2)}$$

$$\rho_w c_w A_s \frac{dh_7}{dt} = \dot{m}_{10} + \dot{m}_8 - f_{h7} \dot{m}_7 - f_{h6}(\dot{m}_{11} + \dot{m}_9) \quad \text{(A.1.2)}$$

The Eq A.1.1 describes the energy balance in the hot node of the thermal storage, the Eq A.1.2 is the energy balance of the cold node and the Eq A.1.2 is the mass balance of the hot node expressed in terms of the height. In the derivative term of the energy balances both the height and the temperature are present $\frac{d(h_7 T_7)}{dt}$ and $\frac{d((h_{tot} - h_7) T_6)}{dt}$, in order to have a more suitable formulation for the numerical integration we have to separate the two terms by applying the multiplication rule for derivatives in particular in Eq. A.1.3 :

$$\frac{d(h_7 T_7)}{dt} = \frac{dh_7}{dt} T_7 + h_7 \frac{dT_7}{dt} \tag{A.1.3}$$
$$\frac{d((h_{tot} - h_7) T_6)}{dt} = \frac{dh_7}{dt} T_6 + (h_{tot} - h_7) \frac{dT_6}{dt}$$

By substituting the expression for $\frac{dh_7}{dt}$ in the energy balances from the mass balance we obtain the expression in (2.4.1.8) and (2.4.1.9).

A.1.2 Weight calculation for cost function

The constant weight W_{en-dis} serve the purpose of changing the dimensional units of the thermal discomfort function from [K^2h] to [€], this parameter was found by solving the optimization problem in each control horizon considered, five sample days for each month from Thursday to Monday, with a k value of 0, in this way the total cost function would become:

$$min J_{tot}(t) = \int_{t_0}^{t_f} J_{dis}(t)]dt \tag{A.2.1}$$

Meaning that the optimal controller will solve the optimal control problem trying to minimize the thermal discomfort inside the room for the given period and W_{en-dis} can be set equal to 1 . Once the solution was obtained it was possible to obtain the value of the integral for the two considered terms, furthermore a plausible starting point for the simulation would be to give the same contribution to the energy cost function $\bar{J}_{en}(t)$ and thermal discomfort cost function $\bar{J}_{dis}(t)$. By setting k value to 0.5 and the difference of the two cost function equal to 0, the following expression is obtained:

$$W_{en-dis} = \frac{\int_{t_0}^{t_f} \bar{J}_{en}(t)\, dt}{\int_{t_0}^{t_f} \bar{J}_{dis}(t) dt} \tag{A.2.1}$$

In order to account for the fact that the thermal discomfort cost function will increase once k is set to a value different from 0, the weight was reduced by a factor of 10^2, obtaining the final average value for $W_{en-dis} = 5.12 \left[\frac{€}{K^2h}\right]$

A.1.3 Pseudo Spectral Method

The Pseudo spectral method converts the continuous time problem into a discretized problem in which an m-vector of controls is considered from the initial to the final time $U(\tau) = [U_0(\tau), \dots, U_{m-1}(\tau)]$ and a n-vector $X(\tau) = [X_0(\tau), \dots X_{n-1}(\tau)]$, $\tau \in [0, t_f]$ which minimize the functional :

$$J = H\left(X(t_f), \dot{X}(t_f), t_f\right) + \int_0^{t_f} G(X(\tau), \dot{X}(\tau), U(\tau), \tau)d\tau \quad \text{(A.3.1)}$$

Subject to

$$X(0) = X_0 \quad \text{(A.3.2)}$$
$$X(t_f) = X_f$$
$$X_{min} \leq X(\tau) \leq X_{max}$$
$$U_{min} \leq U(\tau) \leq U_{max}$$

The time transformation $\tau = \frac{t_f}{2}(t + 1)$ is introduced in order to apply this Pseudo spectral methodology, in such a way the Chebyshev interpolating polynomial are defined on the interval $t \in [-1,1]$, the functional become:

$$J = h(x(1), \dot{x}(1), 1) + \int_{-1}^{1} g(x(t), \dot{x}(t), u(t), t)dt \quad \text{(A.3.3)}$$

Subject to

$$x(-1) = x_{-1} \quad \text{(A.3.4)}$$
$$x(1) = x_1$$
$$x_{min} \leq x(t) \leq x_{max}$$
$$u_{min} \leq u(t) \leq u_{max}$$

Once reached this point, to obtain spectral accuracy, the grids on which the physical problem is to be solved must be obtained by spectral methods. Introducing S_m as the space of algebraic polynomials of degree $\leq m$, and let $T_k(t), k, \geq 0, -1 \leq t \leq 1$, denote the orthogonal family of Chebyshev polynomials of the first kind in this space, with respect to the weight function $w(t) = (1 - t^2)^{-\frac{1}{2}}$. The new grid interpolation points will be the extrema

$$t_j = \cos\left(\frac{j\pi}{m}\right), j = 0,1, \dots, m \quad \text{(A.3.5)}$$

Of the m^{th} order Chebyshev polynomial $T_m(t)$.

Now by expanding the state and control in a Chebyshev series of the m^{th} order, the following approximate solution is determined:

$$x_m(t) = \frac{1}{2}a_0T_0(t) + \sum_{n=1}^{m} a_nT_n(t) \quad \text{(A.3.6)}$$
$$u_m(t) = \frac{1}{2}b_0T_0(t) + \sum_{n=1}^{m} b_nT_n(t)$$

Where $\alpha \equiv (a_0, a_1, \dots a_m)$ and $\beta \equiv (b_0, b_1, \dots, b_m)$ are unknown. For simplicity the choice of m can be seen as function of the required accuracy with the truncantion error for x(t) and u(t) $\sum_{n=m+1}^{\infty} a_n T_n(t)$ and $\sum_{n=m+1}^{\infty} b_n T_n(t)$.

Now substituting the state and control approximations and considering the Chebyshev coefficients $\{C_n(\alpha, T)\}$ and $\{B_n(\alpha, \beta, T)\}$ of $h[x_m(t), T]$ and $g(x_m(t), u_m(t), t, T)$ respectively and applying the properties explained in [25] it can be stated that

$$\int_{-1}^{1} q(t)dt = q_0 - \sum_{n=2}^{\infty} \frac{1 + (-1)^n}{n^2 - 1} q_n \tag{A.3.7}$$

If $q(t) = \frac{1}{2} q_0 T_0(t) + \sum_{n=1}^{\infty} q_n T_n(t)$

The functional of the cost function will become

$$J(\alpha, \beta, T) = \frac{1}{2} C_0(\alpha, T) + \sum_{n=1}^{\infty} C_n(\alpha, T) + B_0(\alpha, \beta, T) - \sum_{n=2}^{\infty} B_n(\alpha, \beta, T). \tag{A.3.8}$$

The two coefficients can be calculated by employing the following formula

$$C_n(\alpha, T) = \frac{2}{K} \sum_{i=1}^{K} h[x_m(cos\theta_i), T] \cos\ n\theta_i \tag{A.3.9}$$

$$B_n(\alpha, \beta, T) = \frac{2}{K} \sum_{i=1}^{K} g[x_m(\cos\theta_i), u_m(\cos\theta_i), \cos\theta_i, T] \cos n\theta_i$$

$$(n = 0,1, \dots, N), K > N, \theta_i = \frac{2i - 1}{K} \frac{\pi}{2}$$

The system dynamics are replaced instead by the following approximation

$$\frac{dx_m}{xt} = f_M(x_m(t), u_m(t), t, T) \tag{A.3.10}$$

Where

$$f_M(x_m(t), u_m(t), t, T) = \frac{1}{2} A_0(\alpha, \beta, T) T_0(t) + \sum_{n=1}^{M} A_n\ (\alpha, \beta, T) T_n(t)$$

With

$$A_n(\alpha, \beta, T) = \frac{2}{K} f(x_m(\cos\theta_i), u_m(\cos\theta_i), \cos\theta_i, T) \cos n\theta_i$$

$$(n = 0,1, \dots, M), K > M, \theta_i = \frac{2i - 1}{K} \frac{\pi}{2}$$

The left side of (A.3.10) is a polynomial of degree m-1, while the right side is a polynomial of degree M. if the function f is nonlinear M=m-1.
Finally the optimal controller has been reduced to a parameter optimization problem which can be stated in this way. Find α, β and T so that J(α,β, T) is minimal, subject to the constraints shown in [26], many mathematical programming techniques can be used to solve this constrained problem, the TOMLAB PROPT MATLAB toolbox uses the solver SNOPT.

A.1.4 SNOPT

Sequential quadratic programming (SQP)methods have proved highly effective for solving constrained optimization problems with smooth nonlinear functions in the objective and constraints. In SNOPT are considered problems with general inequality constraints, with available first derivatives and the constraint gradients are sparse.
This particular SQP algorithm uses a smooth augmented Lagrangian merit function and makes explicit provision for infeasibility in the original problem and the QP subproblems. The Hessian of the Lagrangian is approximated using a limited-memory quasi-Newton method.
For the details on the numerical method, the problem formulation and solution is shown in [23]

B. APPENDIX PRICES

B.1.1 Electricity prices, Feed-in tariff and Natural gas prices

The electricity prices were taken from the G.S.E. website [27] for heating period between October 2016 and April 2017, in particular a monthly variation with two price bands, F1 going from 8:00 to 19:00 and F2 for the rest of the day and the weekend, in the table B.1.1 are reported the values:

	F1 [€/kWh]	F2 [€/kWh]
October	0.165	0.159
November	0.179	0.172
December	0.173	0.167
January	0.222	0.213
February	0.170	0.164
March	0.136	0.131
April	0.132	0.127

Table B.1.1 Electricity prices

The Feed-in tariff is the economic contribution given when the PV system produces more energy than necessary and therefore is sold to the grid. In Italy it's regulated by the "Scambio sul Posto" regulation [28], in particular the contribution is calculated as :

$$CCS\ [€/year] = min[Oe; Cei] + CUSf \cdot Es \tag{B.1.1}$$

Where CCS stands for “Contributo in Scambio sul Posto” and is a yearly partial refund of the bills paid during the year, given back by G.S.E to the owner of the plant.The terms of the equation represent:

- Oe “Onere energia” is the product between the kWh of energy taken from the grid and the PUN “Prezzo Unico Nazionale”, which is the price associated with energy production;
- Cei “Controvalore dell’energia immessa” is the product between the [kWh] of energy input into the grid and the “Prezzo zonale orario”, which can be approximated as the PUN;
- CUSf “Corrispettivo Unitario in Scambio Forfettario” , which accounts for all the other items in the bill related to the transmission of energy, the distribution, and other businesses, without the taxes;
- Es “Energia scambiata”, is the minimum value between the energy taken and energy injected in the grid

In this problem case, the is a main assumption, the self consumption will be higher than energy sold to the grid changing the previous formula to:

$$CCS\ [€/year] = (PUN + CUSf) \cdot Es \tag{B.1.2}$$

Given this formula we can switch from a yearly contribution to a hourly contribution without any problem, and therefore $C_{feed_{in}}$ will be :

$$C_{feed_{in}} = PUN + CUSf\ \left[\frac{€}{kWh}\right] \tag{B.1.3}$$

The values of PUN were taken from GSE website [27] with a monthly variation in the period from October 2016 and April 2017 while the values of the CUSf were taken from the bill of a commercial activity close the school in analysis. The values are reported in the Table B 1.1.2

	Pun [€/kWh]	CUSf [€/kWh]
October	0.0538	0.0250
November	0.0583	0.0257
December	0.0564	0.0257
January	0.0724	0.0248
February	0.0554	0.0250
March	0.0445	0.0250
April	0.0431	0.0250

Table B 1.1.2 PUN and CUSf values

The natural gas prices were taken from GSE website [27] , even tough the natural gas price may fluctuate in one month period, the main variation is seasonal, therefore an average monthly value was taken and the respective values are reported in the table below for the period from October 2016 to April 2017:

Table B 1.1.3

	Natural gas price[€/kWh]
October	0.0540
November	0.0591
December	0.0585
January	0.0687
February	0.0645
March	0.0531
April	0.0539

B.1.2 Emissions and Primary energy

Beside the economical analysis, it is also interesting to check how the optimal controller outperforms the RBC in terms of primary energy consumption and CO_2 emissions, in order to do so, an average monthly value that converts kWh consumed to primary energy and CO_2 is needed. The data for PEFs $\left[\frac{\mathrm{kWh_f}}{\mathrm{kWh_{el}}}\right]$ "primary energy factors" and yearly electricity consumption [Gwh] were taken from the Italian TSO " transmission system operator", Terna. For the biomasses only a constant coefficient was considered for indirect consumption and emission considering the production and the transport, in particular a $\mathrm{PEF} = 0.1\left[\frac{\mathrm{kWh_f}}{\mathrm{kW_{el}}}\right]$ and $e_{CO_2} = 25\left[\frac{\mathrm{g}}{\mathrm{kW_{el}}}\right]$, meanwhile other renewable resources were considered with a zero contribution to emissions and primary energy consumption.

Now in order to find the average monthly value, the composition of electrical energy produced every hour yearly is needed, however it is rather difficult to find data on the amount of energy imported and exported and the mix of production of foreign countries, therefore only national production was considered. The final monthly values were taken from an energy equality analysis, that consider also grid losses with a constant coefficient. However these numbers consider the national mix, since Lombardy mix is known, the parameters were reweighted with respect to Lombardy average mix taken from Lombardy energy monitoring website [29] . The final values are reported in Table B 1.2.1

Table B 1.2.1

	PFE [kWhf/kwhel]	ECO2 [g/kWhe]
October	1.314	336
November	1.221	313
December	1.345	344
January	1.345	343
February	1.354	344
March	1.244	318
April	1.128	289

The value of PEFs during the year result in being pretty low, considering that the European average is around 2 $\left[\frac{kWh_f}{kWh_{el}}\right]$, however this is due to the fact that a large part of energy in Lombardy is produced by using renewable energies, especially Hydroelectric, in fact fuel fired electricity accounts only for around the 50% of the total production.

C. LIST OF FIGURES

C.1.1 Rule based control scatterplots

In these plots are reported the scatterplots for each temperature band for the rule based controller

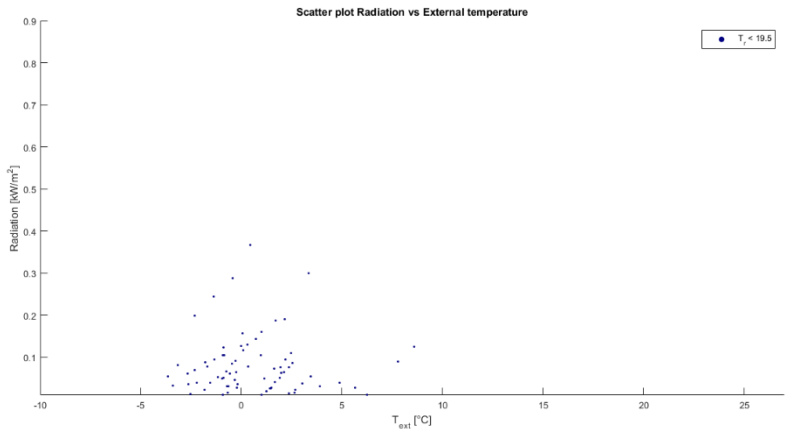

Figure C 1.1.1 Scatter plot $T_{room} < 19.5$ [°C]

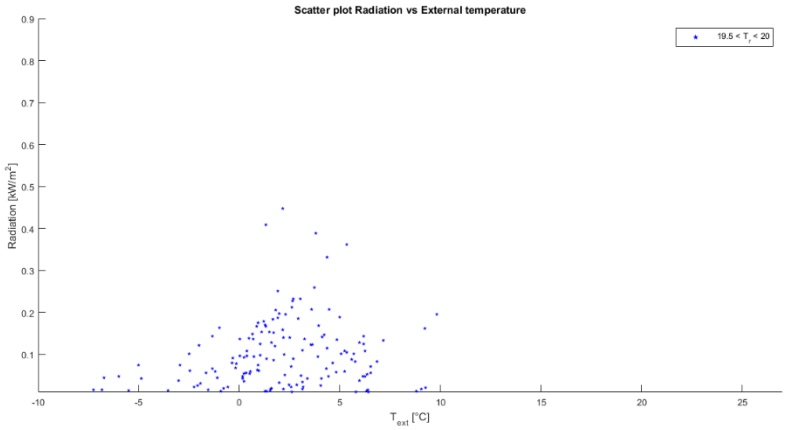

Figure C 1.1.2 Scatter plot $19.5 \leq T_{room} \leq 20$[°C]

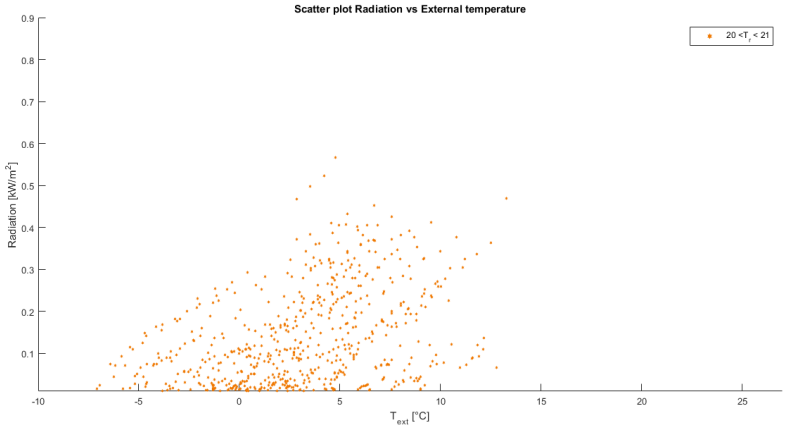

Figure C 1.1.3 Scatter plot $20 \leq T_{room} \leq 21$[°C]

Figure C 1.1.4 Scatter plot $21 \leq T_{room} \leq 22$[°C]

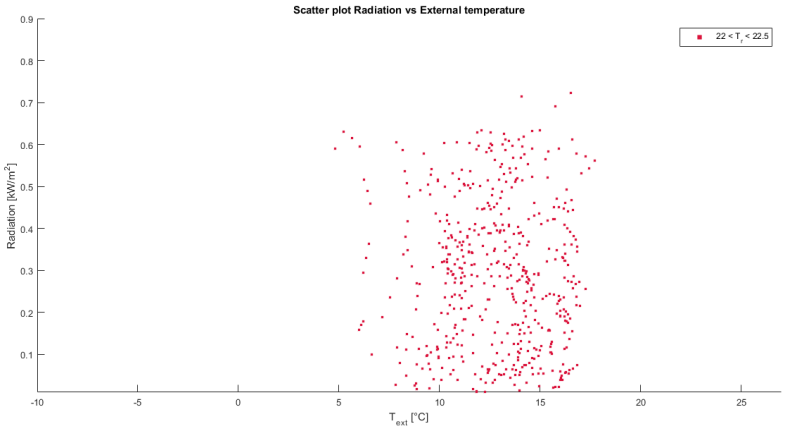

Figure C 1.1.5 Scatter plot $22 \leq T_{room} \leq 22.5[°C]$

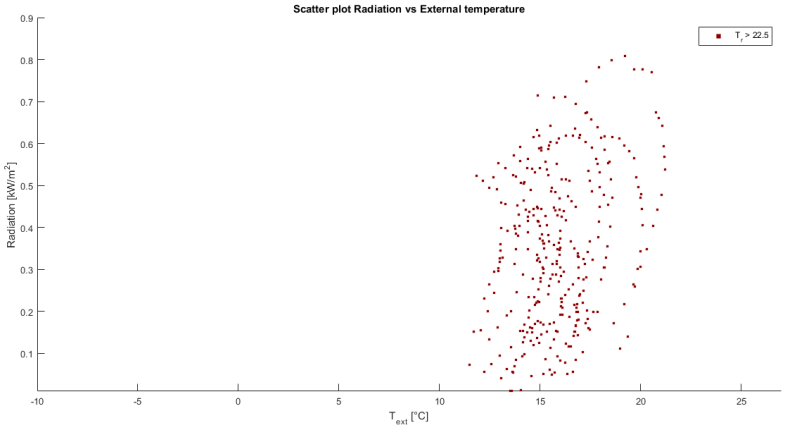

Figure C 1.1.6 Scatter plot $T_{room} > 22.5[°C]$

C.1.2 Sequential rule based scatter plots

In this plots are reported the scatterplots for the sequential rule based controller

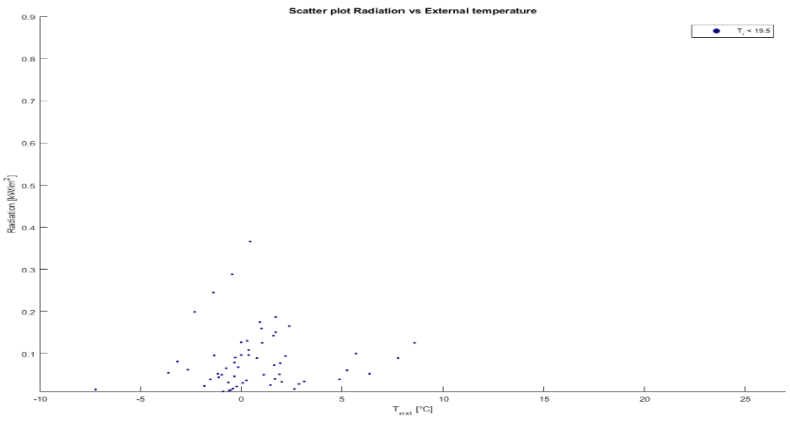

Figure C 1.2.1 Scatter plot $T_{room} < 19.5$ [°C]

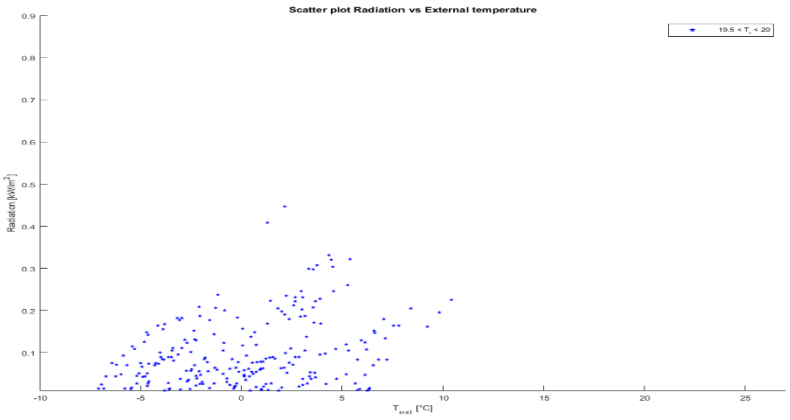

Figure C 1.2.2 Scatter plot $19.5 \leq T_{room} \leq 20$[°C]

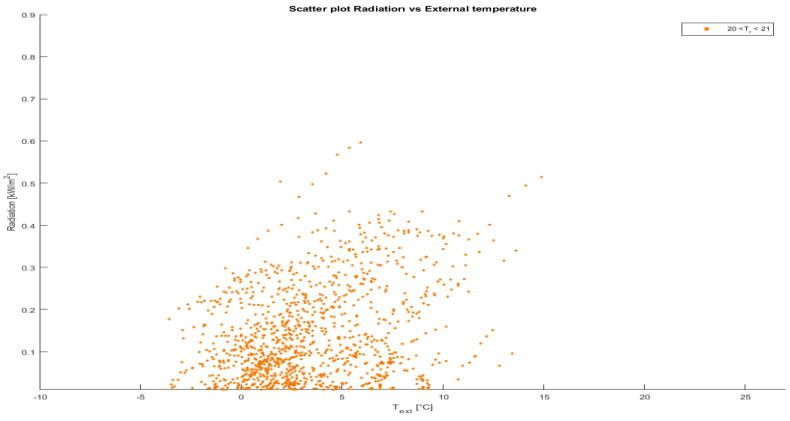

Figure C 1.2.3 Scatter plot $20 \leq T_{room} \leq 21$[°C]

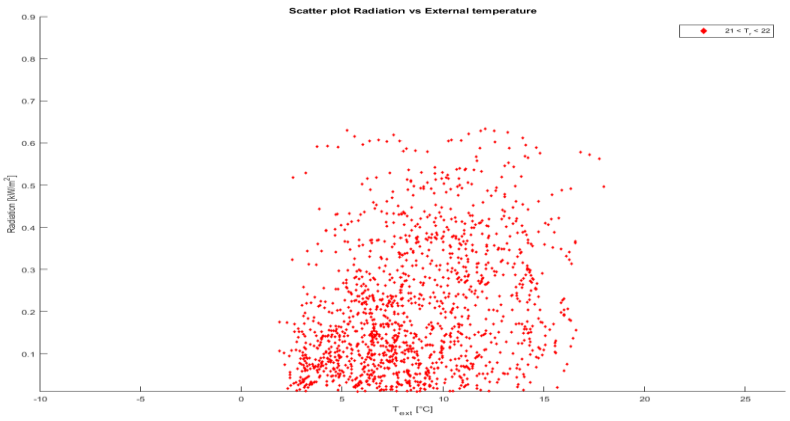

Figure C 1.2.4 Scatter plot $21 \leq T_{room} \leq 22$[°C]

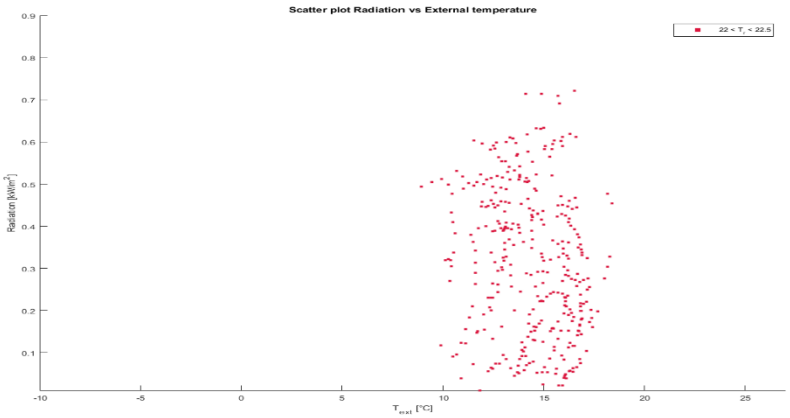

Figure C 1.2.5 Scatter plot $22 \leq T_{room} \leq 22.5$[°C]

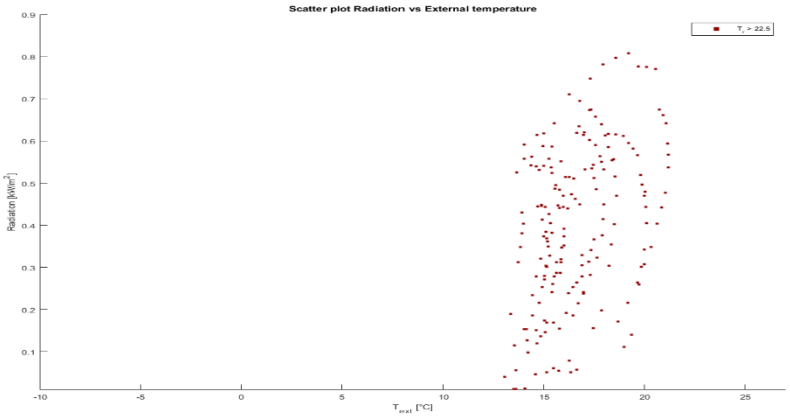

Figure C 1.2.6 Scatter plot $T_{room} > 22.5$[°C]

C.1.3 Rule based control monthly results

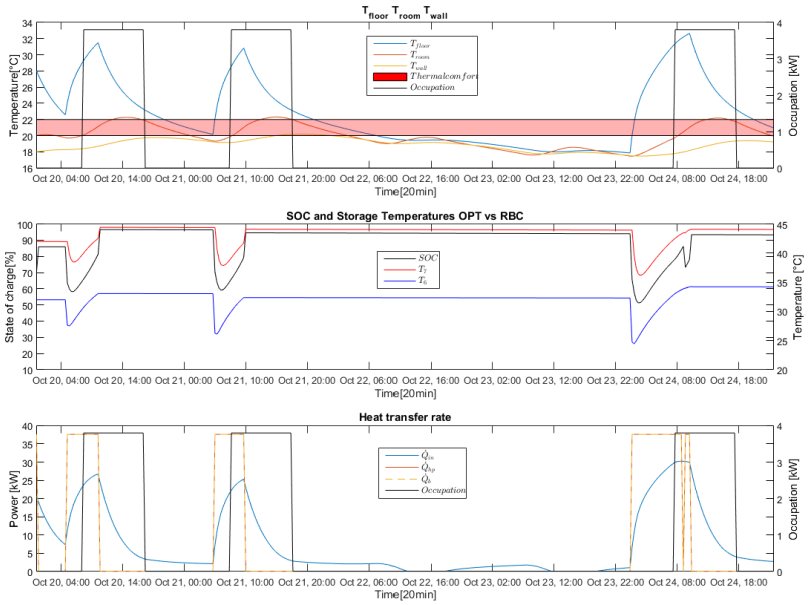

Figure C 1.3.1 October results for RBC, 1) T_{floor}, T_{room} and T_{wall} vs ϕ_o 2) T_7 and T_6 State of charge 3) $\dot{Q}_{in}$, $\dot{Q}_{hp}$ and $\dot{Q}_b$ vs ϕ_o

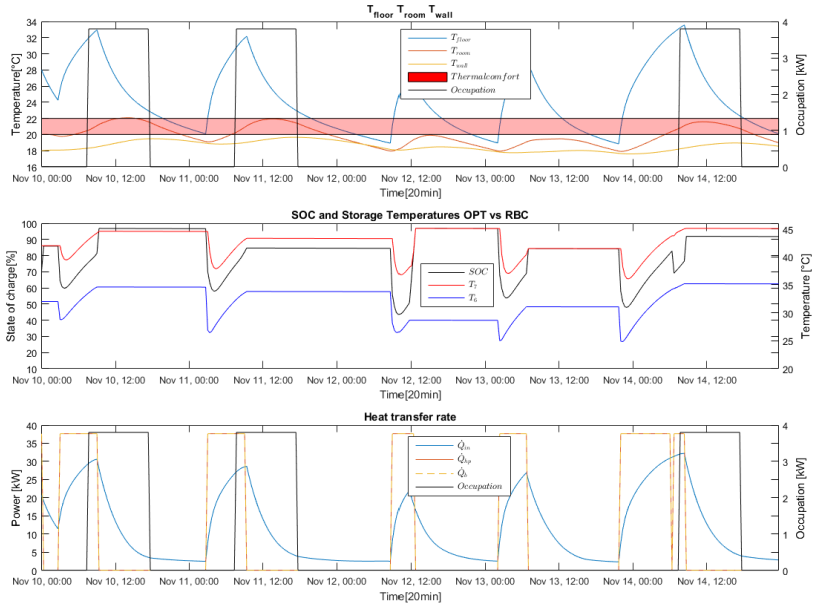

Figure C 1.3.2 November results for RBC, 1) T_{floor}, T_{room} and T_{wall} vs ϕ_o 2) T_7 and T_6 vs State of charge 3) $\dot{Q}_{in}$, $\dot{Q}_{hp}$ and $\dot{Q}_b$ vs ϕ_o

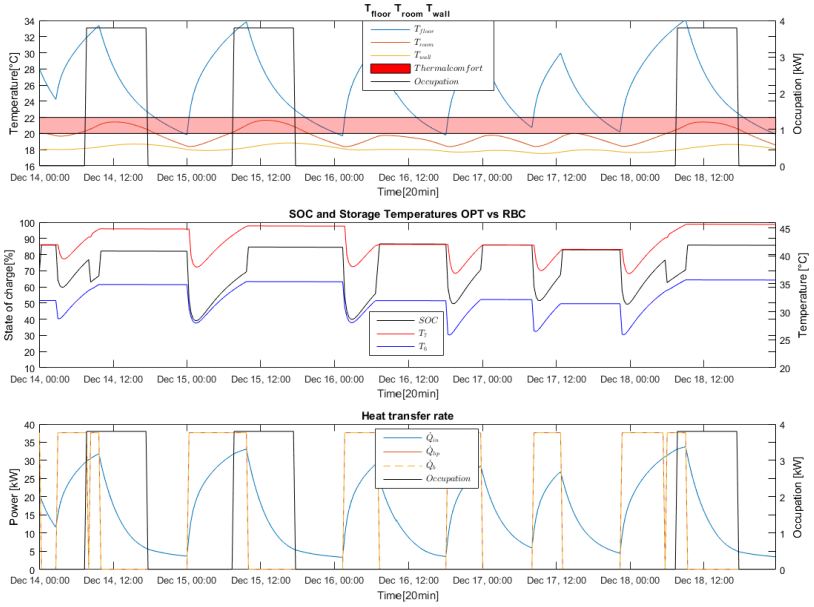

Figure C 1.3.3 December results for RBC, 1) T_{floor}, T_{room} and T_{wall} vs ϕ_o 2) T_7 and T_6 vs State of charge 3) $\dot{Q}_{in}$, $\dot{Q}_{hp}$ and $\dot{Q}_b$ vs ϕ_o

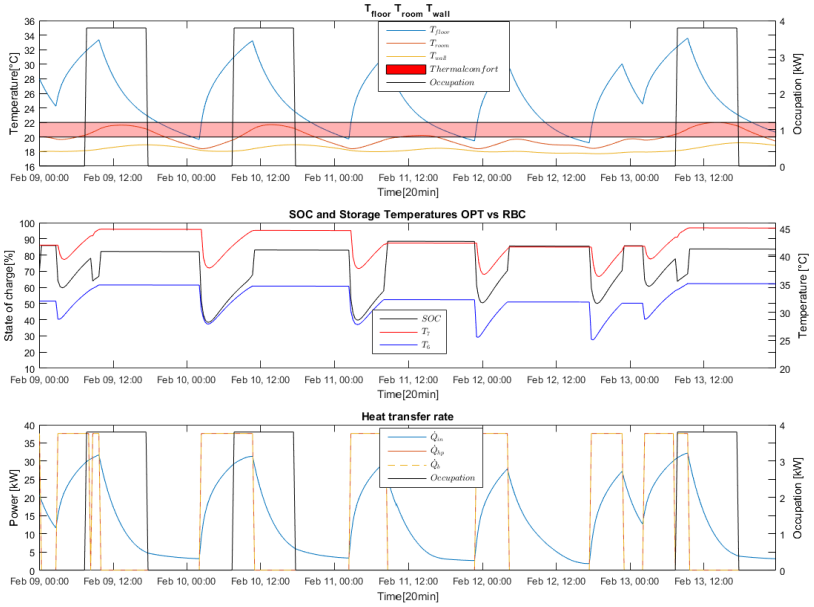

Figure C 1.3.4 February results for RBC, 1) T_{floor}, T_{room} and T_{wall} vs ϕ_o 2) T_7 and T_6 vs State of charge 3) $\dot{Q}_{in}$, $\dot{Q}_{hp}$ and $\dot{Q}_b$ vs ϕ_o

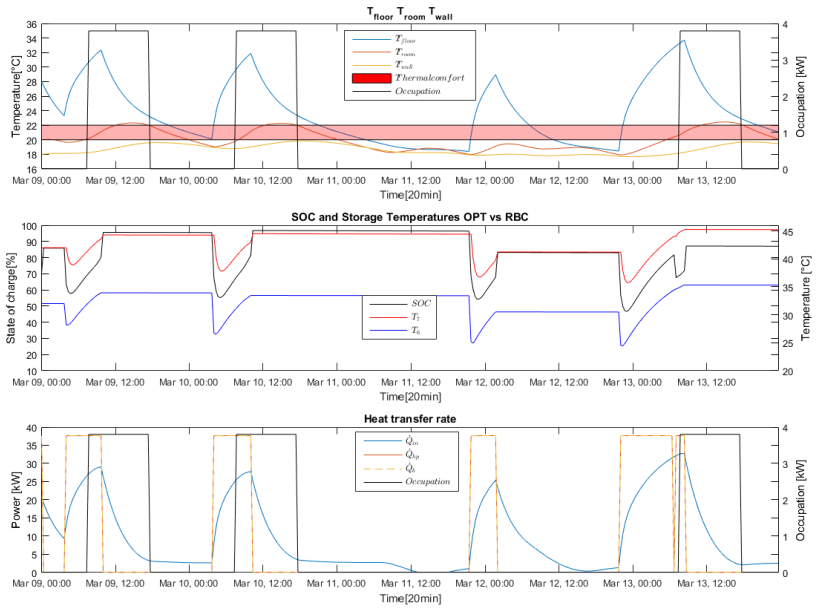

Figure C 1.3.5 March results for RBC, 1) T_{floor}, T_{room} and T_{wall} vs ϕ_o 2) T_7 and T_6 vs State of charge 3) $\dot{Q}_{in}$, $\dot{Q}_{hp}$ and $\dot{Q}_b$ vs ϕ_o

C.1.4 Sequential rule based controller monthly plots

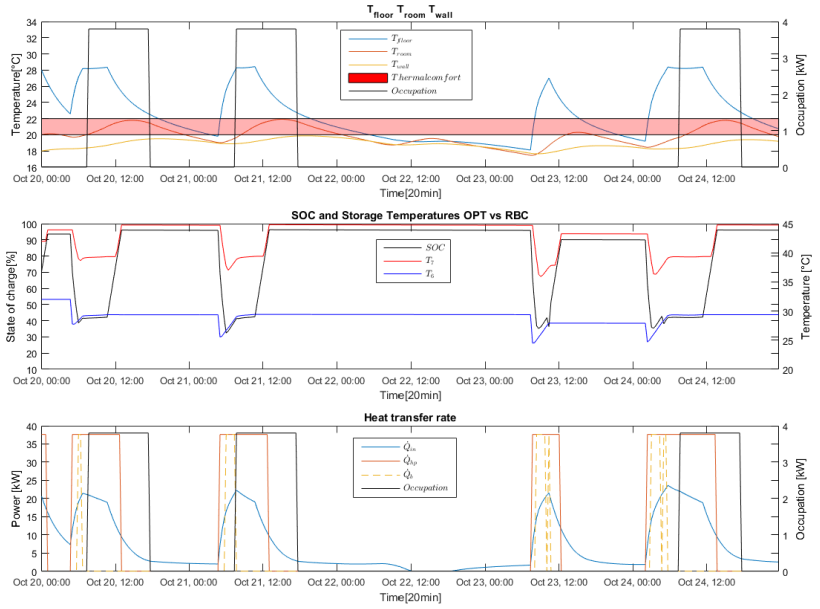

Figure C 1.4.1 October results for sequential RBC, 1) T_{floor}, T_{room} and T_{wall} vs ϕ_o 2) T_7 and T_6 vs State of charge 3) $\dot{Q}_{in}$, $\dot{Q}_{hp}$ and $\dot{Q}_b$ vs ϕ_o

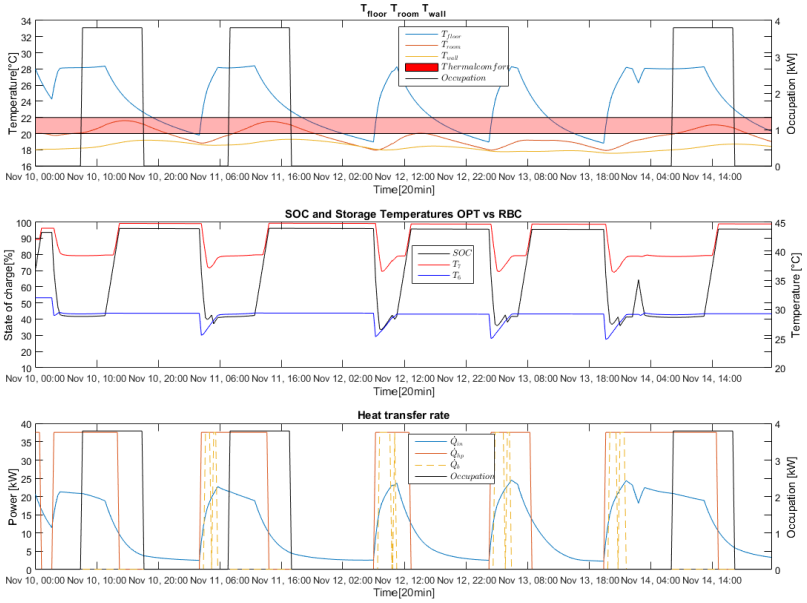

Figure C 1.4.2 November results for sequential RBC, 1) T_{floor}, T_{room} and T_{wall} vs ϕ_o 2) T_7 and T_6 vs State of charge 3) $\dot{Q}_{in}$, $\dot{Q}_{hp}$ and $\dot{Q}_b$ vs ϕ_o

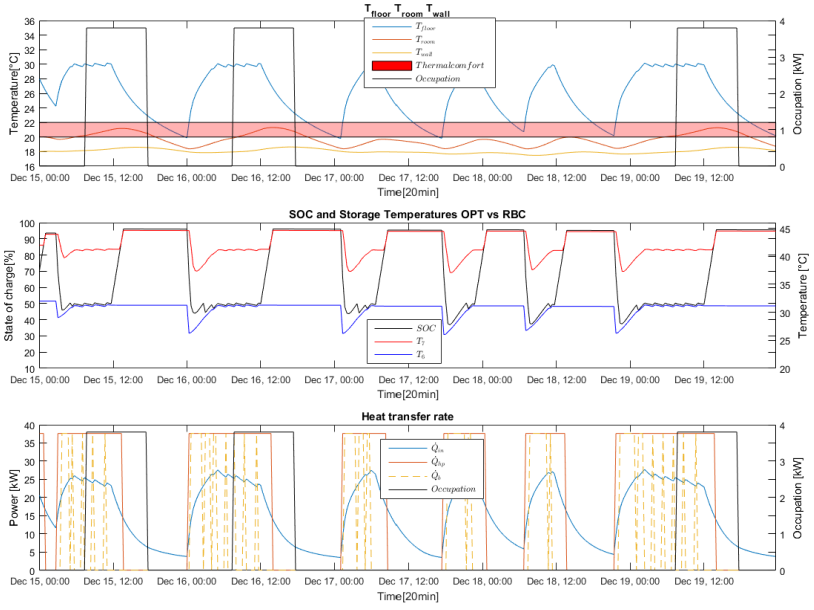

Figure C 1.4.3 December results for sequential RBC, 1) T_{floor}, T_{room} and T_{wall} vs ϕ_o 2) T_7 and T_6 vs State of charge 3) $\dot{Q}_{in}$, $\dot{Q}_{hp}$ and $\dot{Q}_b$ vs ϕ_o

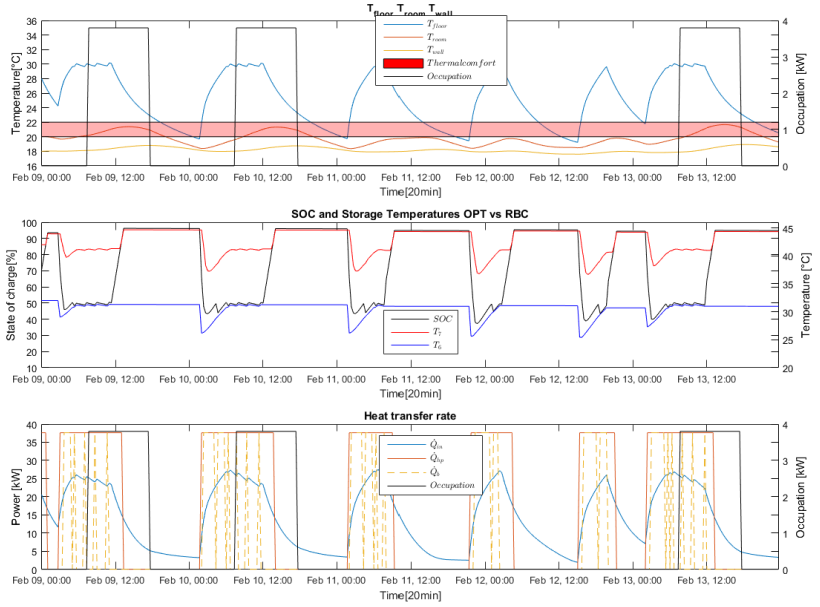

Figure C 1.4.4 February results for sequential RBC, 1) T_{floor}, T_{room} and T_{wall} vs ϕ_o 2) T_7 and T_6 vs State of charge 3) $\dot{Q}_{in}$, $\dot{Q}_{hp}$ and $\dot{Q}_b$ vs ϕ_o

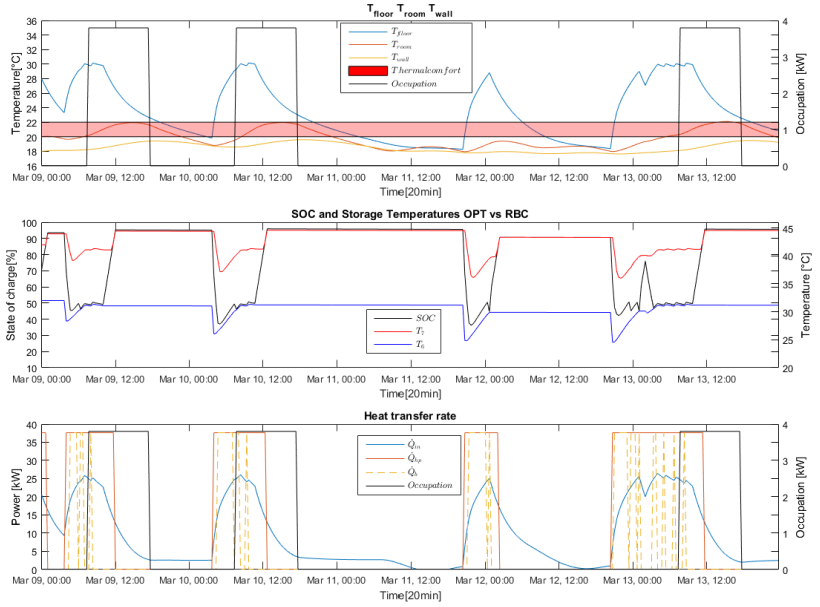

Figure C 1.4.5 March results for sequential RBC, 1) T_{floor}, T_{room} and T_{wall} vs ϕ_o 2) T_7 and T_6 vs State of charge 3) $\dot{Q}_{in}$, $\dot{Q}_{hp}$ and $\dot{Q}_b$ vs ϕ_o

C.1.5 Optimal controller monthly results

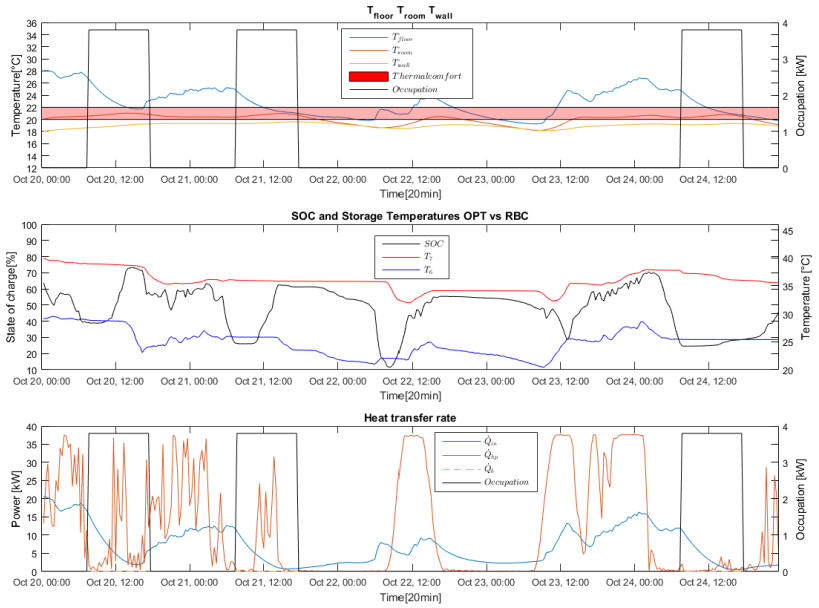

Figure C 1.5.1 October results for optimal controller, 1) T_{floor}, T_{room} and T_{wall} vs ϕ_o 2) T_7 and T_6 vs State of charge 3) $\dot{Q}_{in}$, $\dot{Q}_{hp}$ and $\dot{Q}_b$ vs ϕ_o

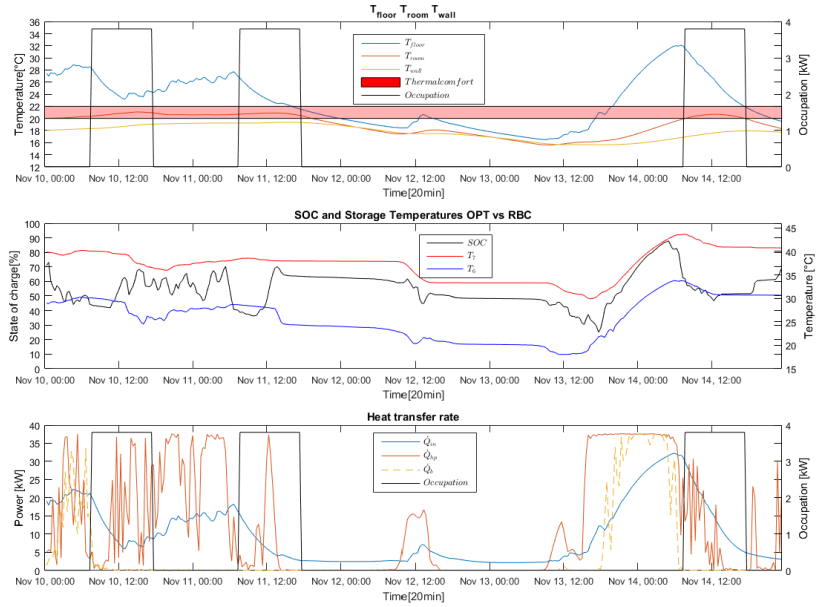

Figure C 1.5.2 November results for optimal controller, 1) T_{floor}, T_{room} and T_{wall} vs ϕ_o 2) T_7 and T_6 vs State of charge 3) $\dot{Q}_{in}$, $\dot{Q}_{hp}$ and $\dot{Q}_b$ vs ϕ_o

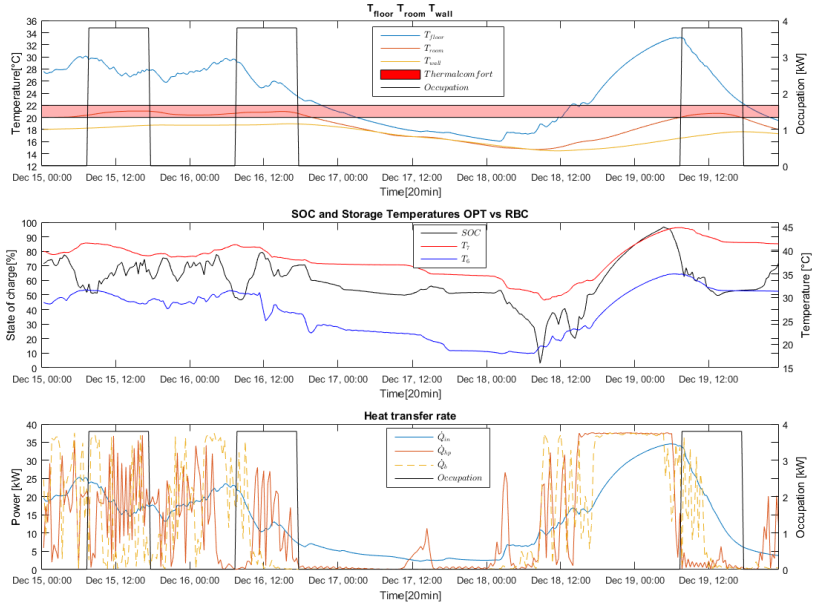

Figure C 1.5.3 December results for optimal controller, 1) T_{floor}, T_{room} and T_{wall} vs ϕ_o 2) T_7 and T_6 vs State of charge 3) $\dot{Q}_{in}$, $\dot{Q}_{hp}$ and $\dot{Q}_b$ vs ϕ_o

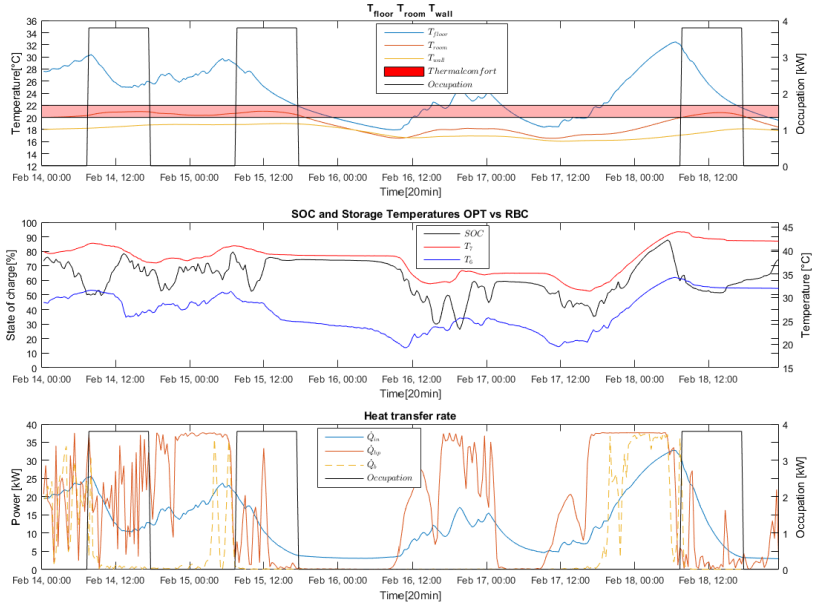

Figure C 1.5.4 February results for optimal controller, 1) T_{floor}, T_{room} and T_{wall} vs ϕ_o 2) T_7 and T_6 vs State of charge 3) $\dot{Q}_{in}$, $\dot{Q}_{hp}$ and $\dot{Q}_b$ vs ϕ_o

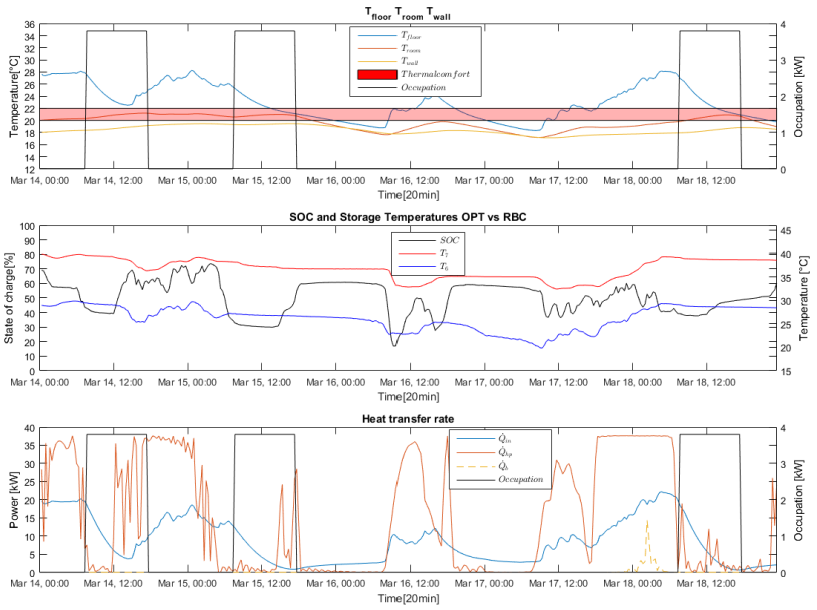

Figure C 1.5.5 March results for optimal controller, 1) T_{floor}, T_{room} and T_{wall} vs ϕ_o 2) T_7 and T_6 vs State of charge 3) $\dot{Q}_{in}$, $\dot{Q}_{hp}$ and $\dot{Q}_b$ vs ϕ_o

C.1.6 Daily comparison optimal controller vs

sequential RBC

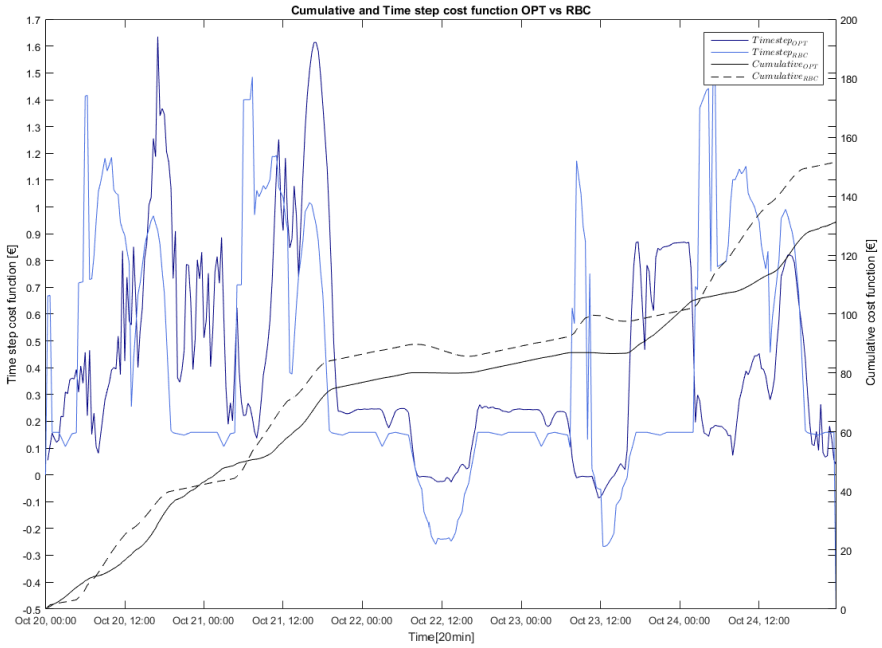

Figure C 1.6.1 October time step cost function and cumulative cost function vs time

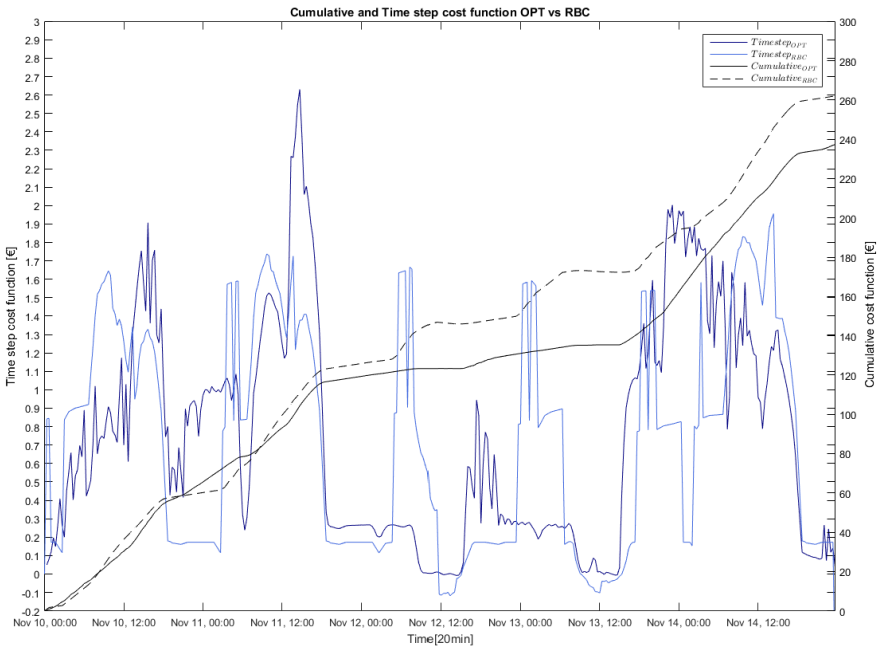

Figure C 1.6.2 November time step cost function and cumulative cost function vs time

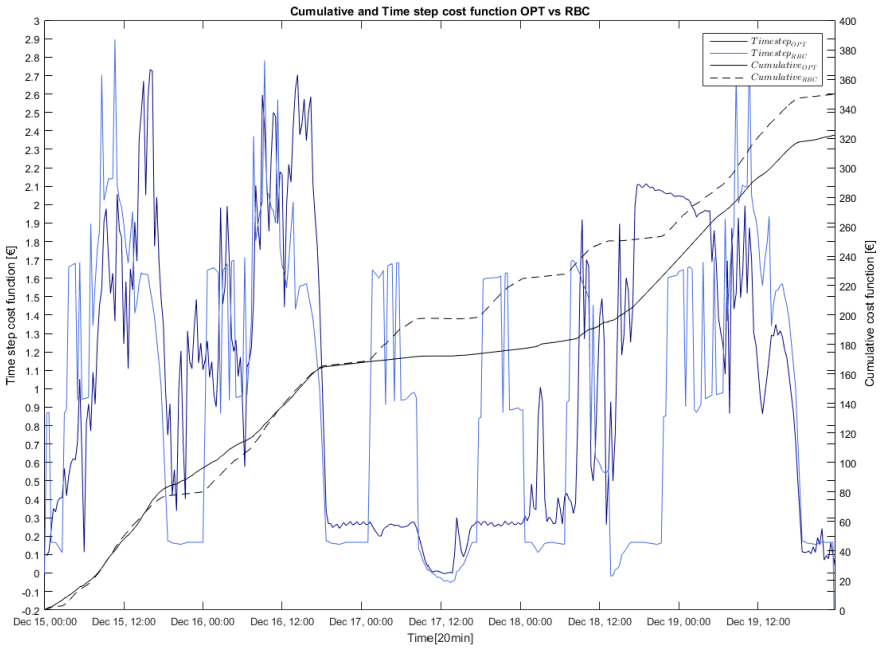

Figure C 1.6.3 December time step cost function and cumulative cost function vs time

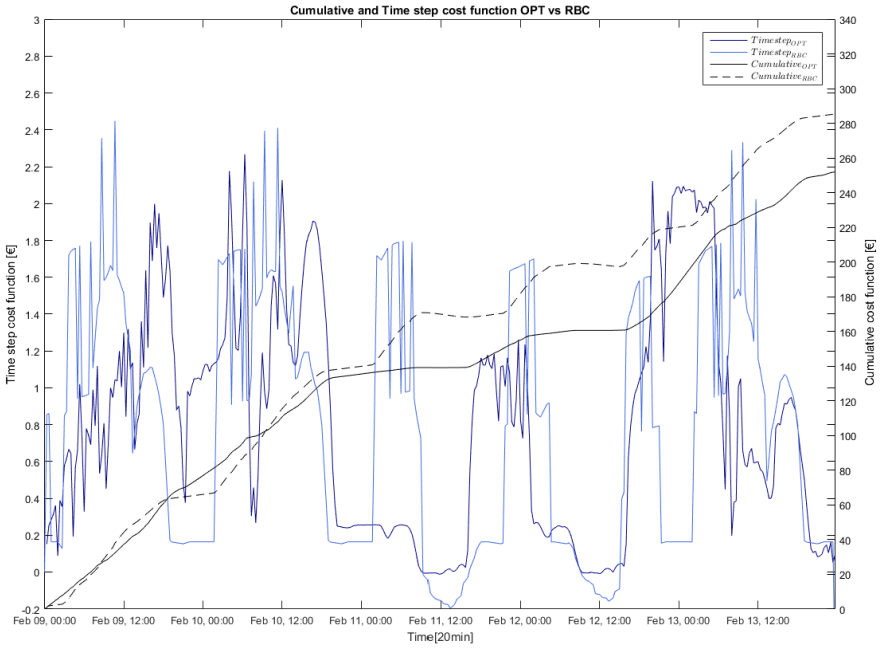

Figure C 1.6.4 February time step cost function and cumulative cost function vs time

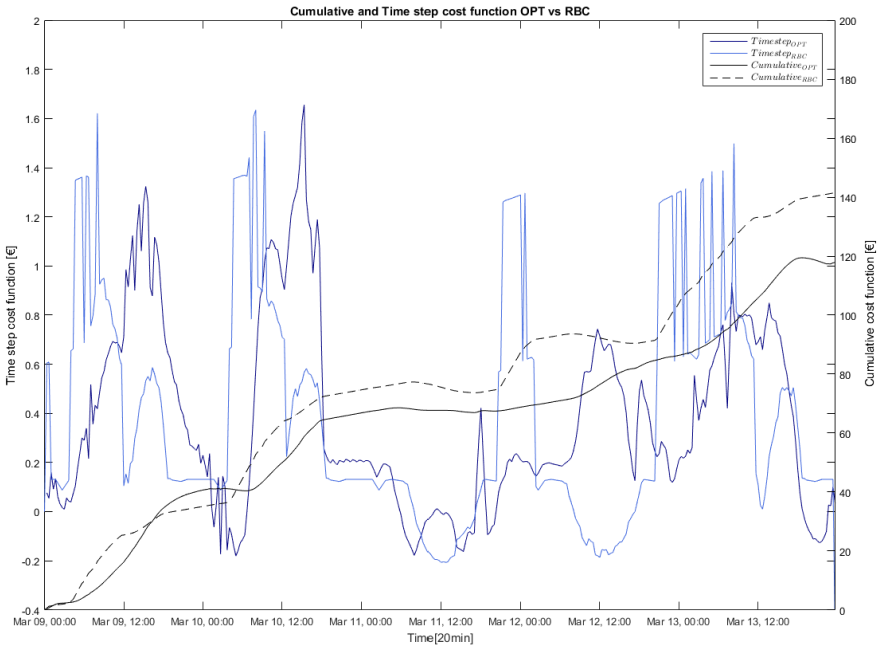

Figure C 1.6.5 March time step cost function and cumulative cost function vs time

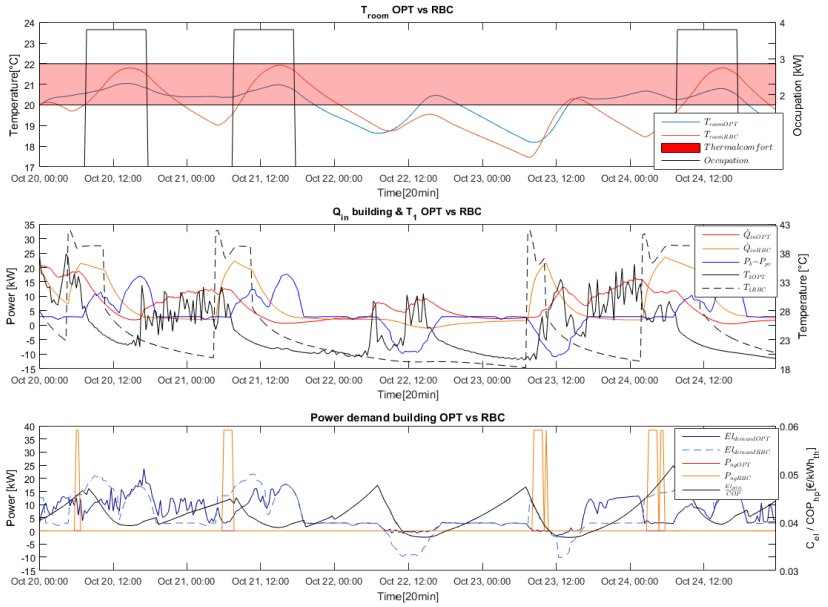

Figure C 1.6.6 October OPT vs RBC 1) T_{room} vs Occupation heat gain, 2) $\dot{Q}_{in} = G_{fr}(T_f - T_r)$, $P_b - P_v$ vs T_1 3) Electricity demand, P_{ng} vs $\frac{C_{el}}{COP}$

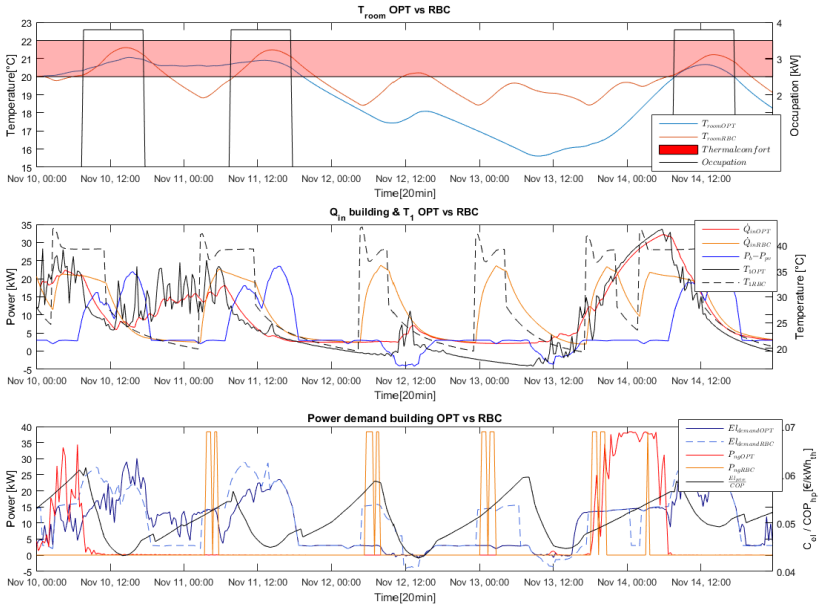

Figure C 1.6.7 November OPT vs RBC 1) T_{room} vs Occupation heat gain, 2) $\dot{Q}_{in} = G_{fr}(T_f - T_r)$, $P_b - P_v$ vs T_1 3) Electricity demand, P_{ng} vs $\frac{C_{el}}{COP}$

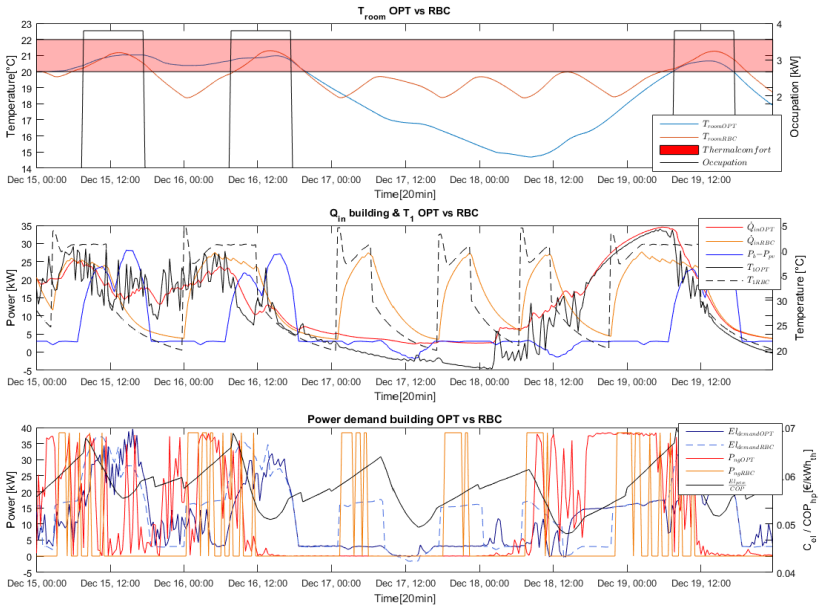

Figure C 1.6.8 December OPT vs RBC 1) T_{room} vs Occupation heat gain, 2) $\dot{Q}_{in} = G_{fr}(T_f - T_r)$, $P_b - P_v$ vs T_1 3) Electricity demand, P_{ng} vs $\frac{C_{el}}{COP}$

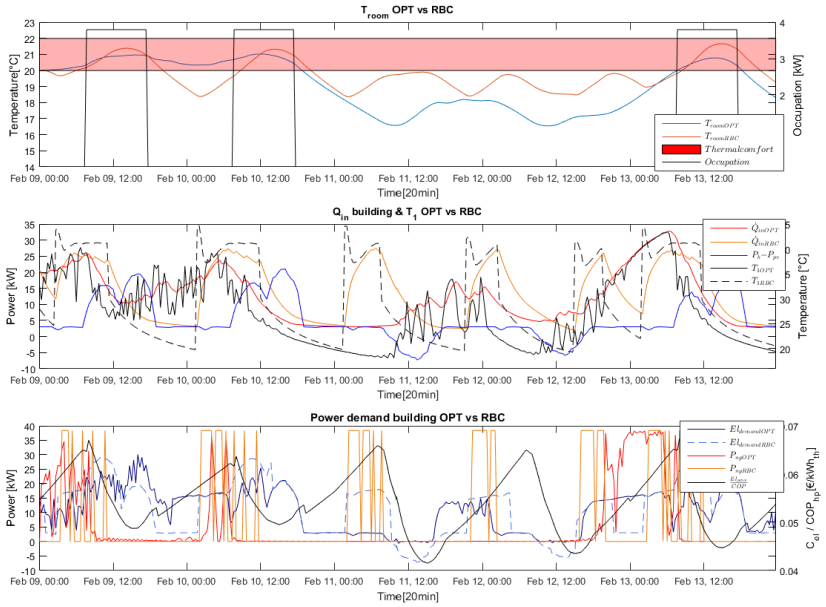

Figure C 1.6.9 February OPT vs RBC 1) T_{room} vs Occupation heat gain, 2) $\dot{Q}_{in} = G_{fr}(T_f - T_r)$, $P_b - P_v$ vs T_1 3) Electricity demand, P_{ng} vs $\frac{C_{el}}{COP}$

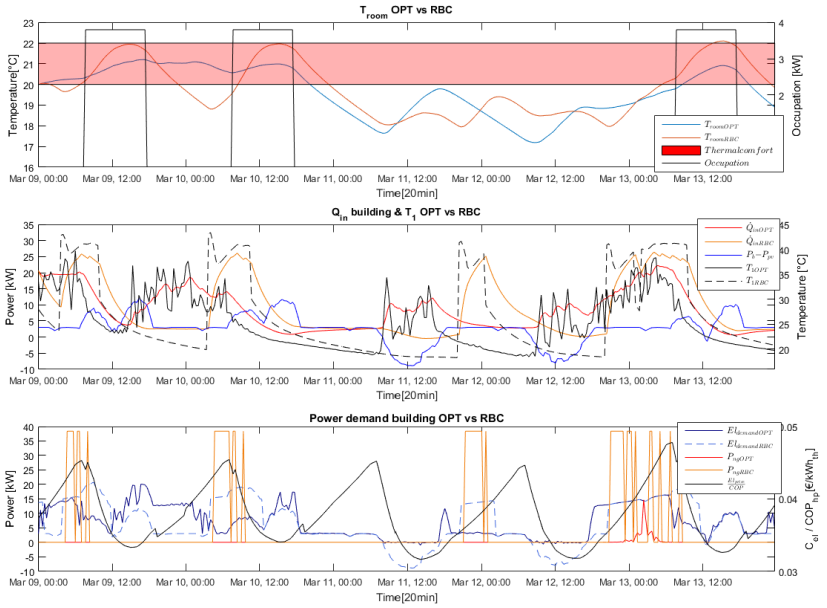

Figure C 1.6.10 March OPT vs RBC 1) T_{room} vs Occupation heat gain, 2) $\dot{Q}_{in} = G_{fr}(T_f - T_r)$, $P_b - P_v$ vs T_1 3) Electricity demand, P_{ng} vs $\frac{C_{el}}{COP}$

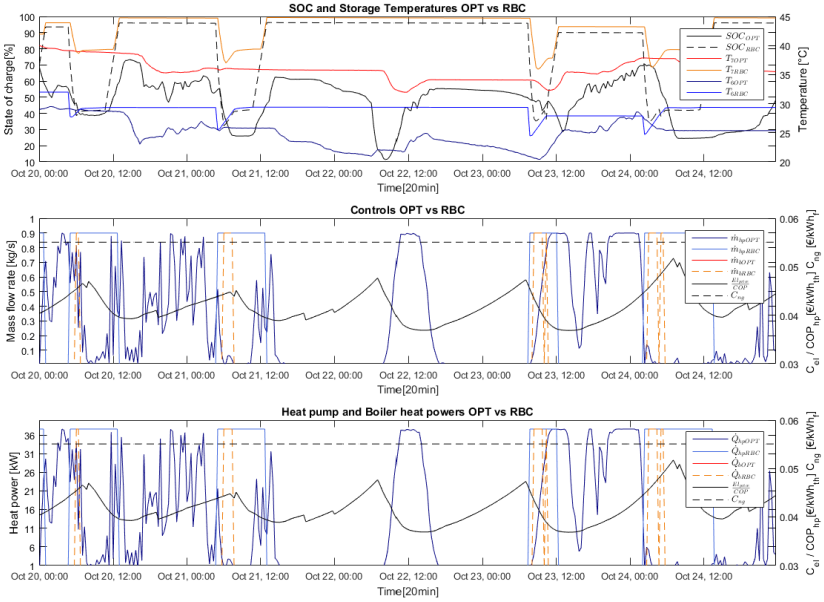

Figure C 1.6.11 October OPT vs RBC 1) SOC vs T_7 and T_6, 2) $\dot{m}_{10}$ and $\dot{m}_8$ vs C_{ng} and $\frac{C_{el}}{COP}$, 3) $\dot{Q}_{hp}$ and $\dot{Q}_b$ vs C_{ng} and $\frac{C_{el}}{COP}$

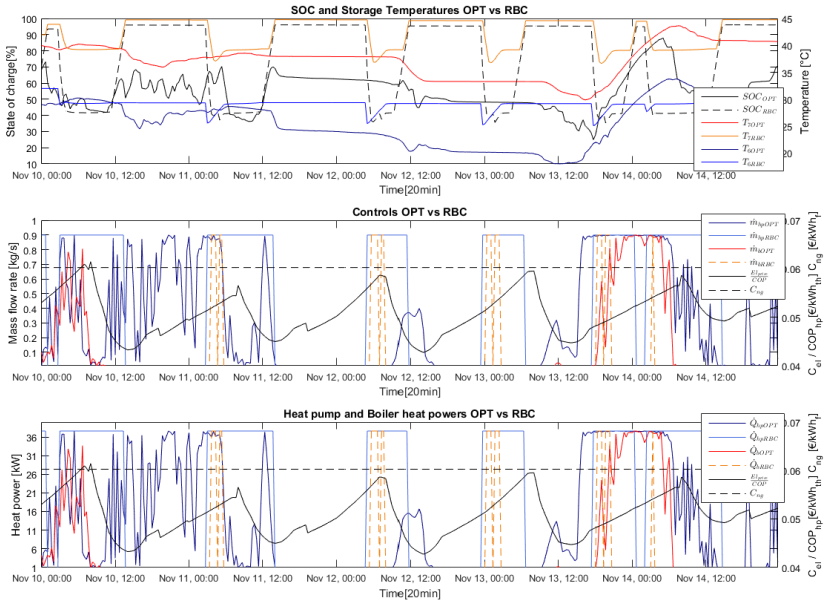

Figure C 1.6.11 November OPT vs RBC 1) SOC vs T_7 and T_6, 2) $\dot{m}_{10}$ and $\dot{m}_8$ vs C_{ng} and $\frac{C_{el}}{COP}$, 3) $\dot{Q}_{hp}$ and $\dot{Q}_b$ vs C_{ng} and $\frac{C_{el}}{COP}$

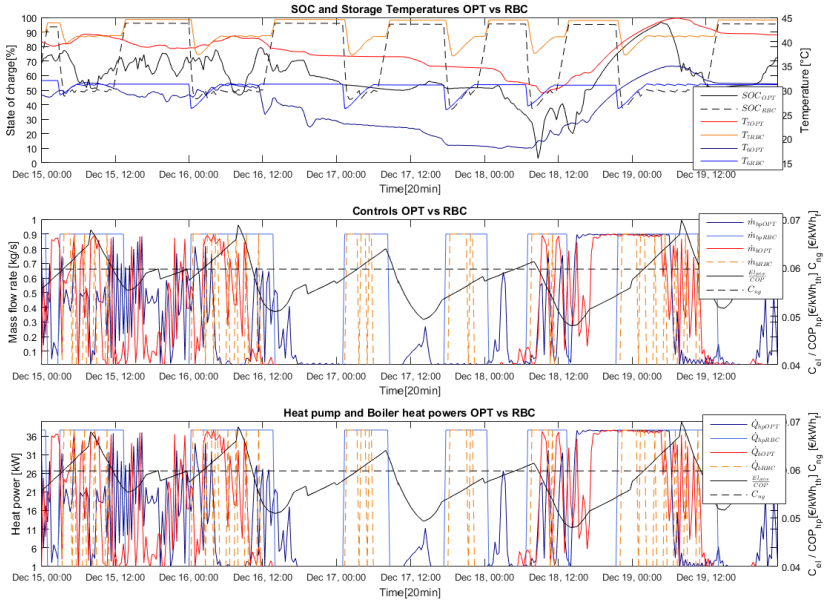

Figure C 1.6.12 December OPT vs RBC 1) SOC vs T_7 and T_6, 2) $\dot{m}_{10}$ and $\dot{m}_8$ vs C_{ng} and $\frac{C_{el}}{COP}$, 3) $\dot{Q}_{hp}$ and $\dot{Q}_b$ vs C_{ng} and $\frac{C_{el}}{COP}$

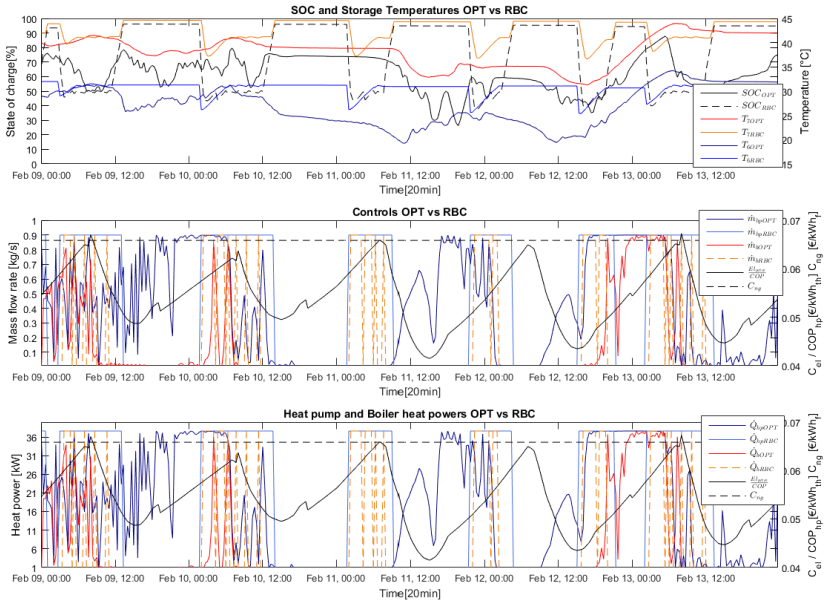

Figure C 1.6.13 February OPT vs RBC 1) SOC vs T_7 and T_6, 2) $\dot{m}_{10}$ and $\dot{m}_8$ vs C_{ng} and $\frac{C_{el}}{COP}$, 3) $\dot{Q}_{hp}$ and $\dot{Q}_b$ vs C_{ng} and $\frac{C_{el}}{COP}$

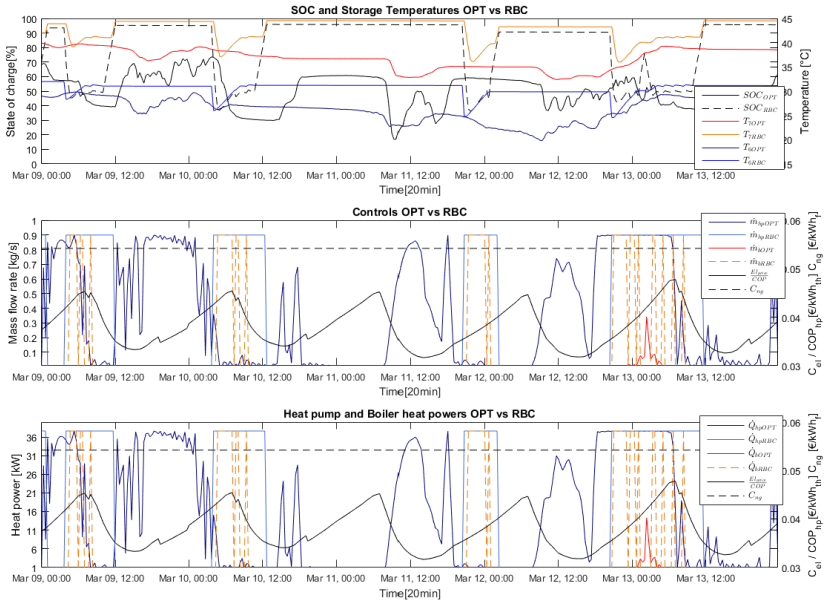

Figure C 1.6.11 March OPT vs RBC 1) SOC vs T_7 and T_6, 2) $\dot{m}_{10}$ and $\dot{m}_8$ vs C_{ng} and $\frac{C_{el}}{COP}$, 3) $\dot{Q}_{hp}$ and $\dot{Q}_b$ vs C_{ng} and $\frac{C_{el}}{COP}$